PHOTOCATALYTIC DEGRADATION OF ORGANIC POLLUTANTS BY TIO_2 CATALYSTS SUPPORTED ON ADSORBENTS

ATREYEE BHATTACHARYYA

NATIONAL UNIVERSITY OF SINGAPORE

2004

PHOTOCATALYTIC DEGRADATION OF ORGANIC POLLUTANTS BY TIO_2 CATALYSTS SUPPORTED ON ADSORBENTS

BY

ATREYEE BHATTACHARYYA (M. SC., NUS)

A THESIS SUBMITTED

FOR THE DEGREE OF MASTER OF ENGINEERING

DEPARTMENT OF CHEMICAL AND BIOMOLECULAR ENGINEERING

NATIONAL UNIVERSITY OF SINGAPORE

2004

ACKNOWLEDGEMENTS

At first, I would like to express my sincere gratitude to my supervisors Assoc. Prof. Madhumita B. Ray and Assoc. Prof. Sibudjing Kawi for their patient guidance, strong support and encouragement during the entire course of this research work. They also helped me to look into the minute details of the problem. Sometimes I got impatient and made several errors but they bear with me cheerfully and guided me towards the right direction. I am thankful to Prof. M. B. Ray for carefully reading earlier versions of this thesis and pointing out several mistakes. I would also like to express my gratitude to Assoc. Prof. Ajay. K Ray for allowing me to use his lab at the initial stages of my experiments and also for his many helpful suggestions.

The assistance provided by the technicians of the department was indispensable. I would like to take this opportunity to thank them all and in particular, I would like to mention Ms. Jamie Siew Woon, Ms. Sylvia Wan and Mr. Boey Kok Hong, for their always extended helping hand to fix the technical matters. Special thanks go to Mr. Qin Zhen for his assistance during this research.

I am grateful to all my friends and other members of our research group. They created a wonderful and enjoyable workplace for me and always helped me whenever I was in trouble. Special thanks to my friends Pavan and Paritam and lab mates specially Dr. Shen, Ho Xu, Tiang who helped me in different ways in my work

Finally I would like to acknowledge the National University of Singapore for providing financial support to this project and research scholarship through the period of my M.Eng.

CONTENTS

SUMMARY

Advanced oxidation processes (AOP) are proven to be very effective for removing low concentration of organic pollutants from various waste streams. Titanium-di-oxide (TiO_2) induced photocatalysis is an established AOP for the treatment of contaminated air and water streams, which is evident from many publications in this area over the last two decades. However, there are certain limitations of using bare TiO_2 in photocatalytic reactors. For example, due to small size (about 4-30 nm) TiO_2 aggregates rapidly in a suspension loosing its effective surface area as well as the catalytic efficiency. Being nonporous, TiO_2 exhibits low adsorption ability for the pollutants, especially for the non-polar organic compounds due to its polar surface. For photocatalytic decomposition of a target compound, adsorption of it on the TiO_2 surface is essential prior to the surface reaction. Furthermore, organic pollutants generally occur in low concentrations (ppm level or below) and pre-concentration of the substrates on the surface where photons are adsorbed is a desirable feature for effective photodegradation.

Recently, new attempts have been made to improve low adsorption ability of non-porous TiO_2 particles by surface augmentation using inert supports. The enhanced decomposition rates are attributed to the increased condensation of organic substrates on the supported catalyst by adsorption and the reduced electron-hole recombination process on the surface. Although, considerable research has been conducted on the immobilization of TiO_2 on adsorbents, detail characterization and performance evaluation of these catalysts in diverse applications are far from optimal.

In this work, TiO_2 photocatalysts supported on various adsorbents were developed, characterized and evaluated. Various adsorbents as catalyst support were selected based on the surface area and pore size. Three different adsorbents, mesoporous (MCM-41), microporous (β-zeolite) and pillared structure (Al-pillared montmorillonite) were chosen and different loadings (10-80 %) of TiO_2 were impregnated on the adsorbent surface using sol-gel method. The catalysts were characterized by several analytical techniques including XRD, SEM-EDX, XPS, and BET analyzer. An azo-dye, orange II dye was chosen as the model compound to determine the photocatalyic efficiency of the supported catalysts in aqueous medium.

The objective of this work is to compare the performances of three TiO_2 supported catalysts in degrading orange II under different operating conditions. In addition, the performances of these catalysts were also compared with those of bare TiO_2 prepared by sol-gel method and commercially available catalyst (Degussa-P25).

NOMENCLATURE

P/P_0	Realative pressure
L	Crystallite size (nm)
q	Amount of organics adsorbed on the catalyst (mg/g)
q_m	Maximum adsorption capacity (mg)
C_s	Equilibrium concentration (ppm)
K	Adsorption equilibrium constant (l/mg)
C	Concentration (ppm)
r_0	Initial reaction rate (mg/l min)
k	Reaction rate constant (mg/l min)
C_0	Initial concentration (ppm)
k_1	First order rate constant (min^{-1})
TOC	Total organic carbon (ppm)

Greek Symbols

λ	wavelength of X-ray radiation (nm)
θ	XRD scanning angle (º)
β	line width at half maximum height (radian)

LIST OF FIGURES

LIST OF TABLES

CHAPTER 1
INTRODUCTION

1.1 Introduction

Advanced oxidation processes are effective remediation and treatment methods due to their ability of complete degradation of wide variety of pollutants including organic, inorganic and microbial substances. Photocatalysis using semiconductors such as titanium di-oxide (TiO_2) is well established advanced oxidation process (AOP) for the purification of contaminated air and wastewater streams which is evident from the large number of publications (Schiavello, 1988; Serpone and Pelizzetti, 1989; Ollis and Al-Ekabi, 1993) in this area over the last two decades. This technique has been applied successfully to air purification, especially for the destruction of volatile organic compounds (VOCs) in gas phase. In case of water purification, this technique offers several advantages such as the use of oxygen as the only oxidant, the capability of simultaneous oxidation and reduction reactions, low costs and use of solar light.

TiO_2 has several advantages such as the ability of using solar energy, operation at ambient temperature, and good photochemical and mechanical resistance. However, there are certain limitations of using bare TiO_2 as: (i) due to small size (about 4-30 nm) TiO_2 aggregates rapidly loosing its effective surface area as well as catalytic efficiency (Qiang et al., 2001), (ii) TiO_2 is nonporous exhibiting low adsorption ability (Torimoto et al., 1997), and (iii) it is poor adsorbent especially to non-polar organic compounds due to its polar surface (Xu and Langford, 1995; Lepore et al., 1996). Adsorption and pre-

concentration of the substrate on the catalyst surface are essential prior to the surface reaction.

Immobilizing TiO_2 on substrates such as ceramic (Sunada and Heller, 1998), glass matrix, quartz, stainless steel plate (Fennandez et al., 1995) and fiber glass (Shifu, 1996) eliminates the problem of agglomeration, although the photocatalytic efficiency of immobilized TiO_2 is less than that of the suspended TiO_2 particles (Matthews, 1990; Xu and Langford, 1997). Besides, the specific surface area also decreases due to the fixing of the TiO_2 on non-porous supports reducing the adsorption capacity. For photocatalytic decomposition of a target compound, adsorption of it on the TiO_2 surface is essential prior to the surface reaction. Furthermore, organic pollutants generally occur in low concentrations (ppm level or below) and pre-concentration of the substrates on the surface where photons are adsorbed is a desirable feature for effective photodegradation.

In recent years, attempts have been made to support fine TiO_2 on porous adsorbent materials like silica (Anpo, 1986; Anderson and Bard, 1995; Lepore et al., 1996; Xu et al., 1999) alumina (Minero et al., 1992; Anderson and Bard, 1997), activated carbon (Torimoto et al., 1997; Hermann et al., 1999; Yoneama and Torimoto, 2000) clay (Tanguay, 1989; Ooka, 1999; Shimizu et al. 2002) and zeolites (Sampath et al., 1994; Xu and Langford, 1995, 1997). Review of recent research on photodecomposition using TiO_2 supported on various adsorbents revealed following advantages over bare TiO_2.

(i) It provides higher specific surface area and introduces more effective adsorption sites than bare TiO_2 (Anderson and Bard, 1995, 1997; Takeda et al., 1995, 1997; Xu and Langford, 1995, 1997; Torimoto et al. 1997). The support with appropriate absorbability has great significance in photocatalytic degradation of organic pollutants in dilute concentration.

(ii) The decomposition rates are reported to increase due to the condensation of organic substrates on the supported catalyst by adsorption, providing high concentration environment around the supported TiO_2 (Minero et al., 1992; Takeda et al., 1995; Anderson and Bard, 1995; Torimoto et al., 1997).

(iii) Acidic nature of the supports prevents electron and hole recombination improving photocatalytic efficiency (Lopez, 2001).

(iv) The support prevents the growth of large TiO_2 crystallites and prevents the conversion of rutile from anatase (Xu and Langford, 1997; Hsien et al., 2001).

(v) During photodegradation, intermediates are formed and also adsorbed on supported photocatalyst surfaces and then further oxidized. Thus, toxic intermediates, if formed are not released in the solution and/or air atmosphere directly and thereby preventing secondary pollution by intermediates (Torimoto et al., 1996).

An extensive literature survey indicated that most studies on enhancement of photodegradation were performed by using TiO_2 supported on different microporous zeolites (Sampath et al., 1994; Xu and Langford, 1995, 1997), activated carbon (Torimoto et al., 1997; Hermann et al., 1999; Yoneama and Torimoto, 2000) and silica (Anpo et al., 1986; Anderson and Bard, 1995; Lepore et al., 1996; Xu et al., 1999). Decomposition rates of the substrates from previous investigation were found to increase due to one or more of the reasons such as increased surface area of the catalyst, increased adsorption of the organic substrates, effective separation of photogenerated electron and holes on the supported catalyst, and stabilization of reactive intermediates (Minero et al., 1992; Takeda et al., 1995; Anderson and Bard, 19995; Torimoto et al., 1997). The efficiency of supported TiO_2 catalysts is influenced by several factors such as the crystalline structure and particle size of TiO_2, porous structure of adsorbent and preparation method. Surface

area should be high enough which could provide uniform dispersion of nanoparticle TiO_2. The high photocatalytic activity of supported TiO_2 was obtained than that of bare TiO_2 due to smaller particle TiO_2 (thus a large surface area) and higher adsorptivity toward organic substrate.

In the case of TiO_2 loaded on microporous zeolite, apparent rate decreased with the increase of TiO_2 coating thickness as the light penetration through catalysts was insufficient as the thickness of the coating increased (Sampath et al., 1994). Activated carbon having higher adsorption capacity exhibited lower photodecomposition rate presumably due to retardation of easy diffusion of the adsorbed substrate (Takeda et al., 1995). If adsorbed substrates are tightly bound to the adsorbent supports, they may not be involved in photodecomposition reaction. Another important phenomenon can be observed from previous research that zeolite and silica with their small pore diameter couldn't accommodate the large molecule substrate in their porous surface from waste stream to enhance substrate photodegradation behavior.

Although extensive research on supported TiO_2 photocatalysis has been performed, but improvement of the photocatalyst performance, to increase the low photon efficiencies, subsequent increase in overall rate and decrease the conversion time is an active research area. Previous studies indicate that photocatalytic activity of supported TiO_2 can be enhanced significantly for parent compound degradation, although complete mineralization has seldom been demonstrated in the above studies. In addition, systematic parametric studies are required for greater application of this potentially useful process for treatment of wide variety of pollutants in different media.

1.2 Scope of the Present Study

Since the surface area and pore size of the adsorbent support are two important factors in determining the adsorption capacity of organic substrate, in this work, three different kinds of supports, mesoporous, microporous, pillared materilas whose surface area and pore size are higher than conventional adsorbent supports, have been chosen to compare their selective adsorption and photocatalytic degradation efficiency for organic substrate in water. The supports used in this study are: (i) MCM-41, a mesoporous support with very large surface area compared to other molecular sieve (> 900 m^2/g), regular hexagonal array of uniform pores with a broad spectrum of pore diameters between 1.5-10 nm, (ii) β-zeolite, a large-pore microporous support compare to other conventional zeolite (surface area 660-680 m^2/g,) with pore sizes of about 0.76 nm (Stelzer et al., 1998) and surface acidity, (iii) Al-pillared montmorillonite (AlPC), a pillared structure support with higher surface area than typical microporous zeolite (surface area = 280-380 m^2/g, Tanguay et al., 1989; Occelli, 1986; Salerno and Mendioroz., 2002) and pore volume which is beneficial for organic compounds to reach and leave the active sites on the surface (Ding et al., 1999; Shimizu et al., 2002). Orange II dye was chosen as the model compound to determine the photocatalyic efficiency of the prepared photocatalysts in aqueous medium

The objectives of this work are: (i) preparation and characterization of the TiO_2 catalysts supported on MCM-41, Al-pillared montmorillonite and β-zeolite simultaneously with bare TiO_2; (ii) to evaluate relative photocatalytic performances of three supported TiO_2 catalysts; (iii) to compare the photocatalytic efficiency of the supported TiO_2 catalysts with bare TiO_2 and commercially available Degussa-P25; and (iv) comprehensive

evaluation of process parameters such as crystallographic structure and particle size of the catalyst, different amount of TiO_2 (wt %) loading on the adsorbent supports, amount of catalysts, initial concentrations of orange II, pH on photocatalytic efficiency in degrading the azo-dye orange II.

CHAPTER 2
LITERATURE REVIEW

2.1 Background

In recent decades, the inorganic materials with their unique and fascinating properties and well defined pore size distribution and surface areas have opened new possibilities in industrial application as adsorbent. The reason for the success of these porous materials originates from (i) their very high surface area, (ii) their adsorption properties and to control the strength and concentration of their active acid sites, (iii) the variety of shape and the dimensions of their pores that are similar in size to many substrate molecules of interest and (iv) their easy regenerability (Kim and Yoon, 2001; Aguado et al., 2002). Some previous research on the improvement of photocatalytic activity by the effect of adsorbent support is reported in the following section.

The role of inert support (alumina and silica) on photocatalytic degradation of organic compounds was reported by Minero et al. (1992). They concluded that the rate of photodegradation was not much affected by the initial adsorption. According to Takeda et al. 1995, the photocatalytic activity of TiO_2 on porous adsorbent support is greatly influenced by the nature of the inert support used in catalyst preparation. They suggested that moderate adsorption capacity is necessary to obtain highest photodegradation efficiency. It is essential for photocatalytic process that adsorbed substrate should be easily moved to photoactive sites of TiO_2 particles (Takeda et al., 1995 and Yoneyama and Tiromoto, 2000).

Takeda et al. (1997) and Yoneyama and Torimoto (2000) also pointed at major influence of diffusion. If adsorbed substrates are tightly bound to the adsorbent supports, they may not be involved in photodecomposition reaction. Takeda et al. 1995 performed similar photodegradation experiments of gaseous propionaldehyde using TiO_2 catalysts supported on different adsorbents. They observed that the highest photodegradation rate was obtained with the use of TiO_2 supported on mordenite. High amount of adsorption was observed for mordenite support yet adsorption strength was moderate enough to allow the diffusion of adsorbed propionaldehyde to the loaded TiO_2. Adsorbent having higher adsorption constant such as activated carbon exhibited lower decomposition rate presumably due to the retardation of easy diffusion of the adsorbed priponaldehyde (Takeda et al., 1995). The same photodecomposition rate of three kinds of chlorinated methanes by TiO_2 supported on activated carbon indicated that rate of supply of those methanes were not greatly different (Torimoto et al., 1997). In a different study, suspended mixture of titania and commercially available activated carbon (Merck) under UV illumination showed photocatalytic degradation of aqueous phenol with an efficiency 2.5 times higher than titania alone (Matos et al., 1998). Matos and his coworkers explained that adsorption of phenol on activated followed by a mass transfer to photoactive titania facilitated the improved rate.

Takeda et al. (1995) noticed an optimal loading of TiO_2 (50 wt%) on mordenite support producing a high decomposition rate for gaseous propionaldehyde and beyond this optimal loading decomposition rate decreased due to a decrease in the adsorption of propionaldehyde. Chen et al. (1999) suggested that adsorption behavior of organics on porous adsorbents strongly depends on the characteristic of pores, their shape, size and chemical properties.

Rate enhancement by the supported catalyst can be improved by decreasing the diffusion path length of the adsorbate. Decrease of diffusion path length can be achieved experimentally by improving the dispersion of TiO_2 particles on adsorbent support.

Ding et al. (1999) and Xu et al. (1999) concluded that dispersion of TiO_2 on the adsorbent with high surface area would be effective to increase the number of surface active sites and to improve kinetic rates. The inert supports also considerably enhanced the lifetime of reactive oxygen species in bulk solution (Reddy et al., 2003).

Torimoto and his coworkers (1996) also noticed that most of the intermediates were collected in solution phase if the naked TiO_2 was used as photocatalyst for propyzamide degradation in aqueous phase whereas most of the intermediates were found on catalyst surface when TiO_2 was loaded on mordenite, silica and activated carbon. The composite catalysts (TiO_2 loaded on adsorbent support) can be used for pollution abatement because some intermediates which might be more toxic than original substrate can be adsorbed by the adsorbent support of loaded TiO_2 and further stabilized.

The enhanced photodecomposition rate of propyzamide (Takeda et al., 1998), salicylic acid (Anderson and Bard, 1997), benzene and chlorobenzene (Hsien et al., 2001), cyclohexane (Shimizu et al., 2002), mythylene blue (Belhekar et al., 2002) dissolved in water, gaseous pyridine (Sampath et al., 1994), propynaldehyde (Takeda et al., 1995) was observed in experiments by many researchers. Supported catalyst enhances the electron density on the conduction band of TiO_2 in composite catalyst as the supported TiO_2 absorbs more incident photons (due to dispersion of TiO_2 on the high surface area support) than bare TiO_2 alone.

Beaune et al. (1993) and Brueva et al. (2001) also investigated photocatalytic activity of supported TiO_2 on zeolite, where catalytic activity was affected by the acidic nature of

adsorbent supports. It might influence the selectivity of reaction through chemisorption on Lewis or Bronsted strong acid sites, induced by aluminum atoms. Shimizu et al. (2002) and Ooka et al. (2003) suggested that oxide in interlayer space of pillared clay or pillared montmorillonite is effective to improve selective photooxidation.

Hsien et al. (2001) and Shimizu et al. (2002) observed that hydrophobicity and hydrophilicity also played an important role in determining the photocatalytic activity for molecular sieves and pillared clays. For the decomposition of hydrophobic compounds such as benzene, monochlorobenzene and dichlorobenzene, TiO_2 supported on molecular sieve produced better activitiy than the commercial anatase TiO_2 or even Degussa P-25. According to Hsien et al. (2001), higher adsorption capacity was observed toward phenol for microporous Na-Y zeolite and Na-mordenite than MCM-41 whereas adsorption capacity toward benzene was similar for three molecular sieve supports. Water molecules, which are more polar than phenol and benzene might compete with the aromatics for adsorption. Conversely, molecular sieve itself, especially MCM-41, favors adsorption of water than aromatic compounds when comparing with TiO_2. But adsorption capacity of supported TiO_2 on Na-Y zeolite, Na-mordenite and MCM-41 increased with TiO_2 loading on the adsorbents which indicated that dispersed TiO_2 on the molecular sieve surfaces might improve the adsorption of aromatics.

Xu and Langford (1997) studied the photocatalytic activity by using various TiO_2 supported on zeolites. They indicated that well defined porous structure of zeolite offer a special environment for the formation of fine TiO_2 crystallites and prevent the conversion of rutile phase. Lepore et al. (1996) and Xu and Langford (1997) observed from powder XRD method that TiO_2 formed on the support was fine crystallites of anatase.

Hisanaga and Tanaka (2002) investigated that the enhancement of photocatalytic activity of benzene in gas phase was not only affected by adsorption of benzene on zeolite. Water adsorption was also an important factor for photocatalysis and high alumina content of zeolite was favorable to water adsorption and hence increased the formation of reactive species such as OH radicals. Xu and Langford (1997) also indicated that highest photocatalytic activity was observed for a support containing low Si/Al ratio in the framework and relatively large pore size.

Malinowska et al. (2003) concluded that photocatalytic efficiency is affected by the type and nature of the pollutants as well as the adsorbent support. It was observed from the previous investigations on supported photocatalysts that some catalysts are quite promising. However, detail characterization and performance evaluation of TiO_2 supported on adsorbent in diverse applications especially related to large scale applications are far from optimal.

2.2 Adsorbent Supports

The ever growing importance of inorganic materials with well defined pore size distribution has attained a great deal of attention in both industrial and fundamental studies due to their unique pore structure and adsorption properties. The most important family in this type of materials is zeolites which are crystalline aluminosilicates with molecular sieve properties.

The term molecular sieve was derived from McBain (1932) when he found that chabazite, a mineral had a property of selective adsorption of molecules smaller than 5 Å in diameter (Zhao et al., 1996). Zeolites and zeotypes materials are formed by corner-

sharing SiO_4^- tetrahedra, with the possibility to replace a few SiO_4^- units by AlO_4^- units, and protons or an equivalent amount of cations to maintain the electronic neutrality of the structure. They are characterized by a regular three dimensional pore structure of molecular dimension, with narrow pore size distribution in the micropore region (Lopez, 2001; Carati et al., 2003). Because of this unique feature they are also called molecular sieve. They act as shape selective materials controlling reaction selectivity. There are some effects of zeolite structure to enhance photocatalytic activity of supported TiO_2 such as stabilization of reactive species such as hydroxyl radicals or intermediates and absorption of substrate.

2.2.1 Classification of Porosity

According to definition of IUPAC, porous materials are classified into three main categories depending on their pore diameter:

Microporous: pore size< 2 nm (pore diameter in the range 0.3-2 nm)

Mesoporous: pore size 2-50 nm

Macroporous: pore size >50 nm

2.2.2 MCM-41

More recently, the expansion of pore size of zeotype materials with controlled pore size distribution from micropore region to mesopore region was developed and extensively studied in response to increasing demands of selective adsorption of large organic molecule from waste water or air (Zhao et al., 1996). In 1992, researchers at Mobil Corporation discovered M41S family of silicate/aluminosilicate mesoporous molecular sieves with exceptionally large pore structures (Beck et al., 1992; Kresge et al.,

1992). After calcinations, these mesoporous materials exhibited ordered arrangement of pores. MCM-41, is a member of M41S family of silicate/aluminosilicate with large surface area (>800 m^2/g). It attracted considerable attention to many researchers because of its regular hexagonal array (Figure 2.1a) of uniform pores with a broad spectrum pore diameters between 1.5-10 nm. The pore diameter of MCM-41 is larger than zeolitic channels which allow faster diffusion of large organic molecules (Beck et al., 1992; Kresge et al., 1992). MCM-41 has been investigated extensively because other members in this family like cubic MCM-48 and lamellar MCM-50 are either difficult to synthesize or thermodynamically unstable (Vartuli et al., 1994). The mesoporous structure can be controlled by sophisticated choice of templates (surfactants), adding of auxiliary organic chemicals and changing reaction parameters like temperature, composition, and pH. Typically, uniform mesopores with the diameter in the range of 5-10 nm could be obtained by using $C_nH_{2n+1}N^+(CH_3)_3$ as a template, where $8<n<16$ (Chen and Lin, 2002). MCM-41 with more effective inter-channel accessibility allows faster mass transport for reactant and products in catalytic reaction and in adsorption of bigger molecule. In our studies purely siliceous MCM-41 was prepared with surface area about 1022 m^2/g and narrow pore size distribution centered at 2.5 to 2.8 nm.

2.2.3 Montmorillonite

Pillared montmorillonite, belonging to smectite mineral group, is a new type of pillared clay (Figure 2.1b.) where octahedral pillar of metal oxides is sandwiched between the tetrahedral silicate sheets (Ooka et al., 1999; Malla et al., 1989). The silicate layers are propped apart by the oxide pillars and some zeolitic micropores are formed between the

silicate layers. The pore size of montmorillonite is larger than that of conventional zeolites. The extent of pore opening of the interlayer of the pillared clay is dependent on the type of metal oxides used. Various metal oxides pillars such as TiO_2, SiO_2, Al_2O_3, Fe_2O_3, ZrO_2 and Cr_2O_3 have been used (Han and Yamanaka, 1998). The size of the pillars can be estimated from the basal spacing of the clays before and after pillaring. Montmorillonite has been used as adsorbent, catalyst and catalyst support due to its porous structure and surface acidity and shape selectivity. Pillared clays generally exhibit bimodoal pore size distribution with pore size bigger than zeolites, which shows advantage in adsorption of large molecule. They possess both Brønsted and Lewis acidity which mainly derive from clay layer structural hydroxyl groups and metal oxide pillars, respectively (Ding et al., 2001). The acidic nature of interlayer space of clay is effective to improve the selectivity of catalyst for the photodegradation. It also possesses high cation exchange capacity (CEC). The pore size of pillared montmorillonite can be varied from 0.5 nm to 2 nm depending on the synthesis conditions, such as type of the starting clay materials, cation exchange capacity (CEC) of clays, type of metal oxide pillars and temperature of thermal treatment. Al-pillared montmorillonite was chosen as one of our catalyst supports (surface area 280-350 m^2/g).

2.2.4 β-zeolite

β (beta)-zeolite is large pore zeolite containing three dimensional 12 membered-ring, with interconnected channel systems (Figure 2.1c) and pore diameters of 0.55nm × 0.55nm and 0.76 nm × 0.64 nm first synthesized by Wadlinger and his coworkers (Borade and Clearfield, 1996). The structure of β-Zeolite consists of an intergrowth of two distinct but closely related structures termed Polymorphs A and B. The polymorphs grow as two-

dimensional sheets and the sheets randomly alternate between the two. Both polymorphs have a three dimensional network of 12-ring pores with a surface area of 650-680 m2/g.

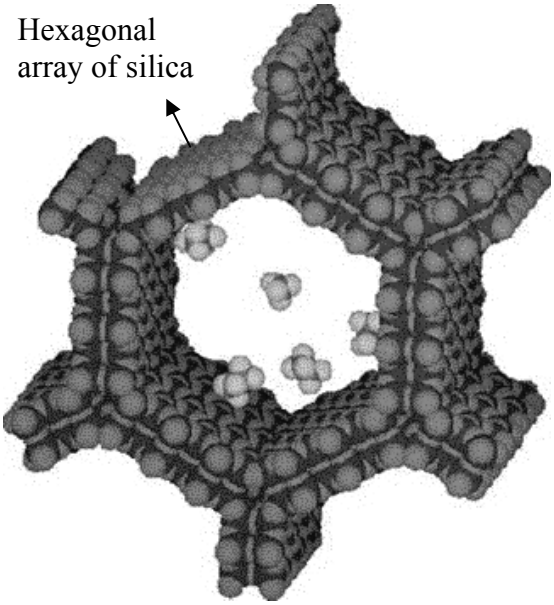

a. Pure MCM-41

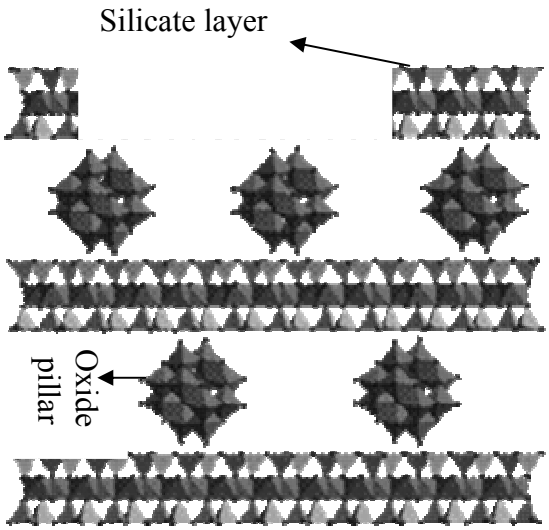

b. Pure pillared montmorillonite

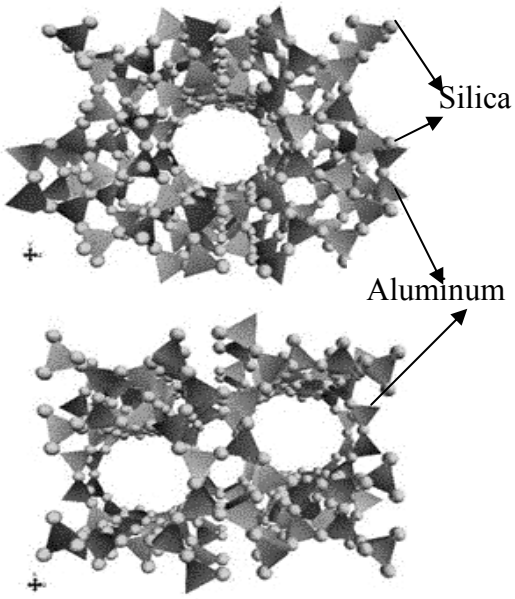

c. Pure β-zeolite

Figure 2.1. Structure of pure MCM-41 (a), pure pillared montmorillonite (b) and pure β-zeolite (c)

This zeolite may offer interesting opportunities as an adsorbent, since it combines three important characterictics: large pores, high Si/Al synthesis ratio, and a tridirectional network of pores. In addition, the dimensions of one type of pores (0.55 nm × 0.55 nm) can originate shape selectivity effects. It is also a promising (Yoo and Smirniotis, 2002) adsorbent and catalyst because it possess high density of Bronsted acid sites and favorable pore structure compared to other zeolites.

Acidic properties of zeolite help to activate molecular oxygen. In this work, β-zeolite with Si/Al ratio = 20 with surface area about 612 m^2/g was chosen as another support. It was reported that Al-rich β-zeolite has low crystallinity.

2.3 Principles of Heterogeneous Photocatalysis

Semiconductor photocatalysis has attained a great deal of attention over last twenty years due to its many advantages in water purification. The basic principles of the photocatalysis are presented in the following section.

A semiconductor is characterized by an electronic structure (Figure 2.2) in which highest energy valence band (vb) and lowest energy conduction band (cb) are separated by a bandgap i.e a region of forbidden energies in a perfect crystal.

When photon energy higher or equal to bandgap energy is absorbed by semiconductor particle (like TiO_2), an electron (e^-) from the valence band is promoted to the conduction band with simultaneous creation of hole (h^+) in valence band.

$$TiO_2 + h\nu \rightarrow e^-_{CB} + h^+_{VB} \qquad (2.1)$$

The electron e_{cb}^- and hole h_{vb}^+ charge carriers formed can recombine on the surface or in the bulk of the particle within few nanoseconds or can be trapped on the surface where

they can react with donor $(Red_2)_{ads}$ or acceptor $(Ox_1)_{ads}$ species adsorbed or close to the surface of the particle. Thereby, subsequent oxidation and reduction reactions are initiated. Photodegradation combines oxidative pathways which could be performed by direct hole attack or performed by very reactive free radicals possessing high oxidizing power, principally hydroxyl radicals ($OH^{\bullet}$). The oxidative reactions in many cases lead to complete mineralization of organic substrate to CO_2 and H_2O.

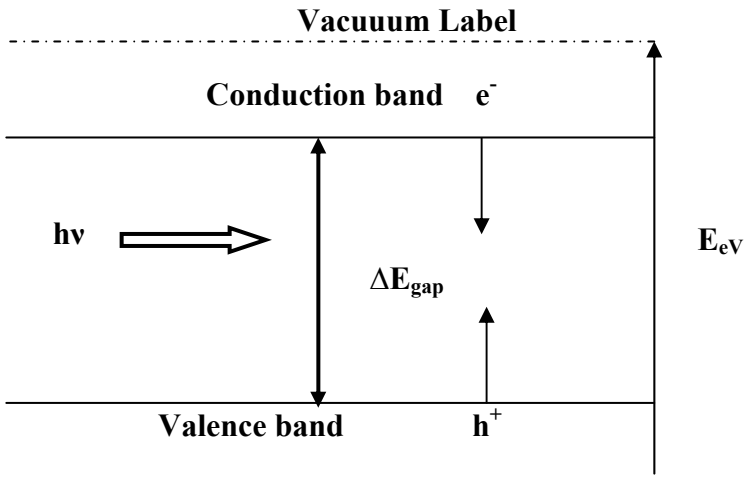

Figure 2.2. Simplified diagram of photogenerated electron-hole pairs

The subsequent redox reactions are described by Hoffmann et al. (1995) as follows:

Trapping of photogenerated electron and hole:

$$TiO^{IV}OH + e^{-}_{cb}e \rightarrow Ti^{III}OH \qquad (2.2)$$

$$TiO^{IV}OH + h^{+}_{vb} \rightarrow (Ti^{IV}OH)^{+} \qquad (2.3)$$

Interfacial electron and hole trapping by adsorbed species:

$$TiO^{III}OH + O_2 \rightarrow (Ti^{IV}OH) + O_2^{\bullet -} \qquad (2.4)$$

$$(TiO^{IV}OH^{\bullet})^{+} + \mathrm{Re}\,d \rightarrow (Ti^{IV}OH) + \mathrm{Re}\,d^{\bullet+} \qquad (2.5)$$

The organic substrates are adsorbed on the TiO_2-adsorbent catalyst surface (Figure 2.3) from the bulk solution. Subsequently the organic substrates are diffused from the inert surface or pore sites to the photo active centre of the supported catalyst. The oxidation of organics takes place at the active centre. The resulting intermediates are also adsorbed on the catalyst surface and further oxidized. These photocatalytic reactions were found to proceed with high efficiency and selectivity where charge separation plays an important role in determining the efficiency.

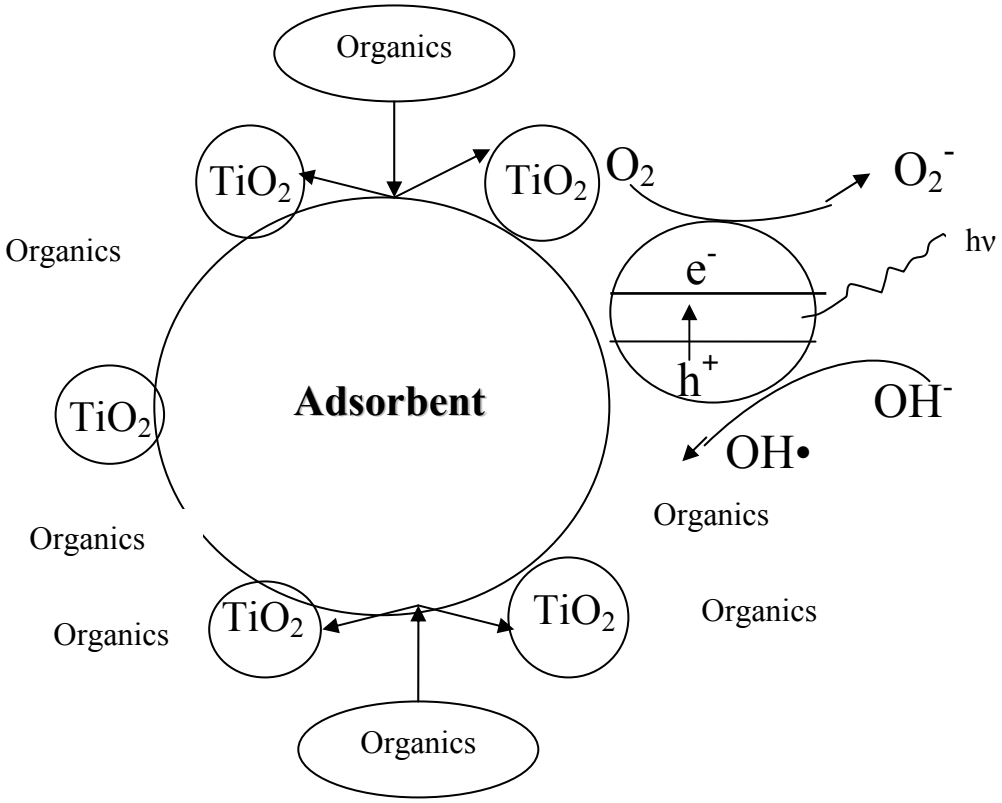

Figure 2.3. Schematic representation of TiO_2 supported on adsorbent

Adsorbent support also controls the dispersion of TiO_2 and local structure of active sites of the supported catalysts. A schematic diagram of the adsorption process is shown below.

2.4 Photocatalytic Use of TiO_2

A proper light source is very important to generate holes and electrons for specific semiconductor material. Lower band gap energy of semiconductor material is preferable as it can be activated by higher wavelength visible light, which exhibits low energy. Knowing the band gap energy of particular semiconductor material, the required threshold wavelength of light source can be easily calculated by the simple equation (2.6). The wavelength of light source should be equal or less than the threshold wavelength of that corresponding semiconductor material to activate the catalyst.

$$\lambda_{bg}(nm) = \frac{1240}{E_{bg}(eV)} \tag{2.6}$$

TiO_2 is by far the most useful material for photocatalytic purposes because of its exceptional optical electronic properties, chemical stability, non-toxicity and low cost. Photocatalytic characteristics of suspended TiO_2 strongly depend on physical properties of TiO_2 e.g. crystal structure, surface area, surface hydroxyls and particle size. TiO_2 exists in two main crystallographic forms, anatase and rutile. The energy bandgap of anatase (3.23 eV, 384 nm) and rutile (3.02 eV, 411 nm) combine with the valence band positions to generate highly energetic holes at the interface, which get involved in oxidation process. Anatase has been found in most cases much more photoactive than rutile because it possesses a slightly higher Fermi level and a higher degree of surface hydroxylation. Ohthani et al. (1997) reported the effect of crystal structure of suspended TiO_2 on photocatalytic activity. They concluded that photocatalytic activity of amorphous TiO_2 was negligible, whereas photocatalytic activity of anatase crystallites with same particle

size as amorphous TiO_2 is appreciable and there are some relationships between TiO_2 particle size and photocatalytic activity. Some success in enhancing photocatalytic activity had been achieved using ultrafine TiO_2 crystallites instead of bulk TiO_2 materials. Anpo et al. (1987) found an increase in photocatalytic activity for the hydrogenation of CH_3CCH with decreasing particle size smaller than 10 nm. A similar phenomenon was observed for photodegradation of mythelene blue in aqueous suspension for TiO_2 particle larger than 30 nm (Xu et al., 1999). However, some reports showed that photodegradation efficiency does not monotonically increase with decreasing TiO_2 particle size. Some researchers also investigated some optimal particle size for photodecomposition of chloroform in liquid phase (Maira et al., 2000).

In photocatalytic process, if the reaction occurs at the surface of the photocatalyst, the degradation process can be envisaged to occur through several steps:

1. Diffusion of the reactants from the bulk of solution to the surface of the catalyst.
2. Transfer of the reactants from the external surface of the catalyst into the pores.
3. Diffusion of adsorbed reactants from the external surface or pore sites of the catalyst to photoactive centers at the surface of the catalyst.
4. Reaction occurring at the catalytic centres.
5. Desorption of the reaction products from the surface to the bulk solution.

There are various factors that can affect the photocatalytic reaction rates. The pH of the solution determines the surface charge on the semiconductor catalyst. The kinetic regime depends on the substrate concentration, showing most cases Langmuirian behavior (that not necessarily represents the true kinetic regime). The photonic flux is also important because an excess of light promotes a faster electron-hole recombination.

2.5 Catalyst Preparation Method

Catalysts were prepared by sol-gel method as fine particles are formed during sol-gel deposition. This method has several promising advantages over other catalyst preparation methods such as reactive thermal deposition, chemical vapor deposition, solid state dispersion (SSD), ion exchange mechanical mixture, spray pyrolysis and precipitation. Sol-gel method allows better control of texture, composition, homogeneity and structural properties of final solids by controlling parameters such as hydrolysis ratios, complexing ratio, aging temperature and acidity (Reddy et al., 2003; Campanati et al, 2003). Photocatalytic efficiency of the catalyst can be changed by changing the composition of elements in the solution during preparation by this technique. It has low process cost, especially for large scale production.

2.6 Organic Compound Used in Experiment

Dye generated from textile industries are an important source of environmental pollution. It is estimated that from 1 to 15 % of the dye is lost during dyeing process and is released in textile effluents. The release of these color effluents to the ecosystem is a source of esthetic pollution, eutrophication and of the perturbation of aquatic life. Some azo-dyes and their degradation products (as aromatic amines) are highly carcinogenic (Augugliaro et al., 2002; Guillard et al., 2003). Decolorization of dye effluents has therefore received increasing attention. Among the dyes, available in the market today, approximately 50-70% are azo compounds followed by anthraquinone group. Azo dyes can be divided into monoazo, diazo, triazo classes according to the presence of one or

more azo bonds. Some azo bonds (-N=N-) are found in various categories i.e. acid, basic, direct, azoic, pigments. Some azo dyes and their dye precursors have been suspected to be human carcinogens as they form toxic aromatic amines. Therefore azo dyes are pollutants of high environmental impact and were selected as more relevant group of dyes for examination of the photodegradation behavior.

Orange II, azo dye was chosen as the model compound to determine the photocatalyic efficiency of the above photocatalysts mentioned earlier (section 2.2.2-2.2.4) in aqueous medium. The structure of orange II is shown in Figure 2.4. Here we will investigate the relative performance of the three supported photocatalysts compare to unsupported or bare TiO_2 in degradation of orange II under different operating conditions.

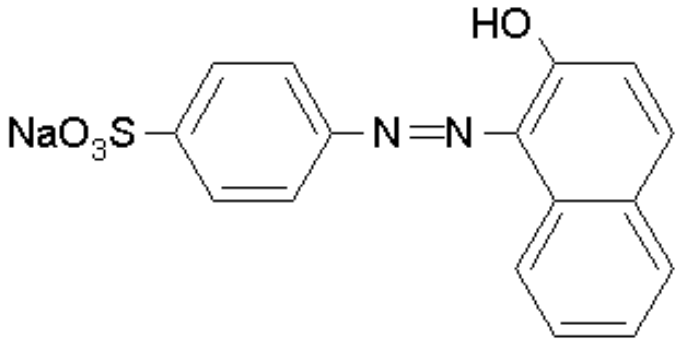

Figure 2.4 Chemical structure of orange II

CHAPTER 3
EXPERIMENTAL SECTION

In this chapter, detailed description of materials, experimental set-up and analytical procedure used in this work are provided.

3.1. Materials

Titanium tetra iso-propoxide and Orange II, an azo dye were purchased from Aldrich (Sigma-Aldrich Co., Germany). The properties of orange II are presented in Table 3.1. The analytical grade Al-pillared montmorillonite (Fluka), β-zeolite (Zeolyst International, UK, Si/Al = 20), Degussa-P25 (Degussa, Germany) were purchased and used without any purification. Pure siliceous MCM-41 was prepared in the lab following a method developed by Kawi et al. (2002). Analytical grade aerosil, HCl (37%) (MERCK, Germany), HNO_3 (65%) (MERCK, Germany), NaOH pellets (Mallinckrodt AR., USA), CTMABr (Aldrich, Sigma-Aldrich, Germany) were used for the preparation of pure MCM-41 and TiO_2 supported on MCM-41, Al-pillared montmorillonite, β-zeolite and unsupported or bare TiO_2.

Table 3.1 Physical Properties of Orange II p-(2-Hydroxy-1-naphthylazo) benzenesulfonic acid, sodium salt

Molecular Formula:	$C_{16}H_{11}N_2NaO_4S$
Molecular Weight:	350.33
Solubility :	116 g/l
Melting point:	164 ºC

3.2 Experimental Details of Catalyst Preparation

3.2.1 Preparation of Pure MCM-41

Purely siliceous MCM-41 was prepared by hydrothermal synthesis (Kawi et al., 2002). Cetyltrimethyl-ammonium bromide (CTMABr) was used as the organic template for this synthesis. In this preparation 6 g of aerosil and 2 g of NaOH were dissolved in 90 g of deionized water under continuous stirring and heating at 60-70 ºC for approximately 30 minutes (mixture A). Another solution (mixture B) was prepared by dissolving 9.1 g of CTMABr in 50 g of deionized water under continuous heating (60-70 ºC) and stirring for 30 minutes till the sol became transparent. Mixture B was added dropwise to mixture A under continuous stirring and pH of this mixture was adjusted to 11 using 2 M HCl. Subsequently, the resulting solution was stirred for another 3 hours at room temperature and mixture was transferred to PP-bottle for hydrothermal treatment for three days at 100 ºC in oven. The solution was filtered and the solid was washed with DI water and dried in oven at 50 ºC. The solid was calcined at 600 ºC for 10 hours to remove the organic template.

3.2.2 Preparation of TiO_2 Supported on Adsorbents and Pure TiO_2

The TiO_2 sol was synthesized by acid catalyzed sol-gel formation method using 30 ml of 1 M HNO_3 and 7.4 ml of titanium tetra-isopropoxide following the hydrolysis reaction (Anderson et al., 1988).

$$Ti\ (iso\text{-}OC_3H_7)_4 + 4H_2O \rightarrow Ti\ (OH)_4 + 4C_3H_7OH \qquad (3.1)$$

Titanium tetra-isopropoxide was added gradually to the 1 M HNO_3 solution (Takeda et al., 1995) under continuous stirring for 1.5 to 2 hours to produce a transparent sol containing 2 gm of TiO_2. Subsequently, the colloid solution was diluted with de-ionized water and pH was adjusted to 3 with the addition of 1 M NaOH resulting in a turbid colloid. The pH adjustment was necessary to prevent the destruction of the structure of adsorbent due to reaction with acid. Depending on the (wt %) loading of TiO_2 on the support, requisite amount of adsorbent (MCM-41, Al-pillared montmorillonite, β-zeolite) was added to the TiO_2 turbid colloid suspension. The resulting mixed suspension was agitated by magnetic stirrer for another 2 hours at room temperature, followed by several centrifugations and washings with de-ionized water until the pH of the supernatant was about 6. The resulting supported TiO_2 catalyst was dried in an oven and subjected to calcination in furnace for 1 hour at 300, 450, 600 and 750 ºC. Finally the products were ground into fine powder and stored in dark. Catalysts supported on MCM-41, montmorillonite and β-zeolite was prepared with different TiO_2 contents (10, 25, 30, 40, 50, 60, and 80 %). Bare TiO_2 without any support was also prepared using the above sol-gel technique and calcined at 300 and 450 ºC.

3.3 Characterization of Catalysts

The synthesized catalysts were characterized using different analytical techniques.

3.3.1 N_2-sorption Isotherm/BET Analysis

The nitrogen adsorption/desorption isotherm of supported and unsupported TiO_2 and adsorbents were obtained at liquid nitrogen temperature 77 K by using Quantachrome

Auto-sorb1 analyzer. Before determining the isotherm, the sample (wt. 0.1g) was out-gassed for 6 hours at 300 ºC under vacuum. The specific surface area has been evaluated by multi point BET (Brunauer-Emmett-Teller) plot. The linearity is restricted to the limited part of the isotherm, usually with P/P_0 in the range of 0.05 to 0.30. The pore volume and pore size distribution were obtained from the desorption branch using Barrett-Joyner-Halenda (BJH) method (based on Kelvin equation).

3.3.2 *XRD Analysis*

The X-ray powder diffraction spectra of unsupported and supported TiO_2 were obtained using Shimadzu XRD-6000 powder diffractometer, where Ni-filtered Cu target Kα-ray (operating at 40 kV and 30 mA, $\lambda = 0.15418$ nm) was used as the X-ray source. The sample was grinded into fine powder and a thin layer was prepared on a metal slide. The sample was placed in a sample holder inside the diffractometer and adjusted the divergence and convergence slit width according to scanning range of 2θ before scanning. The scatter slit width was always fixed at 1 mm for all scanning range. The scanning ranges 2θ = 1.5 to 10°, 5 to 50°, 10 to 80° were used to determine peak characteristics of MCM-41, β-zeolite, Al-pillared montmorillonite and TiO_2 (both supported and unsupported catalysts), respectively. Scanning speed was maintained at 2º per min for all diffraction spectra. For the measurement of low angle peak of MCM-41 and montmorillonite at 2θ = 1.5 to 10°, divergence slit 0.05 mm, and receiving slit 0.15 mm was used. Scanning range of 2θ = 5 to 50°, divergence (0.5 mm), receiving (0.3 mm) slit width were used for pure and TiO_2 supported on β-zeolite. The high angle analysis (2θ = 10 to 80°) was performed for supported and bare TiO_2 and pure Al-pillared

montmorillonite with divergence and receiving slit width of 1 mm and 0.3 mm, respectively.

3.3.3 XPS Analysis

Surface analysis of the supported and unsupported TiO_2 catalysts was carried by X-ray photoelectron spectroscopy (XPS) using high performance Kratos Axis analytical instrument HSI ESCA (electron spectroscopy for chemical analysis). The fine powder of sample was irradiated with mono-energetic soft X-ray and the energy of detected electrons was analyzed. Al Kα (1486.6 eV) X-rays were usually used. Binding energies (BE) for all elements in the sample were calibrated relative to carbon impurity with a C1s band at 248.7 eV. Prior to the XPS study all samples were evacuated in a pretreatment chamber ($P \sim 10^{-3}$ Torr) at room temperature for 1 h and then introduced into the main chamber for XPS measurements.

3.3.4 SEM/ EDX Analysis

Microscopic feature of the supported and unsupported catalysts was obtained from scanning electron microscopy (SEM, JEOL JSM-5600LV). Fine catalyst powder was supported on carbon tape and coated with platinum. Elemental analysis was performed with EDX (energy-dispersive X-ray spectroscopy) with the scanning electron microscope using a silicon detector operating at an accelerating voltage of 15 kV and a beam current of 1.0 mA under vacuum at 10^{-6}–10^{-7} mbar.

3.4 Experimental Details of Batch Adsorption and Photocatalysis

The photocatalytic degradation efficiency of different compositions of TiO_2 loaded MCM-41, MCM-41, Al-pillared montmorillonite, β-zeolite and bare TiO_2 was investigated in aqueous suspension of the catalysts.

3.4.1 Experimental Setup

Batch adsorption of orange II by TiO_2 supported on MCM-41, Al-pillared montmorillonite and β-zeolite was performed in a covered glass beaker fitted with a magnetic stirrer.

The photocatalytic degradation of orange II in catalyst suspension was performed in a semi-batch swirl-flow reactor (Figure 3.1a) (Mehrotra et al., 2003). The apparatus was mainly comprised of photocatalytic reactor, reservoir UV lamp, peristaltic pump, water bath. The semi batch reactor was made of two circular pyrex plates, which are separated by stainless steel cylinder coupled with soft rubber padding, and was covered by aluminum casing (Figure 3.1b). The volume of the reactor used was 63.5 ml. The reaction solution was introduced tangentially into the reactor from a reservoir (volume = 250 ml) through a peristaltic pump. Magnetic stirrer was used to mix the solution in the reservoir. The solution exited from the center of the top of the reactor and returned to the reservoir through silicone tube. The tangential introduction of the solution produced a swirl flow to mix the solution well. The temperature of the reservoir was maintained at 25 ºC through a water jacket surrounding it connected to the waterbath by tubing. A high-pressure mercury vapor lamp (Phillips HPR 125W) with a wavelength of 365 nm and incident light

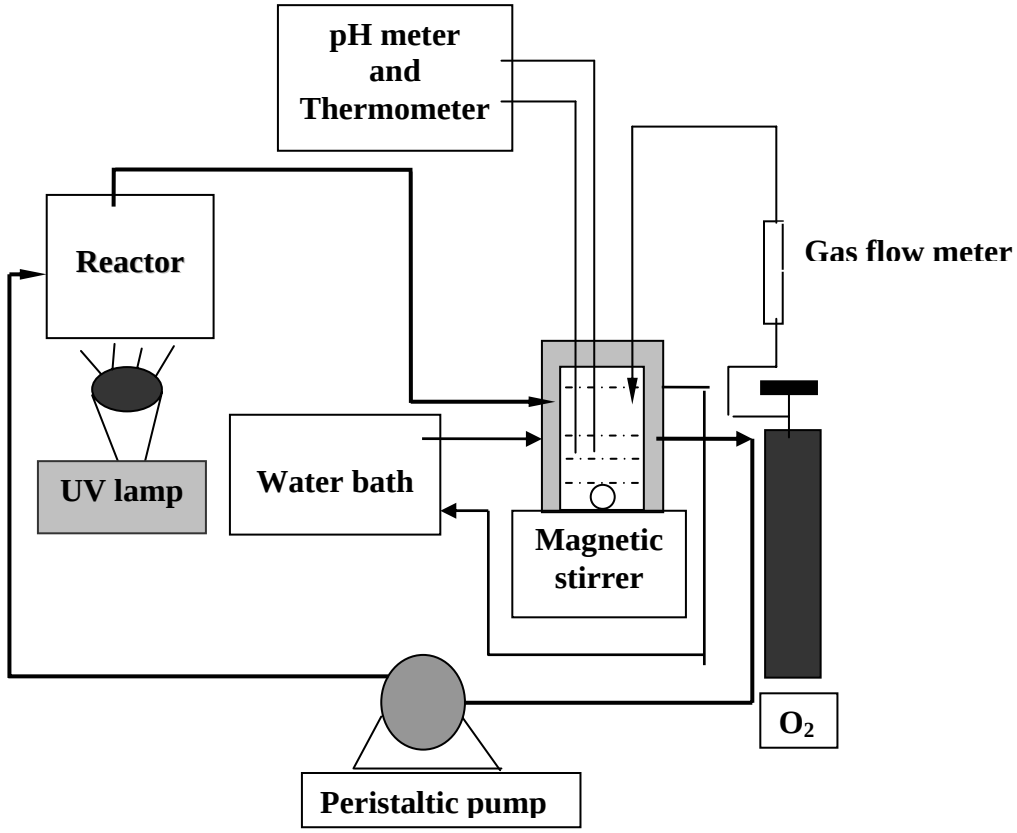

(a)

(b)

Figure 3.1. Schematic diagram (a) and photograph (b) of the experimental set-up.

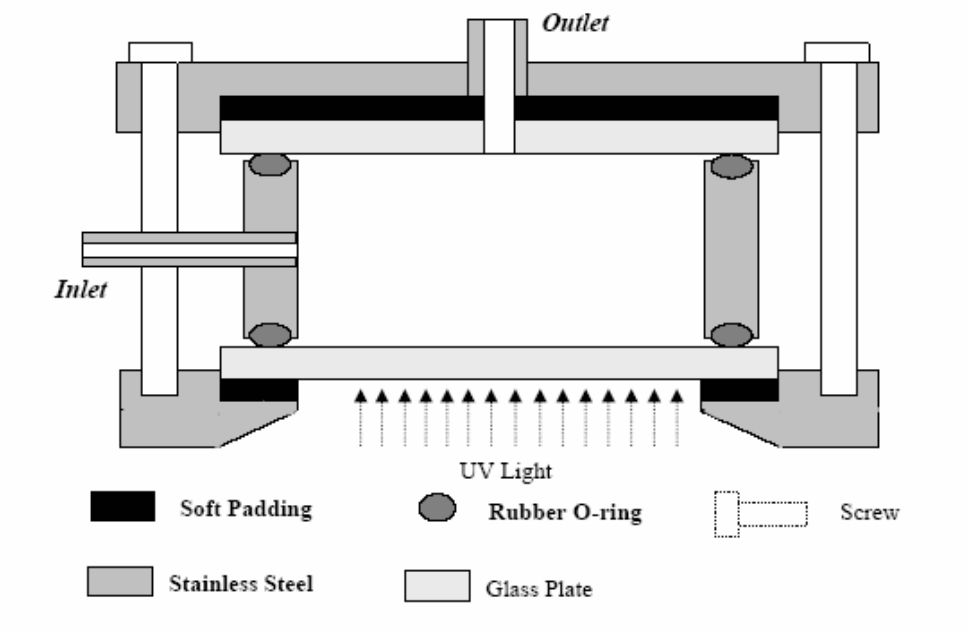

(a)

(b)

Figure 3.2. An illustration (a) and photograph (b) of the swirl flow photocatalytic reactor.

intensity of 213 W/m^2 was used as the UV-light source. The lamp was placed about 0.1 m underneath the bottom glass plate of the reactor on a holder. The light intensity was measured by a digital radiometer (model UVX-36; UVP). The lamp and reactor assemble was placed inside a wooden box painted black so that no stray light can enter the reactor. The lamp was constantly cooled by compressed air to keep the temperature down, thereby protecting the lamp from overheating.

3.4.2 Experimental Procedure

Batch adsorption of orange II by TiO_2 supported on MCM-41, Al-pillared was conducted at different initial concentrations of orange II ranging from 30 -1000 ppm and different catalyst amounts (0.25, 0.5 and 1.0 g/l) under natural pH condition. A total volume of 250 ml of orange II solution was used in the adsorption studies. In all experiments, ultrapure water (Milli Q plus 185, ultra pure water system) was used to make the solution.

In case of photoctalytic experiments, the required amount of catalyst was added in suspension to the aqueous solution of orange II into the reservoir. Although most of the photodegradation experiments were performed at 50 ppm initial concentration of orange II, several experiments were conducted by varying initial substrate concentration of 20 to 250 ppm. The pH of the solution was monitored continuously. While most of the experiments were conducted at natural pH (about 5), in some experiments initial pH was varied from 3-7 using 1 M HCl and 1 M NaOH. Before irradiating the solution with UV light, it was circulated through the reactor in dark for 1-2 hours to ensure that adsorption equilibrium of orange II had been reached. During each run, samples were taken from the

reservoir at suitable time intervals. All samples were filtered with syringe driven Millex Millipore filter (0.1 μm) to remove the catalyst before analysis.

Samples of orange II were analyzed using UV-visible spectrophotometer (Shimadzu UV-1601). Total organic carbon (TOC) was measured by Shimadzu TOC analyzer (5000A, Shimadzu) with ASI-500 autosampler to measure the extent of mineralization under different conditions. Samples of orange II collected during photooxidation were also scanned through UV-visible spectrophotometer (Shimadzu UV-1601) to identify the peaks of the intermediates formed during photodegradation.

CHAPTER 4
RESULTS AND DISCUSSIONS

4.1 Characterization of Catalysts

4.1.1 N_2-sorption and BET Analysis:

The pore diameter, pore volume and specific surface area of the supported catalysts were obtained from nitrogen adsorption/desorption isotherm and multipoint BET analysis (Sing et al., 1985). Nitrogen adsorption and desorption isotherm of pure MCM-41 exhibits a steep inflection at P/P_0 = 0.25-0.31 and reversible type IV isotherm (Figure 4.1a) with a small hysteresis loop (Kresge et al., 1992; Schmidt et al., 1995). Isotherms of pure MCM-41 and 10, 25, 50, 60, and 80% TiO_2 loaded MCM-41 show sharp steep capillary condensation in mesopore region at (P/P_0 = 0.25-0.31), suggesting a narrow pore size distribution. Adsorption at low pressure (P/P_0 < 0.25) is due to mono-multilayer adsorption of N_2 on the wall of mesopore. The BJH desorption Dv (d) curve of MCM-41 as well as TiO_2 loaded MCM-41 showed a narrow pore size distribution. The BJH pore size distribution of 50 (wt %) TiO_2 loaded on MCM-41 is shown in Figure A.1.1a (appendix).

According to BDDT (Brunauer, Deming, Deming and Teller) classification (Brunauer et al.,1940) pure and TiO_2 supported Al-pillared montmorillonite (Figure 4.1b) both exhibited type IV isotherm with a well defined hysteresis loop which is quite similar with previous study on Al-pillared montmorillonite. (Salerno and Mendioroz, 2002). The amount of N_2 sorbed on the pillared clays was much higher than that of raw clays

implying that porous structure was developed by pillaring. (Ooka et al., 1999; Shmizu et al., 2002). This shape of isotherm implies mono-multilayer adsorption on slit shaped pores among plate like particles. It also indicates that both supported and unsupported montmorillonite might contain both micro and mesopores (Ooka et al., 1999).

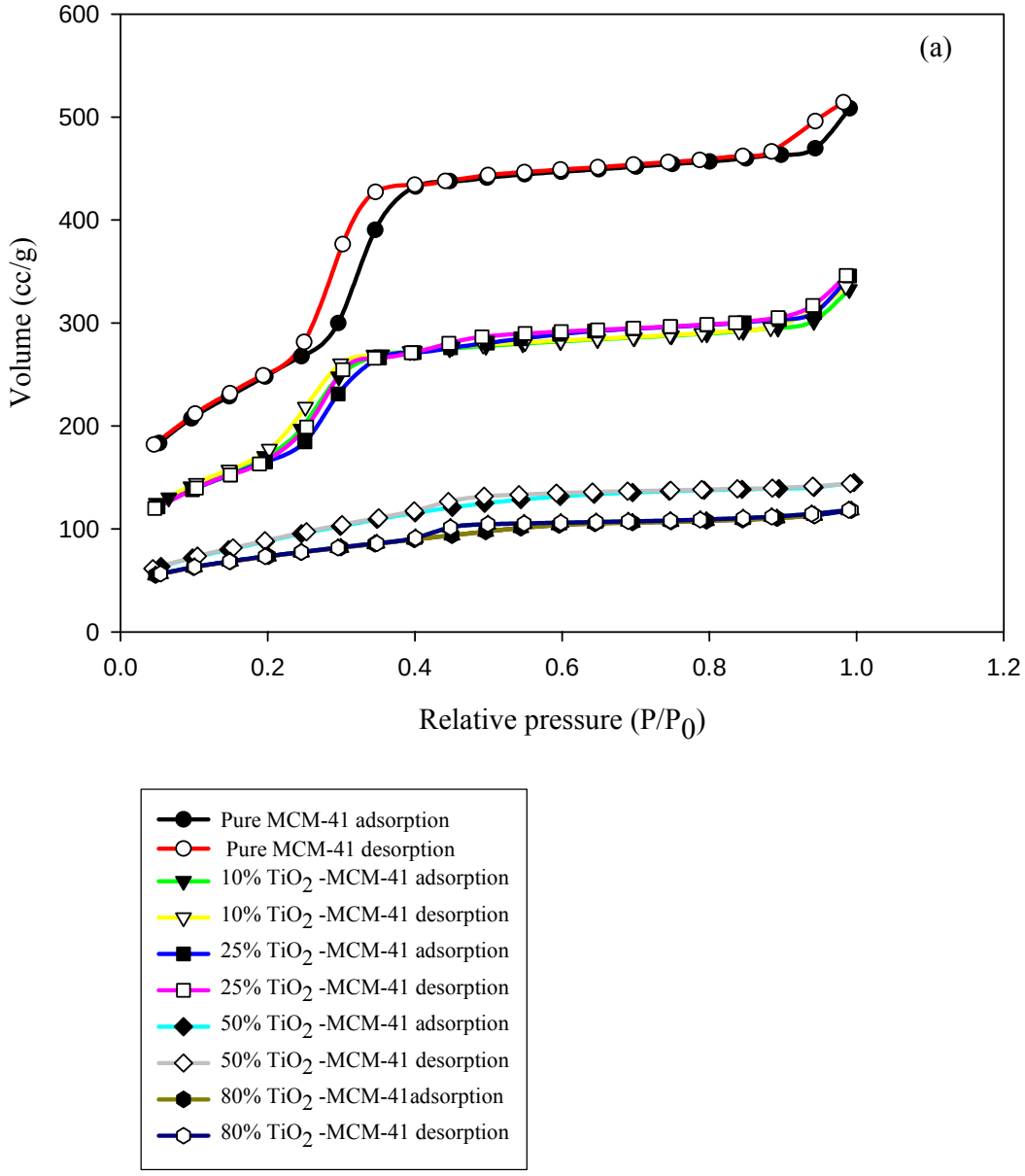

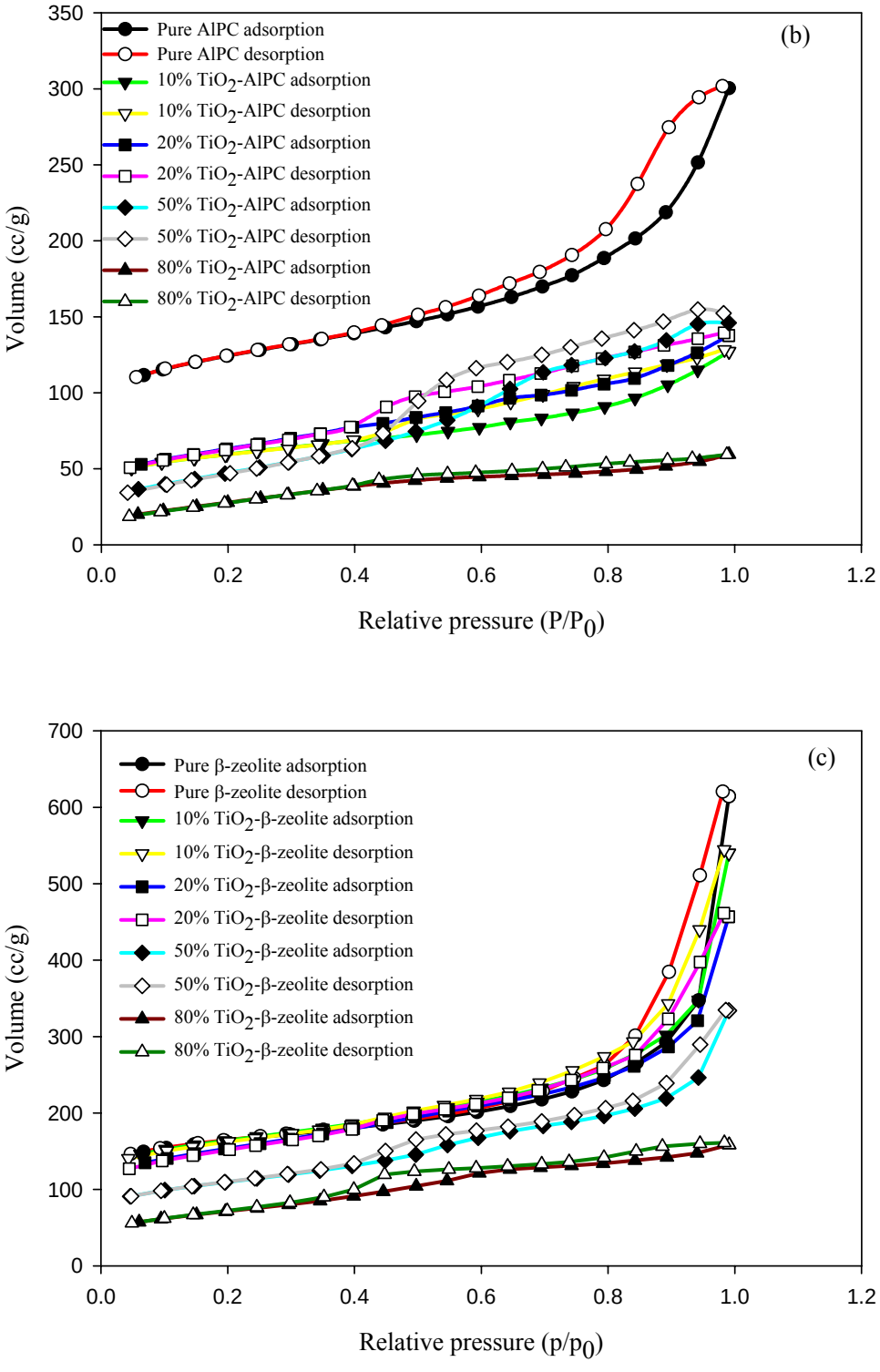

Figure 4.1. N_2 adsorption-desorption isotherms of MCM-41, Al-pillared montmorillonite (AlPC), β-zeolite and supported TiO_2 (wt %) (a, b, c) (calcined at 300 ºC).

Steep characteristic of the curve at higher pressure region during adsorption and prominent hysteresis suggested the increase of mesoporosity in the montmorillonite (Han and Yamanaka, 1998). It was found from BJH pore size distribution that pure and TiO_2 supported montmorillonite with different TiO_2 (wt %) loading exhibited pore size distribution with maximums around 3.7 to 4 nm range. At lower loading, it is suggested that Al-pillared montmorillonite contain two types of pore size aggregates (Salerno and Mendioroz, 2002) of interlayer pores. But at higher loading pores might be only due to mesopores. Pore diameter of pure montmorillonite was about 0.74 nm whereas different TiO_2 (wt %) loaded montmorillonite was about 1.4 to 4 nm. The BJH pore size distribution of 50 (wt %) TiO_2 loaded on Al-pillared montmorillonite is shown in Figure A.1.1b (appendix).

Nitrogen adsorption desorption isotherms with hysteresis loop were obtained for pure and TiO_2 supported β-zeolite (Figure 4.1c). The steep rise of the adsorbed volume (V) at very low P/P_0, followed by a plateau for P/P_0 values approximately between 0.05 and 0.5 indicated characteristic of microporous behavior. However, the presence of a hysteresis loop at relative pressure P/P_0 higher than 0.45 in the adsorption–desorption curves suggested typical presence of mesopores (Ferino et al., 2003). Most likely, mesoporosity of pure and TiO_2 supported β-zeolites is related to the intercrystalline voids resulting from agglomeration of the very small crystallites of β-zeolites (Coutanceau et al., 1997). Pore diameter of pure β-zeolite calculated from BJH method was approximately 0.74 nm. The BJH pore size distribution of 50 (wt %) TiO_2 loaded on β-zeolite is shown in Figure A.1.1c (appendix).

For all catalysts calcined at 300 ºC, with increasing loading (wt %) of TiO_2, surface area of the supported catalysts on MCM-41, montmorillonite and β-zeolite decreased as shown in Figure 4.2. The decrease in surface area is observed to be non-linear to the loading of TiO_2, indicating the adsorbent-TiO_2 is simply not a mechanical mixture, rather titania has been dispersed inside the supports and causes partial blockage of the pores. Significant changes in the pore volume, especially for montmorillonite may suggest that TiO_2 was deposited inside the pores of the support (Figure 4.3). The pore diameter of the TiO_2 supported MCM-41, montmorillonite and β-zeolite, varies from 2.41-1.42 nm, 0.74-2.7nm and 0.75-1.7 nm, respectively with TiO_2 (wt %) loading varying from 10-80% (Table A.1.1) (appendix). But pore diameter of TiO_2 (wt %) loaded on MCM-41 remained constant whereas pore diameter of TiO_2 (wt %) loaded on Al-pillared montmorillonite and β-zeolite increased with the increasing loading (wt %) of TiO_2 on the support. The observed differences in pore diameter do not follow any specific trend, which indicates a random nature of dispersion of TiO_2 on the support.

The BET surface areas of the unsupported TiO_2 (160 m^2/g) and commercial TiO_2 (Degussa-P25, 48 m^2/g) were much lower than that of the supported TiO_2. It was also found that with increasing calcination temperature from 300 to 750 ºC surface area of the supported (50 wt %) TiO_2 catalysts (Table 4.1) decreased. This might be due to the increase in the particle size of TiO_2 on the surface which was confirmed later by XRD analysis.

Table 4.1 BET surface area of 50 (wt %) TiO_2 supported on MCM-41, Al-pillared montmorillonite (AlPC) and β-zeolite at different calcination temperatures.

BET surface area (m^2/g)			
Calcination temperature	**MCM-41**	**AlPC** [a]	**β-zeolite**
300 ºC	527	243	357
450 ºC	513	150	352
600 ºC	487	145	349
750 ºC	374	104	246

[a] represents Al-pillared montmorillonite.

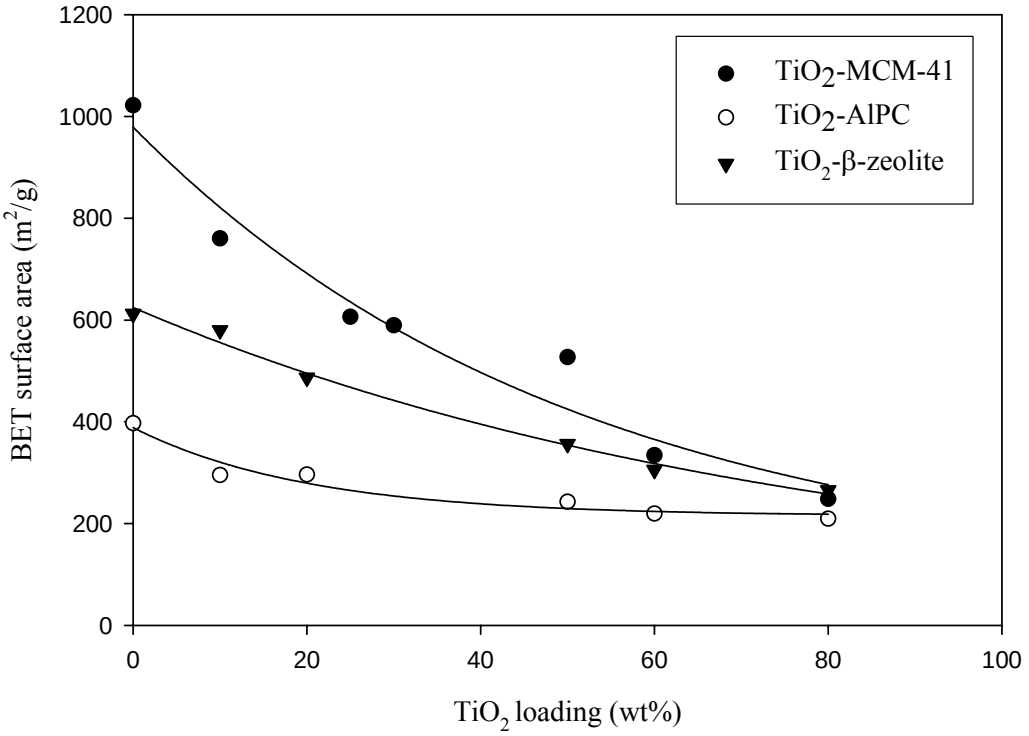

Figure 4.2. BET surface area vs. TiO_2 (wt %) loading on MCM-41, Al-pillared montmorillonite (AlPC) and β-zeolite (calcined at 300 ºC).

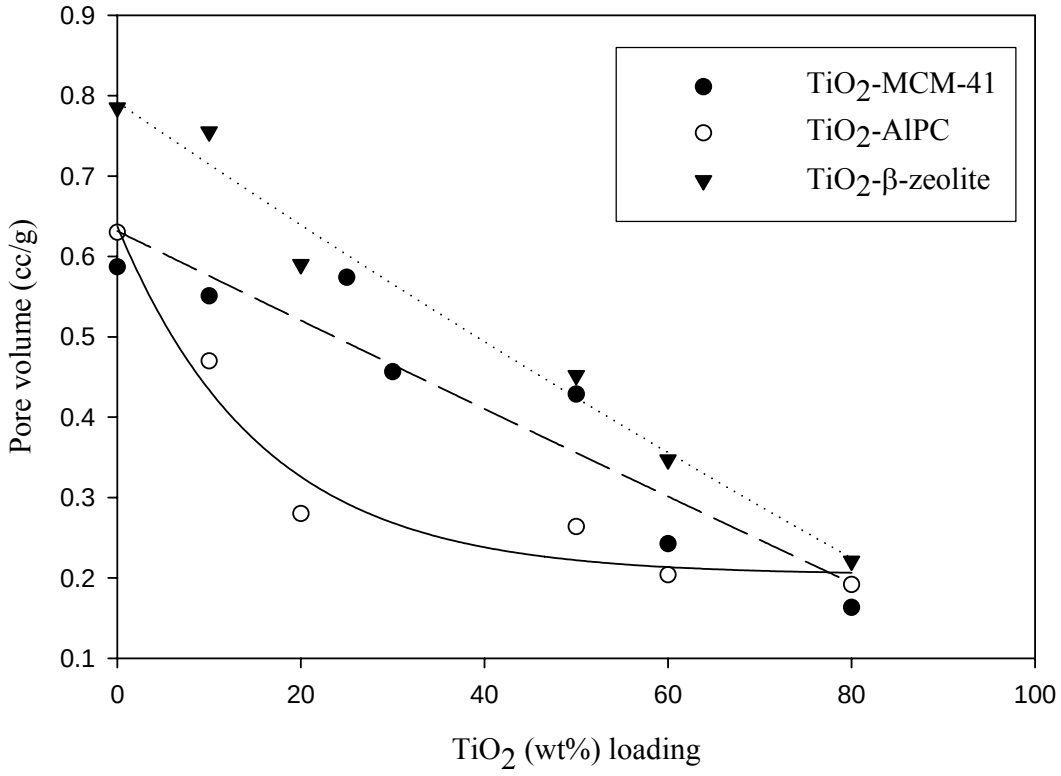

Figure 4.3. Pore volume vs. TiO_2 (wt %) loading on MCM-41, Al-pillared montmorillonite (AlPC) and β-zeolite (calcined at 300 ºC).

4.1.2 XRD Analysis:

X-ray powder diffraction method was used to assess the crystallinity of the supported catalysts. XRD diffraction peak of pure MCM-41 (Figure 4.4a) sample at low angle region ($2\theta = 2.2°$) corresponding to (100) lattice plane could be seen (Beck et al., 1992). The intensity of the (100) peak of MCM-41 decreases with increasing TiO_2 (wt %) loading. Pure Al-pillared montmorillonite showed a d_{001} peak around 4.6º corresponding to basal spacing about 1.7 to1.8 nm (Figure 4.4b) which is comparable with literature (Occelli, 1986; Tanguay et al., 1989; Malla et al., 1989; Yamanaka et al., 1990; Salerno and

Mendioroz, 2002). β-zeolite also exhibited two characteristic peaks at 7.7 and 22.5º respectively (Figure 4.4c).

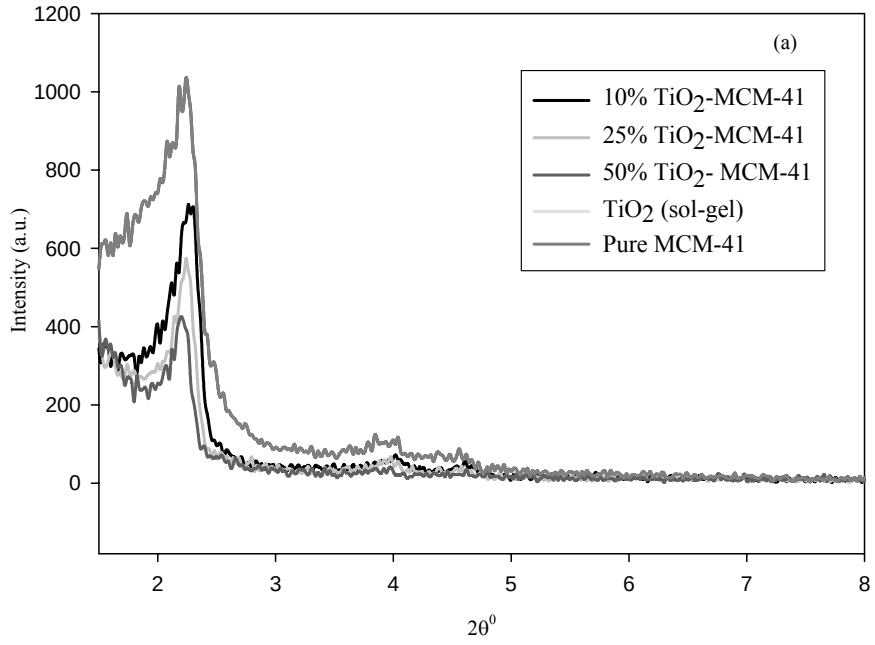

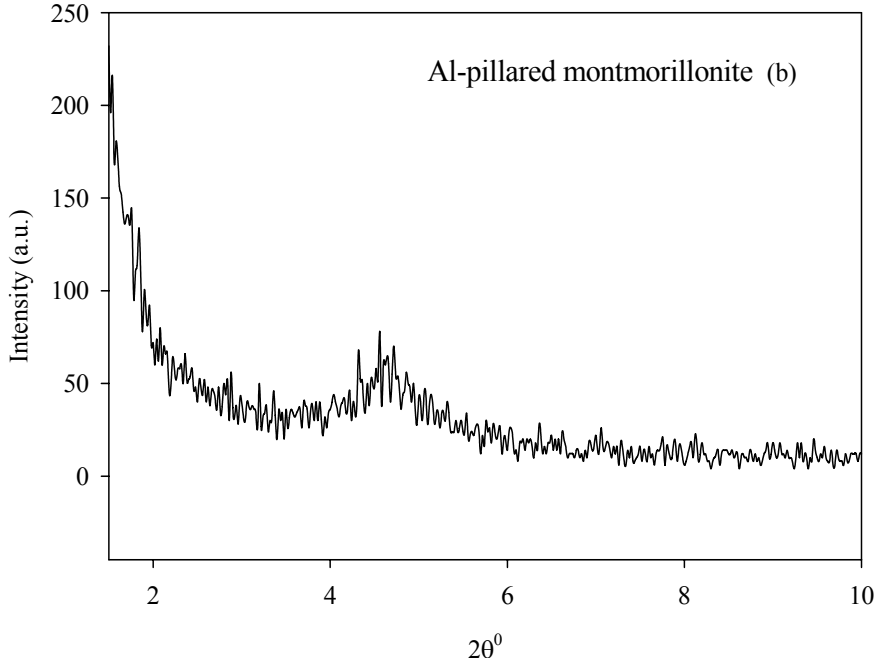

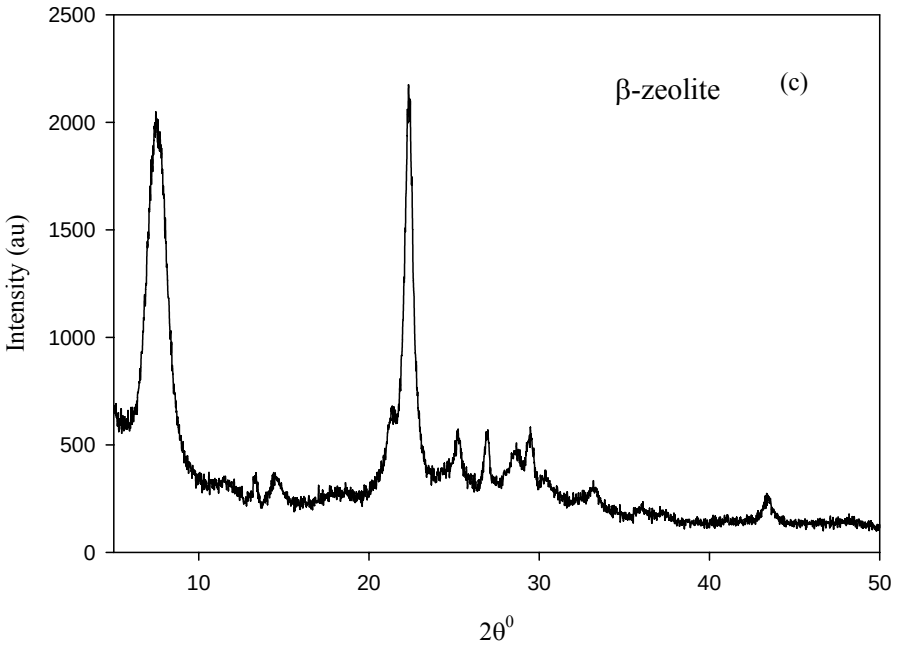

Figure 4.4. XRD spectra of pure MCM-41 (a), montmorillonite (AlPC) (b) and β-zeolite (c).

XRD peaks, characteristic of anatase were observed at 2θ = 25.3° corresponding to (101) orientation (Liqiang et al., 2003) for both bare and supported TiO_2 on MCM-41, montmorillonite and β-zeolite (Figure 4.5). Peaks corresponding to anatase TiO_2 were also appeared at 2θ = 37.8, 48.3, 54.8° with the broader peaks for supported TiO_2 as can be seen in Figure 4.5. No significant peak of rutile was observed at 2θ = 27.42°, although small peaks at 54.5° could be observed in some cases. As expected, with increasing TiO_2 (wt %) loading, sharper peaks of TiO_2 were observed due to increased crystalline feature of TiO_2 (Figure 4.5 a-c). Bare TiO_2 exhibits sharp peak characteristic indicating well defined crystal of TiO_2 (shown in Figure 4.5d).

Low intensity and broad peak characteristic of XRD spectrum of supported TiO_2 on MCM-41 and β-zeolite compared to that of bare TiO_2 indicate that highly dispersed fine

crystallites of anatase TiO_2 were formed on these supports. On the other hand, XRD spectrum of TiO_2 supported on montmorillonite displays sharper TiO_2 peaks, indicating relatively larger TiO_2 crystallites formed on montmorillonite. The nano particles could not be observed as ideal crystals with discrete crystal faces due to fine crystallite size, which was confirmed by the SEM analysis later.

The XRD patterns of TiO_2 supported on MCM-41, Al-pillared montmorillonite and β-zeolite prepared by sol-gel method and calcined at different temperatures are presented in Figure A.1.2 (appendix). The relative peak intensities of the (101) anatase crystallographic plane increased with the increase in calcination temperature suggesting that the crystallinity is improved. Sharp diffraction spectrum indicates that crystallite size of anatase also increased with increasing calcination temperature. The primary anatase crystallite size at different calcination 300-750 ºC was calculated on the (101) diffraction peaks using Scherrer's equation (Zhang et al., 2000) (assuming no crystal distortion in lattice), presented in Table 4.2.

Scherrer's Equation is represented by

$$L = \frac{K\lambda}{\beta \cos\theta} \qquad (4.1)$$

Where L is crystallite size, λ is the wavelength of the X-ray radiation (Cu Kα = 0.15418 nm), K is usually taken as 0.89 and β is the line width at half maximum height, after subtraction of equipment broadening. Scherrer equation is not very reliable methods for accurate determination of particle size however, it can provide approximate anatase crystallites size of the supported catalysts.

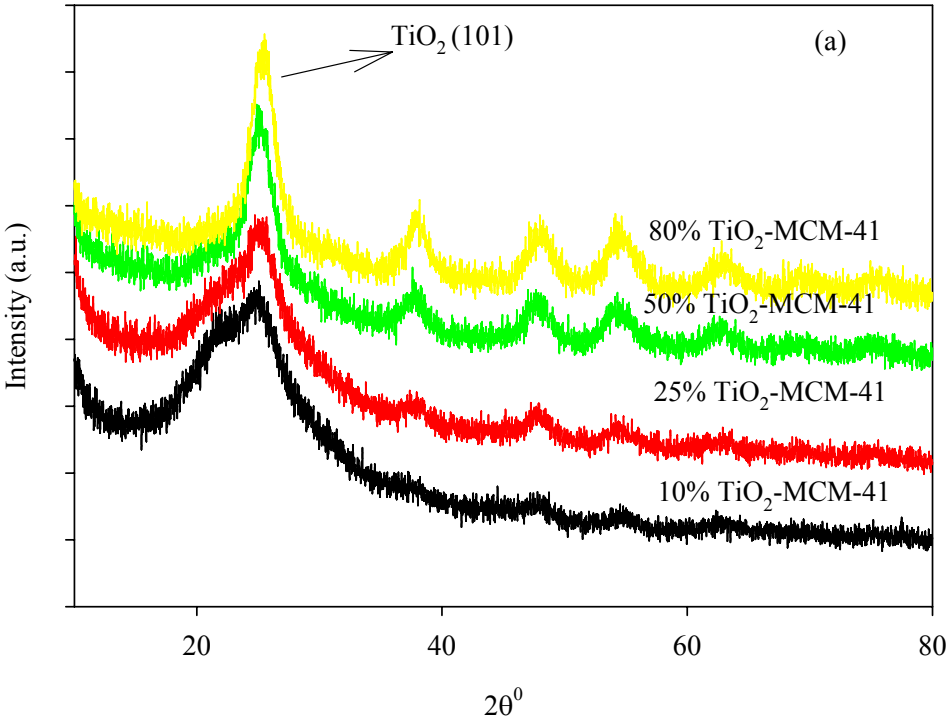
TiO2 (101)
(a)
80% TiO2-MCM-41
50% TiO2-MCM-41
25% TiO2-MCM-41
10% TiO2-MCM-41
Intensity (a.u.)
20
40
60
80
2θ0

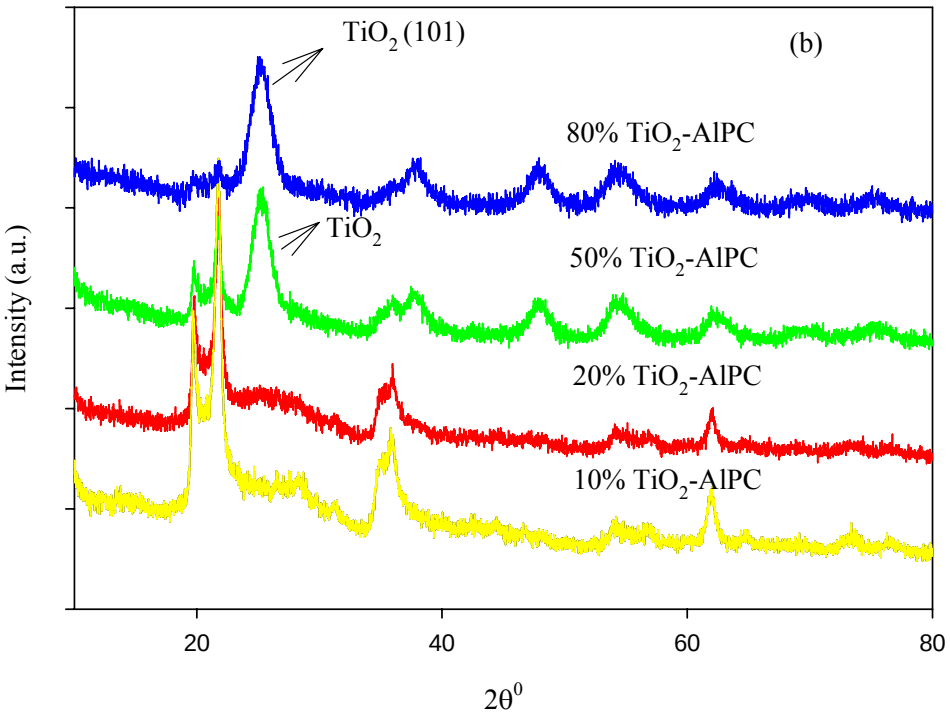
TiO2 (101)
(b)
80% TiO2-AlPC
TiO2
50% TiO2-AlPC
20% TiO2-AlPC
10% TiO2-AlPC
Intensity (a.u.)
20
40
60
80
2θ0

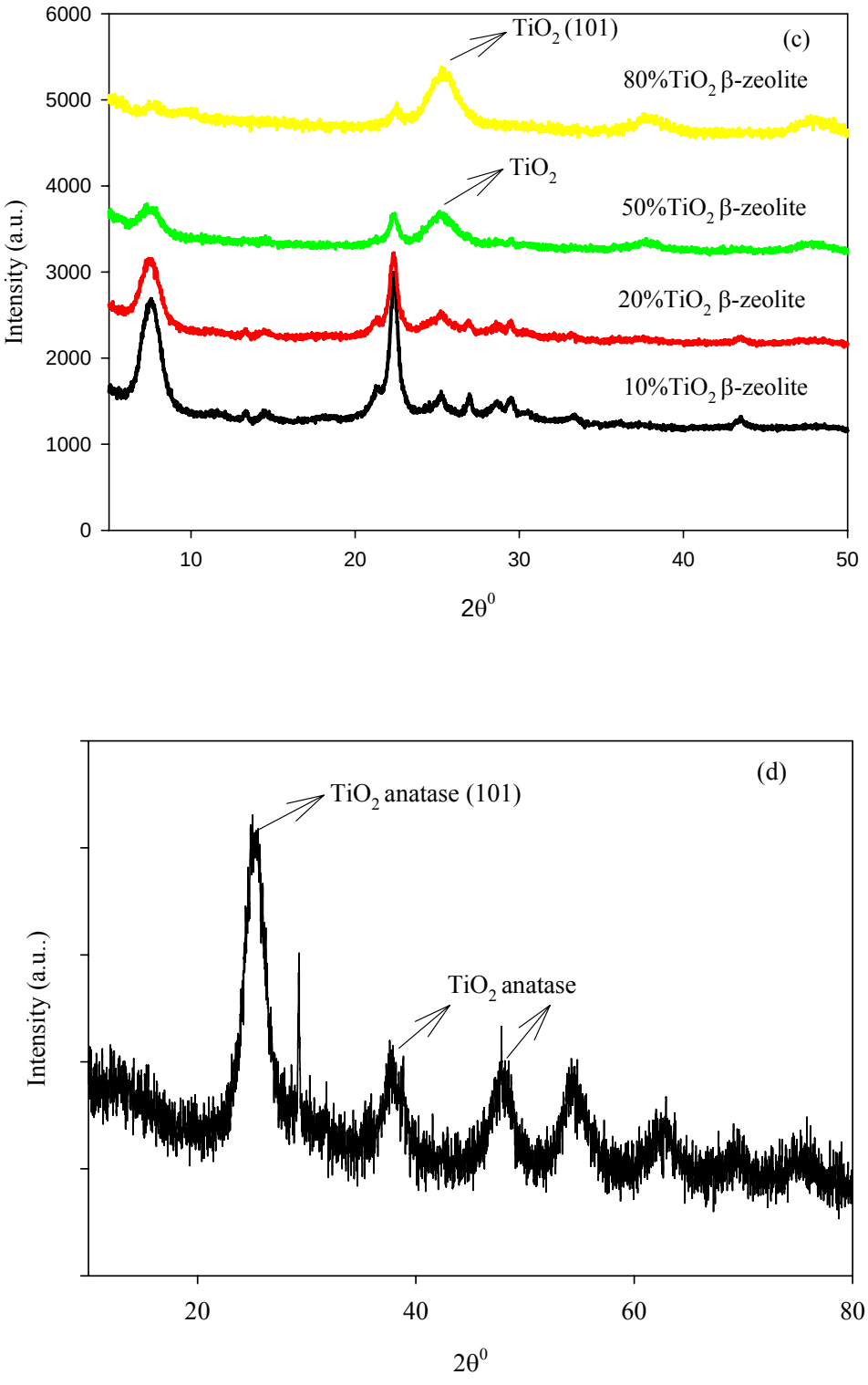

Figure 4.5. XRD pattern of TiO_2 (wt %) loaded on MCM-41 (a), Al-pillared montmorillonite (AlPC) (b), β-zeolite (c) and TiO_2 (sol-gel) (d) (calcined at 300 ºC).

Table 4.2 Crystallite size of TiO_2 calculated using Scherrer's Equation.

Catalyst	300 ºC	450 ºC	600 ºC	750 ºC
50% TiO_2-MCM-41	2.4 nm	6.2 nm	7.4 nm	21.2 nm
50% TiO_2-AlPC [a]	5.6 nm	12.8nm	15.6 nm	20.7 nm
50% TiO_2-β-zeolite	5.5 nm	6.8nm	11.8 nm	17.8 nm

[a] represents Al-pillared montmorillonite.

4.1.3 XPS Analysis

The surface composition and chemical elementary state of the supported catalysts were determined using X-ray Photoelectron Spectroscopy. The relative peak intensity of Ti (2p) core level increased with increasing loading (wt %) of TiO_2, indicating greater coverage of the support surface by Ti on MCM-41, Al-pillared montmorillonite and β-zeolite. As expected, the XPS peak intensity of Si decreased with the increase in the TiO_2 loading. In this section, TiO_2-MCM-41 was used as representative among all three supported catalysts and XPS spectra of different elements of TiO_2 supported on MCM-41 shown in Figure 4.6. The binding energies of Ti (2p) of all three supported catalysts presented in Table 4.3 are essentially similar, which imply that Ti element for all the prepared catalysts exhibits similar state of oxidation and chemical environment. The binding energies of all the elements are in good agreement with the reported values (Anpo et al., 1986; Blasco et al, 1994; Reddy et al., 2001 and Yasuyuki and Ayame, 2001). Comparing the reported binding energies, the oxidation state of Ti corresponds to both tetrahedral and octahedral coordinated Ti.

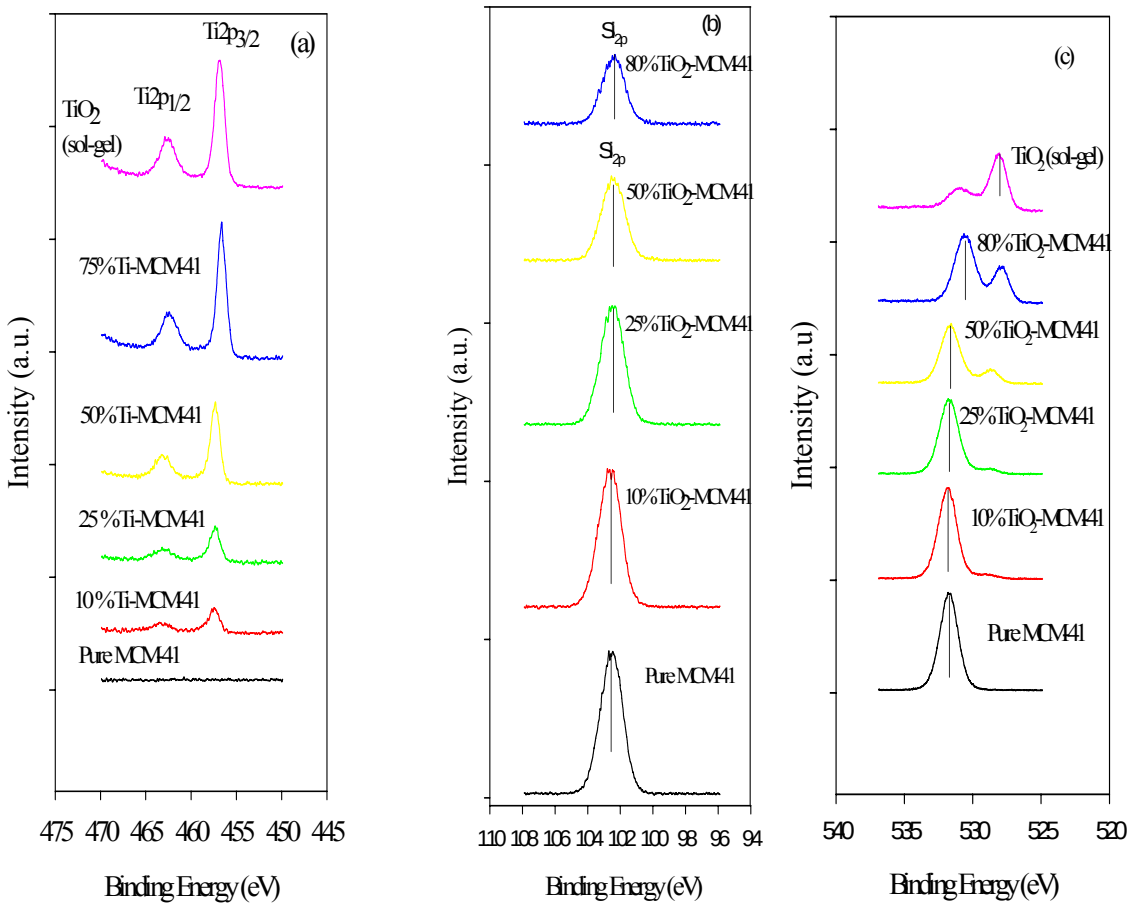

Figure 4.6. XPS spectra of Ti (2p) (a), Si (2p) (b), and O (1s) (c) of different TiO_2 loaded MCM-41 (calcined at 300 ºC) and pure MCM-41.

Table 4.3 Binding energy of different elements present in pure adsorbents and supported TiO_2 catalysts.

Catalyst	Ti (2p) (eV)	Si (2p) (eV)	O (1s) (eV)	Al (2p) (eV)
Pure MCM-41		103.3	532.3	
Pure AlPC [a]		103.2	531.9	74.8
Pure β-zeolite		103.3	531.9	73.9
10% TiO_2-MCM-41	458.5	103.1	532.0	
25% TiO_2-MCM-41	458.5	102.9	532.4	
50% TiO_2-MCM-41	458.6	103.1	532.0	
80% TiO_2-MCM-41	458.7	102.5	531.8	
10%TiO_2-AlPC [a]	458.5	102.8	531.9	74.4
20% TiO_2-AlPC [a]	458.5	102.7	531.9	74.7
50%TiO_2-AlPC [a]	458.7	102.3	531.3	73.9
80%TiO_2-AlPC [a]	458.5	102.1	532.1	75.0
10% TiO_2-β-zeolite	458.7	102.9	532.6	73.5
20% TiO_2-β-zeolite	458.5	102.8	532.8	73.6
50% TiO_2-β-zeolite	458.6	102.4	532.6	73.7
80% TiO_2-β-zeolite	458.7	102.3	529.5	73.3
TiO_2 (sol-gel)	458.9		527.6	

[a] represents Al-pillared montmorillonite.

4.1.4 SEM-EDX Analysis

Morphology of the supports and the supported catalysts was determined using SEM micrographs. It can be seen from Figure 4.7a that pure MCM-41 did not exhibit well-defined crystalline feature while Al-pillared montmorillonite exhibited layered crystalline structure (Figure 4.7c), and pure β-zeolite shows both spherical and rhombic crystals (Figure 4.7e). SEM-EDX micrographs with 50 (wt %) TiO_2 loading were reported in this section. SEM coupled with EDX microprobe, a semi-quantitative elemental analysis was performed at different locations (six to eight positions) for each sample to identify the presence of Ti in all parts of the samples. Peaks of Ti were clearly observed in all of the locations indicating that Ti was present almost all over the support with uniform dispersion. (Figure 4.7 i, j and k). However, SEM micrographs shown in Figure 4.7 b, d and f did not clearly display the crystallites of TiO_2 indicating the formation of fine particles of TiO_2 on the support. Some agglomeration of the fine particles was observed at all loading of TiO_2. Comparatively bigger crystals were formed for bare TiO_2 prepared by the sol-gel method (Figure 4.7 g). SEM micrographs of other TiO_2 loading (10, 25, 20, 80 wt %) on adsorbent supports were reported in appendix (Figure A.1.3 a-i). It can be seen from the micrograph that 80 (wt %) TiO_2 supported on adsorbents exhibits bigger crystallites than other loading. SEM analysis of 50 (wt %) TiO_2-supported MCM-41, Al-pillared montmorillonite and β-zeolite at different calcination temperature were also performed. However, increasing particle size with increasing calcination temperature was not clearly observed from SEM micrographs.

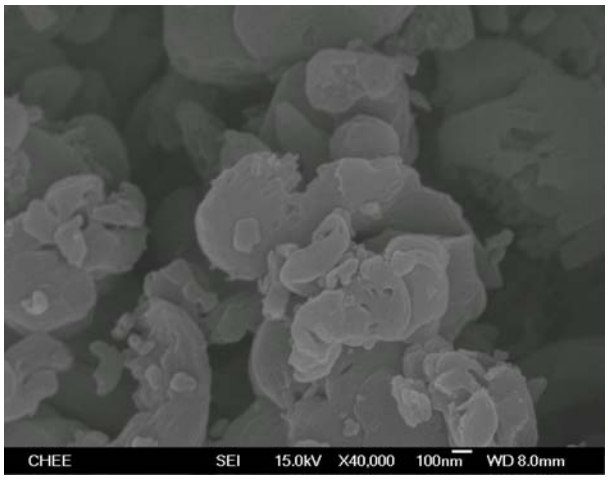

(a) Pure MCM-41

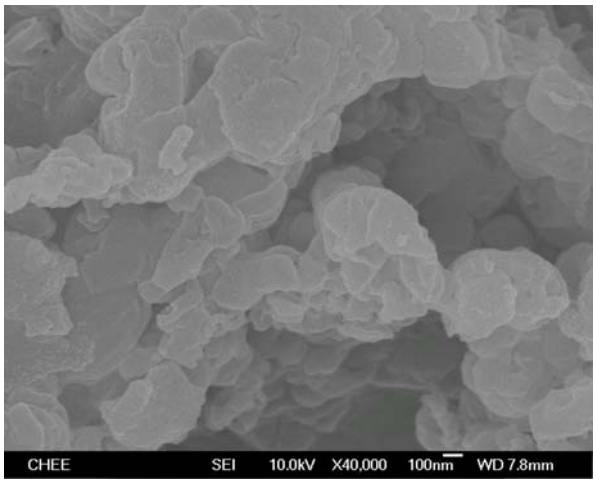

(b) 50% TiO_2-MCM-41

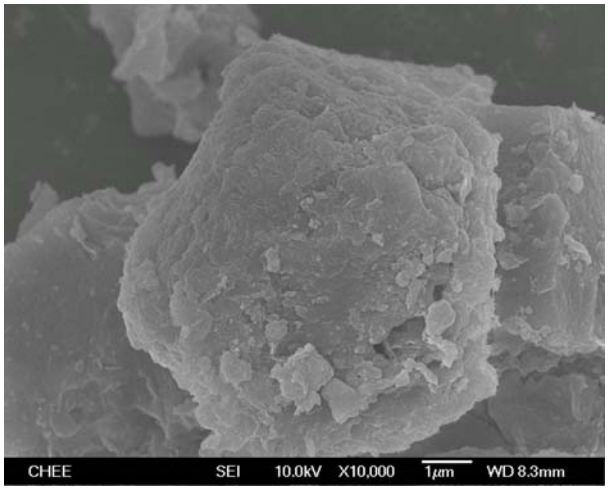

(c) Al-pillared montmorillonite

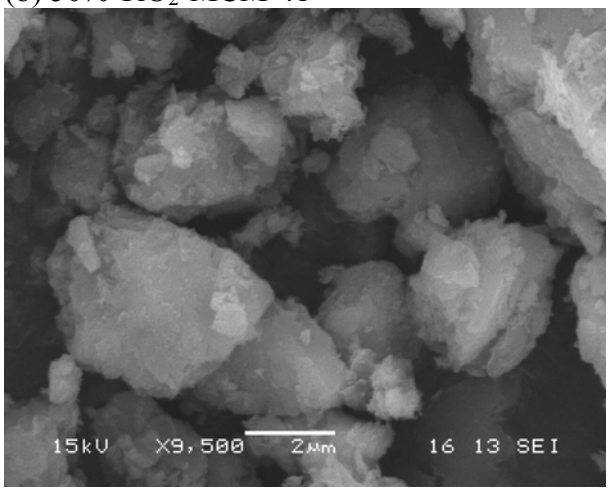

(d) 50% TiO_2-Al-pillared montmorillonite

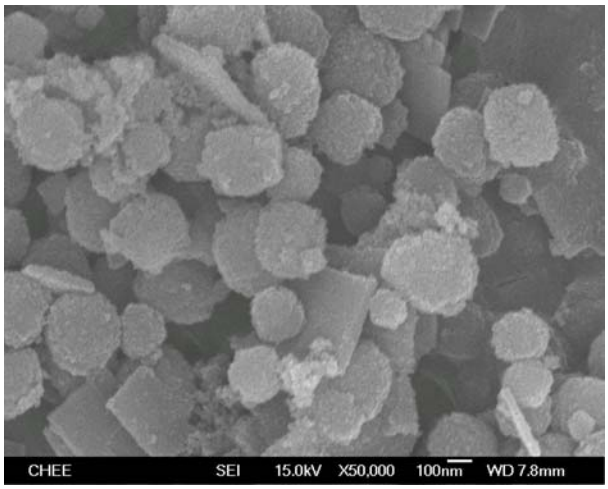

(e) Pure β-zeolite

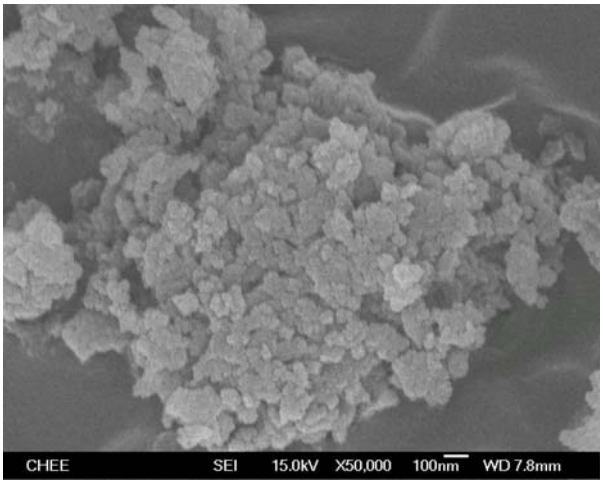

(f) 50% TiO_2-β-zeolite

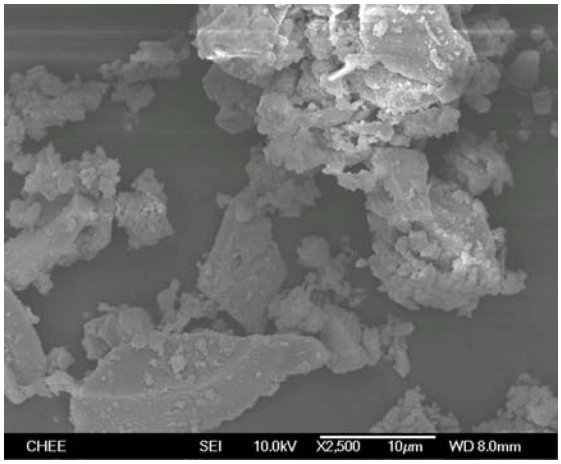

(g) TiO_2 (sol-gel)

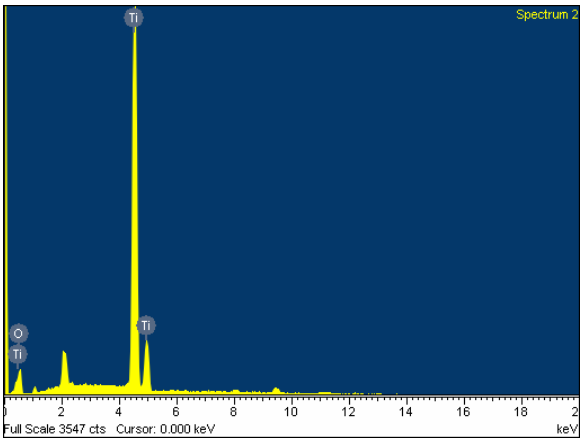

(h) EDX of TiO_2 (sol-gel)

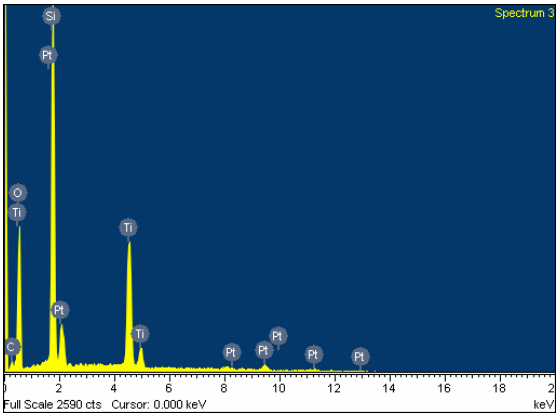

(i) EDX of 50% TiO_2-MCM-41

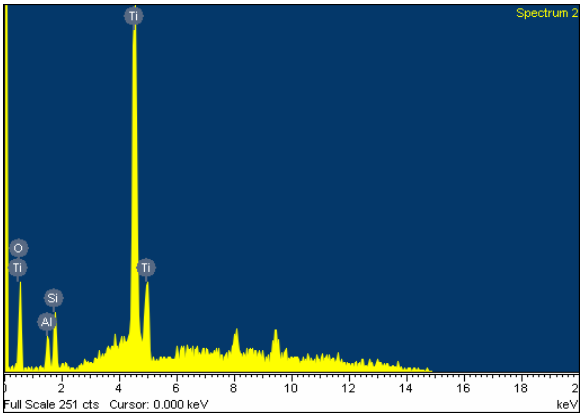

(j) EDX of 50% TiO_2-Al-pillared montmorillonite

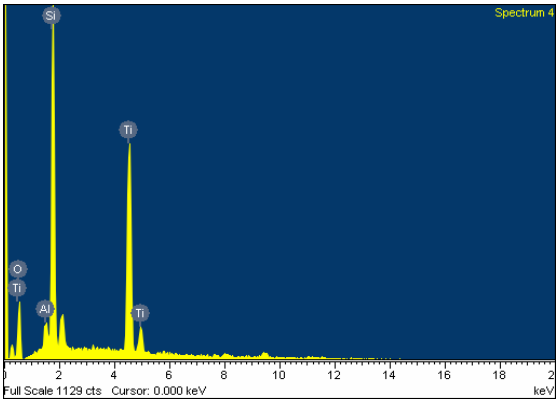

(k) EDX of 50% TiO_2-β-zeolite

Figure 4.7. SEM of pure MCM-41 (a), 50% TiO_2-MCM-41 (b), pure Al-pillared montmorillonite (c), 50% TiO_2-Al-pillared montmorillonite (d), pure β-zeolite (e), 50% TiO_2-β-zeolite (f), TiO_2 (sol-gel) (g), EDX of TiO_2 (sol-gel) (h), 50% TiO_2-MCM-41 (i), 50% TiO_2-Al-pillared montmorillonite (j), 50% TiO_2-β-zeloite (k).

4.2 Batch Adsorption and Photodegradation Study

4.2.1 Adsorption of Orange II

Prior to the photodegradation studies, batch adsorption studies of orange II were conducted using different initial concentrations of the dye and the catalysts. Orange II is an acidic dye, thus shows an interesting adsorption behavior for both pure MCM-41, Al-pillared montmorillonite and β-zeolite and TiO_2 supported on adsorbents. Adsorption isotherm results of orange II for different supported and unsupported catalysts are shown in Figure 4.8, where all the supported catalysts showed very good adsorption characteristics compared to that of bare TiO_2, and Degussa-P25. However, interestingly pristine supports, MCM-41, Al-pillared montmorillonite and β-zeolite with the highest surface areas revealed very poor adsorption behavior for orange II than supported TiO_2. MCM-41 and β-zeolite are mildly acidic in nature whereas montmorillonite is moderately acidic as the pH values of pure MCM-41, β-zeolite and montmorillonite in ultrapure water were approximately 6.96, 6.60 and 5.62 respectively with 0.5 g/l of the individual catalysts in solution. Orange II being slightly acidic, the anion of orange II is subjected to electrostatic repulsion between it and the negative surface of the supports at natural pH.

The acidity of the solution increased with the increased loading (wt %) of TiO_2 on the surface of the supports (Figure 4.9). Free metal ions (Ti^{4+} or Al^{3+}) generated during calcination process of the supported catalysts undergo hydrolysis reaction to produce free H^+ ions in the aqueous solution. The following surface reaction (Sauer et al., 2002 and Guillard et al., 2003) for the supported catalysts is expected to occur below pH 6.8 (pzc of

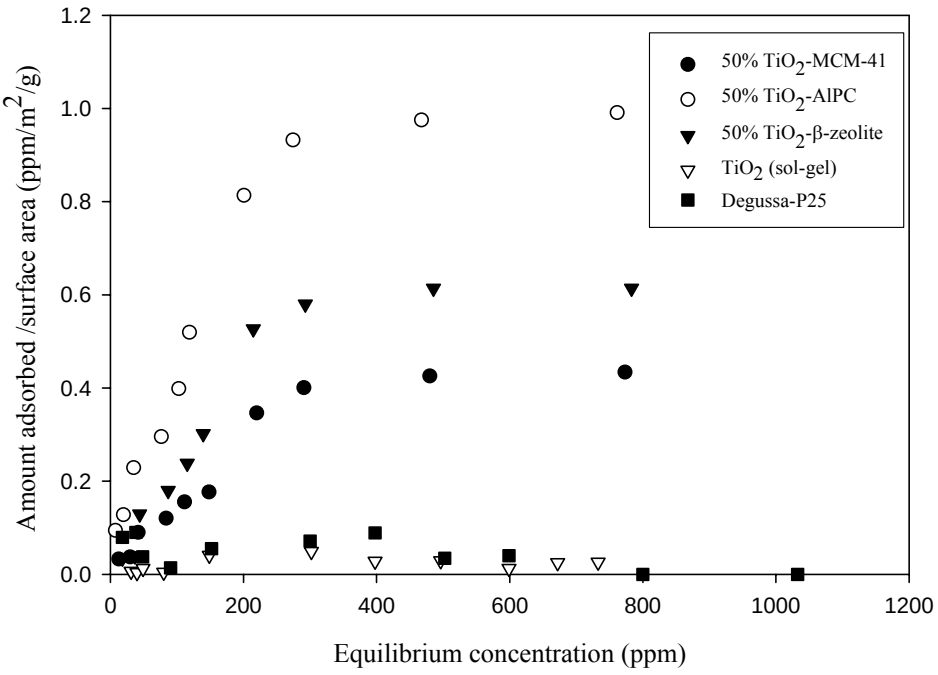

Figure 4.8. Batch adsorption studies of different 50 (wt %) TiO_2-loaded catalysts, Degussa-P25 and TiO_2 prepared by sol-gel (catalyst amount = 0.5 g/l, initial concentration of orange II = 30-1000 ppm, natural pH, calcination temperature = 300°C).

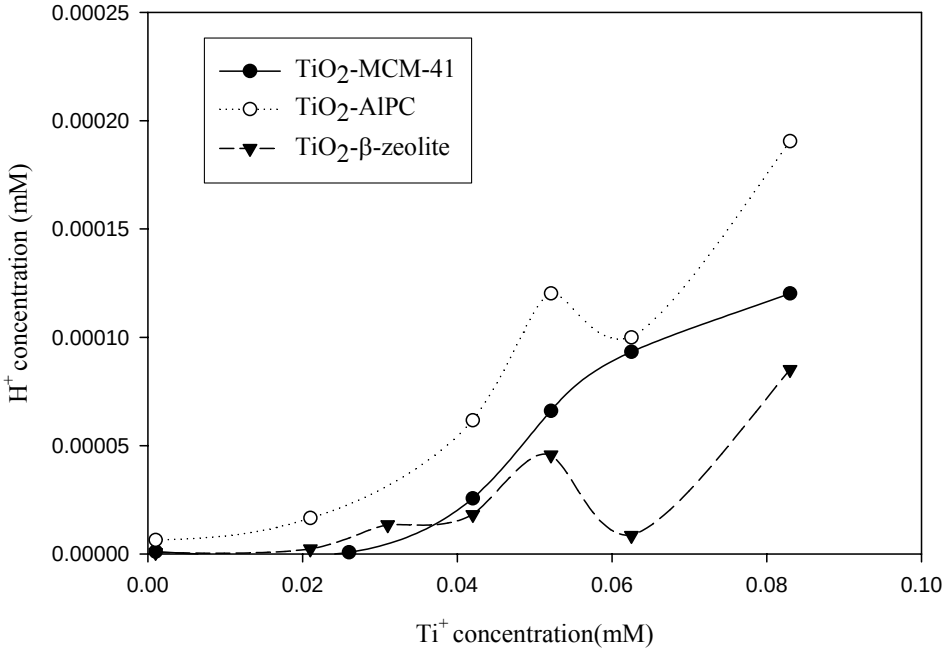

Figure 4.9. H^+ ion concentration vs. Ti^+ ion concentration for different TiO_2 loading on MCM-41, Al-pillared montmorillonite and β-zeolite.

TiO_2) :

$$Ti - OH + H^+ \leftrightarrow TiOH_2^+ \qquad (4.2)$$

(The relevant redox reactions of TiO_2 are provided in Chapter 2, section 2.3 on page 16-17 following Hoffmann et al. 1995). Adsorption increased only with the increasing loading of TiO_2 with maximum adsorption occurring at 50-60 (wt %) loading of TiO_2 (Figure 4.10 a-c). In this case, adsorption of orange II is facilitated due to the electrostatic attraction between anion and positively charged TiO_2 on the surface. Addition of well dispersed TiO_2 reduces the negative surface charge of pure adsorbent supports, while higher surface area of supports contributes to the better adsorption of orange II by supported catalysts. However, with the increased loading of TiO_2 (beyond 50-60 %) the surface area of the catalysts decreases, thus eventually leading to lower adsorption indicating the presence of optimal loading. Incidentally, despite lower surface area of TiO_2-montmorillonite catalysts compared to that of TiO_2 supported on MCM-41 and β-zeolite, orange II exhibited stronger adsorption characteristics for TiO_2-montmorillonite (Figure 4.8 and Figure 4.16). The factors that can attribute to the preferential adsorption of orange II on TiO_2-montmorillonite are: (i) montmorillonite is moderately acidic, (ii) interlayer surface of the pillared clay is hydrophobic and facilitate the adsorption of organics, and (iii) shape selectivity because of its pore structure.

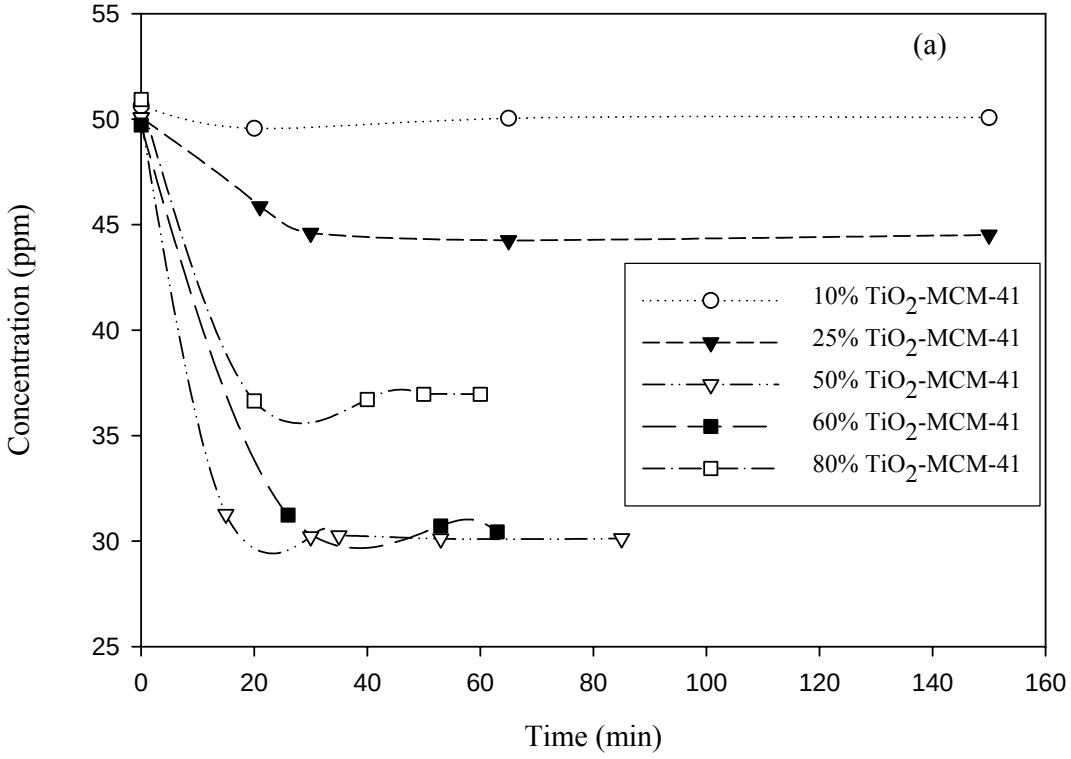
(a)
Concentration (ppm)
Time (min)
10% TiO2-MCM-41
25% TiO2-MCM-41
50% TiO2-MCM-41
60% TiO2-MCM-41
80% TiO2-MCM-41

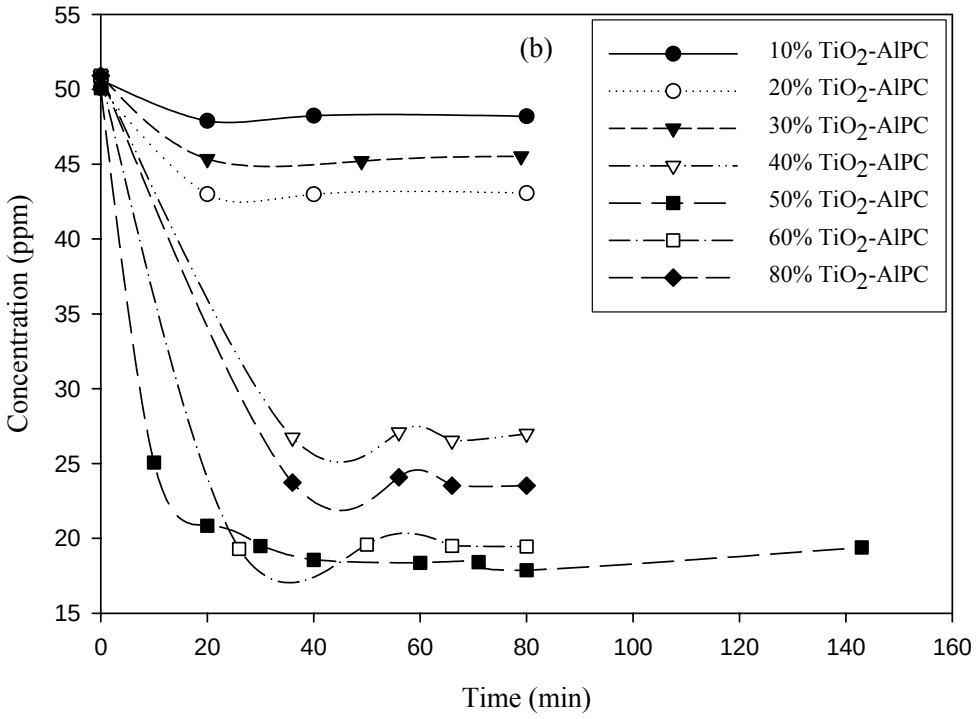
(b)
Concentration (ppm)
Time (min)
10% TiO2-AlPC
20% TiO2-AlPC
30% TiO2-AlPC
40% TiO2-AlPC
50% TiO2-AlPC
60% TiO2-AlPC
80% TiO2-AlPC

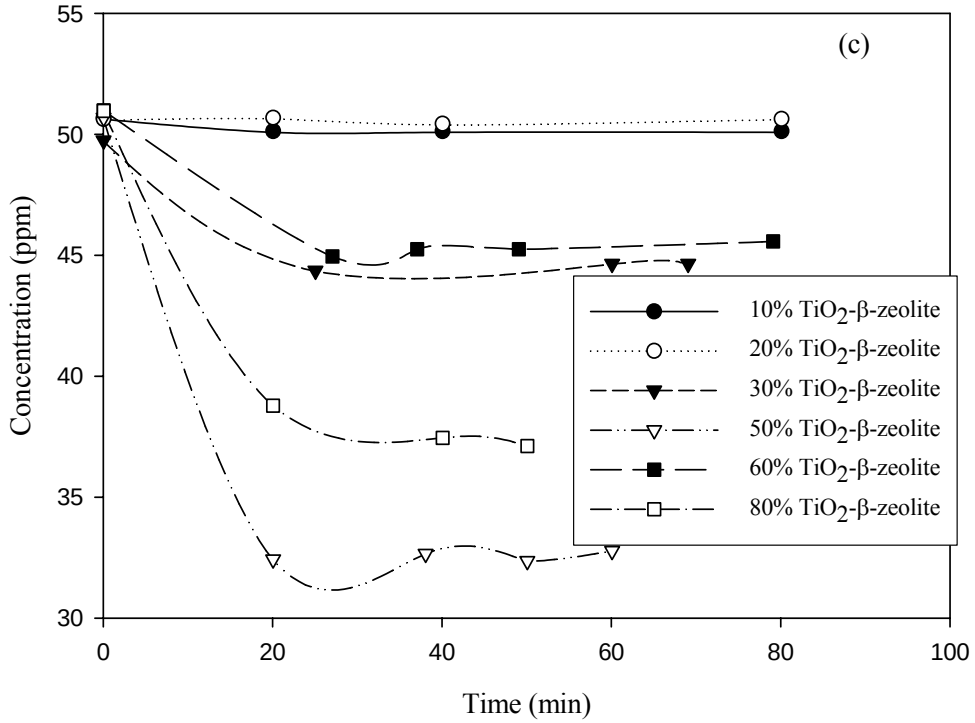

Figure 4.10 Dark adsorption of orange II by different TiO_2 (wt %) loading on MCM-41 (a), Al-pillared montmorillonite (b) and β-zeolite (c) (catalyst amount = 0.5 g/l, initial concentration of orange II = 50 ppm, natural pH, calcination temperature = 300 ºC).

In order to evaluate adsorption equilibrium constant of orange II by three TiO_2 supported catalysts, we consider the following Langmuir and Freundlich isotherm models:

$$\frac{q}{q_m} = \frac{bC}{1+bC} \tag{4.3}$$

$$q = KC^{\frac{1}{n}} \tag{4.4}$$

In both of the isotherm models (4.3) and (4.4), q is the amount of organics adsorbed on the catalyst and C is the equilibrium concentration of organics. In the Langmuir isotherm model (4.3), q_m denotes maximum available adsorption sites and b is the thermodynamic constant. In the Freundlich isotherm model (4.4), n represents Freundlich exponent and K

is the adsorption equilibrium constant. These isotherms models are fitted using least squares method after the following linearization:

$$\frac{1}{q} = \frac{1}{q_m} + \frac{1}{bq_m}\frac{1}{C} \tag{4.5}$$

$$\log(q) = \log(K) + \frac{1}{n}\log(C) \tag{4.6}$$

The Freundlich model fitted better for all the catalyst concentrations indicating possible multilayer adsorption. Freundlich isotherms for TiO_2 supported catalysts (50 wt % TiO_2) are presented in Figure 4.11 a-c, whereas Langmuir isotherms are presented in the Appendix (Figure A.1.4 a-c).

Adsorption equilibrium constants for all the catalysts calculated from Freundlich isotherms are reported in Table 4.4. It can be seen from these results that 50 (wt %) TiO_2 Al-pillared has the highest adsorption equilibrium constant among all three supported TiO_2. Adsorption equilibrium constant (K) of TiO_2 supported MCM-41 and β-zeolite are of similar value.

Overall, it can be observed from Figure 4.8 that the adsorption of orange II was greatly improved on supported TiO_2 catalysts than pristine support and bare TiO_2. Therefore adsorption behavior is not simply contributed by TiO_2, but due to the contribution of both supports and TiO_2.

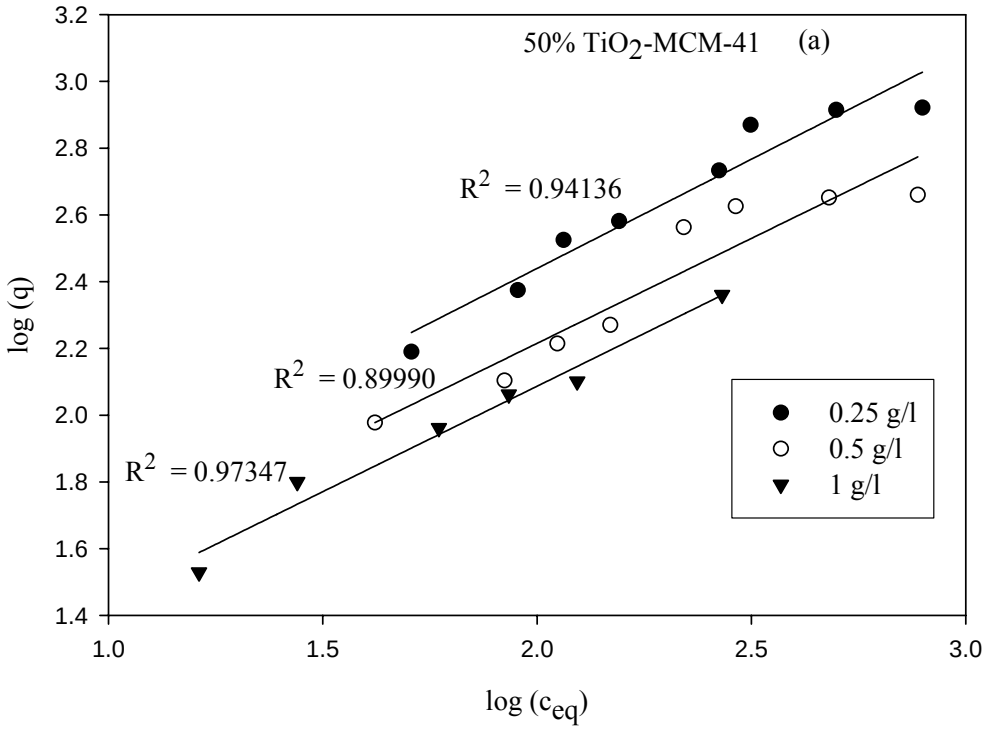
50% TiO2-MCM-41 (a)
R2 = 0.94136
R2 = 0.89990
R2 = 0.97347
0.25 g/l
0.5 g/l
1 g/l
log (q)
log (ceq)
3.2
3.0
2.8
2.6
2.4
2.2
2.0
1.8
1.6
1.4
1.0
1.5
2.0
2.5
3.0

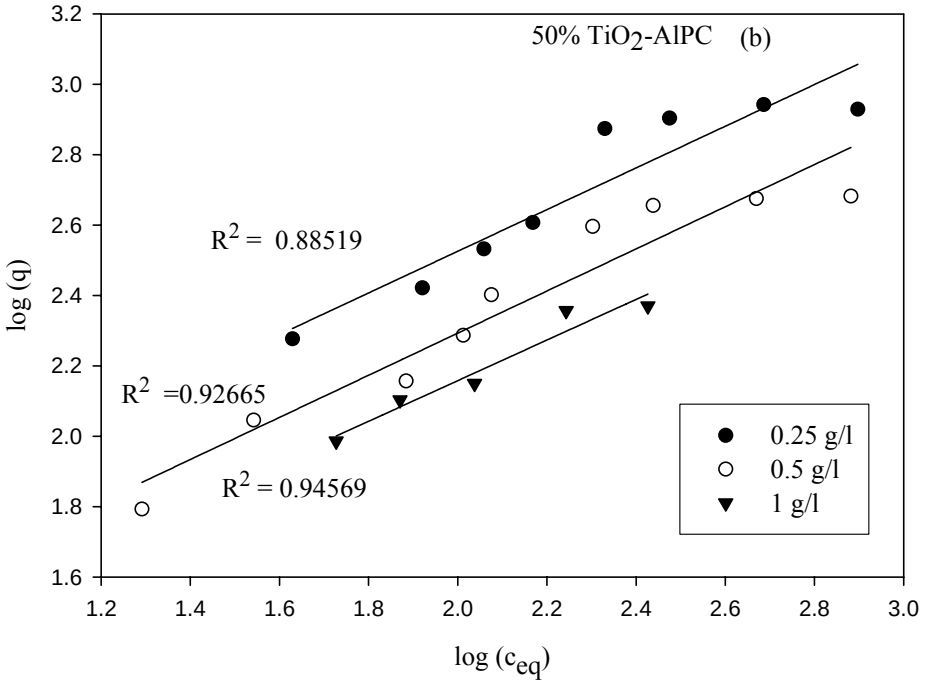
50% TiO2-AlPC (b)
R2 = 0.88519
R2 =0.92665
R2 = 0.94569
0.25 g/l
0.5 g/l
1 g/l
log (q)
log (ceq)
3.2
3.0
2.8
2.6
2.4
2.2
2.0
1.8
1.6
1.2
1.4
1.6
1.8
2.0
2.2
2.4
2.6
2.8
3.0

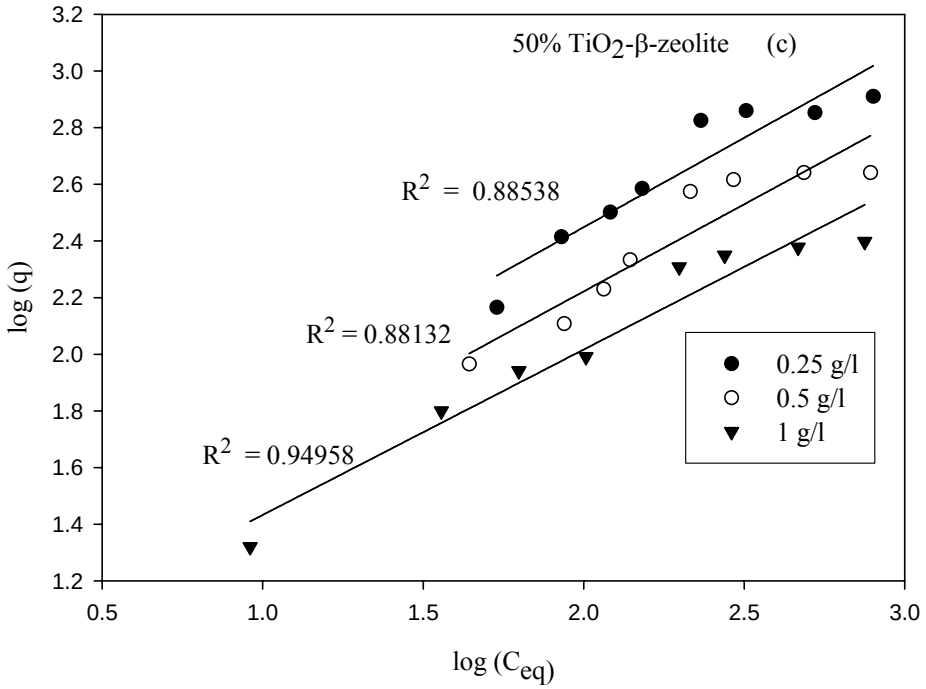

Figure 4.11. Freundlich adsorption isotherm of 50 (wt %) TiO_2 supported on MCM-41 (a), Al-pillared montmorillonite (b) and β-zeolite (c) (Initial concentration = 50-1000 ppm, natural pH, calcination temperature = 300 ºC).

Table 4.4 Freundlich isotherm parameters at different catalyst amount for three different supported TiO_2.

Catalyst	Catalyst amount (g/l)		
	0.25 g/l	**0.5 g/l**	**1 g/l**
50 % TiO_2-MCM41	$q = 13.5\ C^{1/1.53}$	$q = 9.08\ C^{1/1.59}$	$q = 6.64\ C^{1/1.58}$
50 % TiO_2-AlPC[a]	$q = 21.79\ C^{1/1.70}$	$q = 12.47\ C^{1/1.67}$	$q = 10.09\ C^{1/1.73}$
50 % TiO_2-β-zeolite	$q = 15.33\ C^{1/1.58}$	$q = 9.80\ C^{1/1.63}$	$q = 6.92\ C^{1/1.69}$

[a] represents Al-pillared montmorillonite.

4.2.2 Photocatalytic Degradation of Orange II

Photodegradation experiments were conducted at different operating conditions varying the initial concentration of orange II, TiO_2 loading (wt %) on the adsorbents, amount of catalyst, pH, and calcination temperature. In addition, kinetic experiments were also conducted to compare the performance of the supported TiO_2 catalysts with that of Degussa-P25 and bare TiO_2 prepared by sol-gel method. In the following section, effects of the process parameters on photodegradation of orange II are discussed.

Prior to the actual photodegradation experiments with catalysts, photodegradation experiments were conducted using pure MCM-41, montmorillonite and β-zeolite (Figure 4.12). As expected, there was no significant removal of orange II by the supports/adsorbents when the UV-radiation was applied to the solution. These experiments were essential in order to establish the photodegradation efficiency of the TiO_2 catalysts supported on adsorbents over the only adsorption by the adsorbents. It should be noticed that the UV-light was turned on only when the adsorption equilibrium was attained for a certain initial concentration of orange II. It also indicates that the pure adsorbents never participated in the photodegradation of orange II.

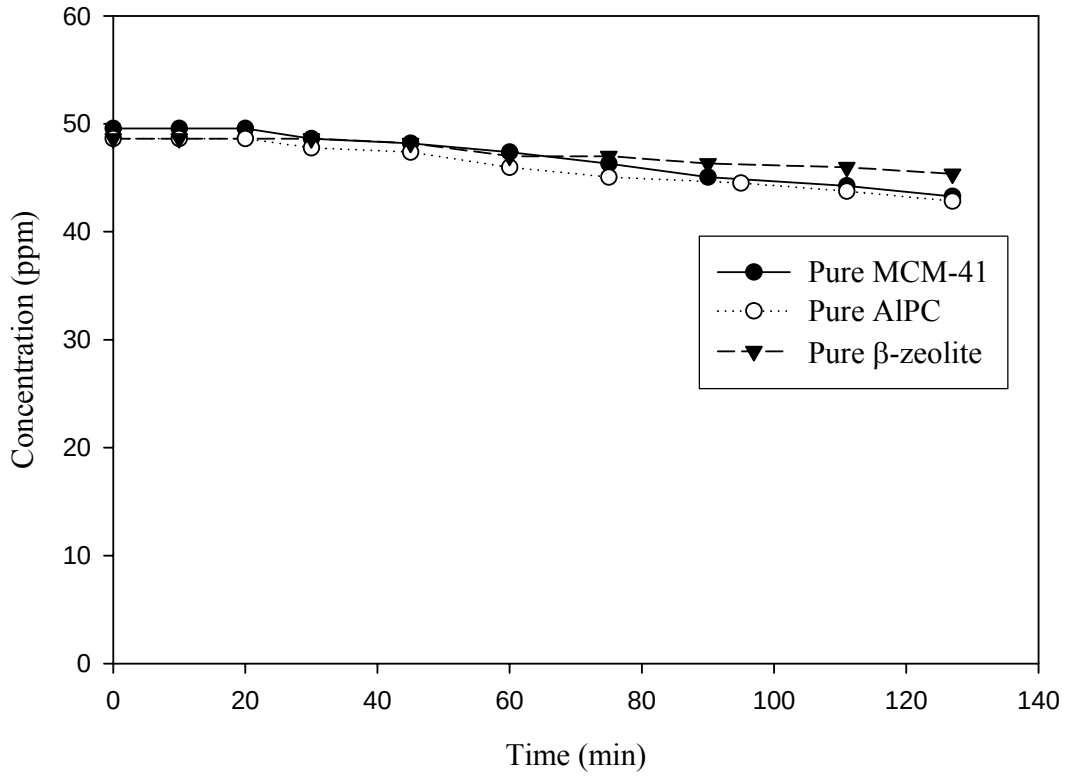

Figure 4.12. Photodegradation of orange II by different supports (catalyst amount = 0.5 g/l, initial concentration of orange II = 50 ppm, natural pH).

4.2.2.1 Effect of Initial Concentration

It is important both from a mechanistic and from an application point of view to investigate the dependence of the photocatalytic degradation rate on the substrate concentration. The photodegradation of orange II by 50 (wt %) TiO_2 supported on MCM-41, Al-pillared montmorillonite and β-zeolite is shown represented in Figure 4.13. The photodegradation rate depends on the probability of hydroxyl radicals formed on the photocatalytic surface and the probability of hydroxyl radicals reacting with dye molecules. Since the life time of the hydroxyl radicals is very short (few nanoseconds), they can react at or near the location where they are formed. The apparent 1^{st} order rate

constants for all three catalysts at different initial concentrations are presented in Table 4.5. As the initial concentration increases, the probability of reaction between oxidizing species and the dye molecules increases leading to the enhancement of photodegradation rate. However, the degradation efficiency of orange II decreased as the concentration of the substrate increased further. This is due to the inhibition of generation of hydroxyl radicals on the catalyst surface as the active sites of the catalyst are covered by high concentration of dye molecules. Another possible cause for decrease in degradation rate was UV screening effect of the dye itself.

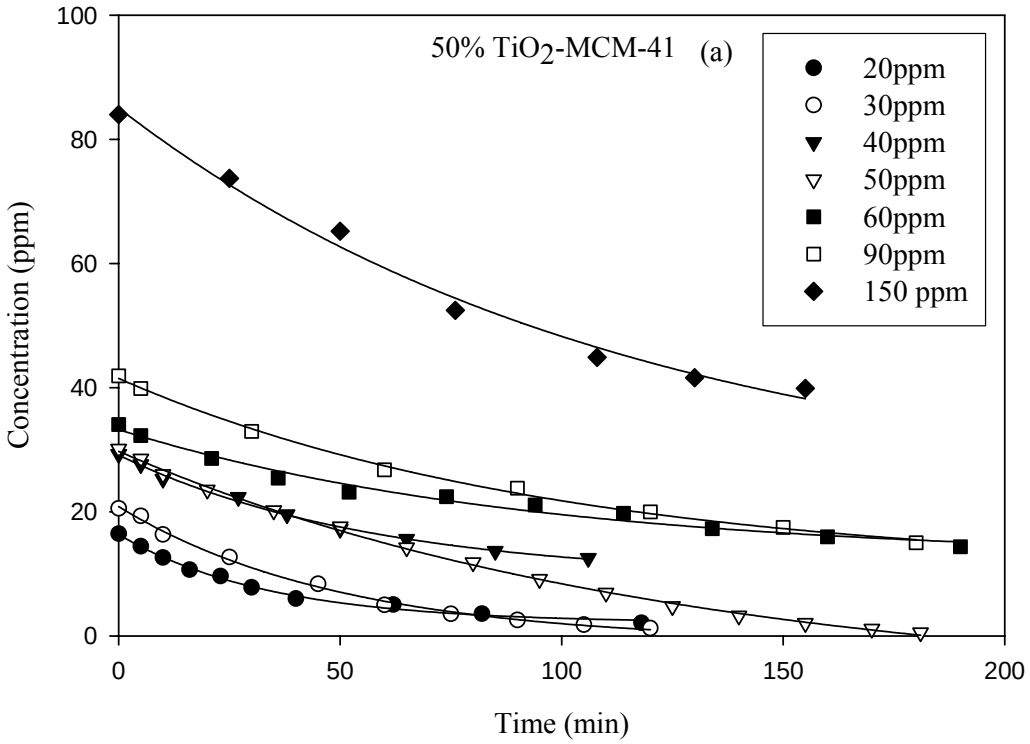

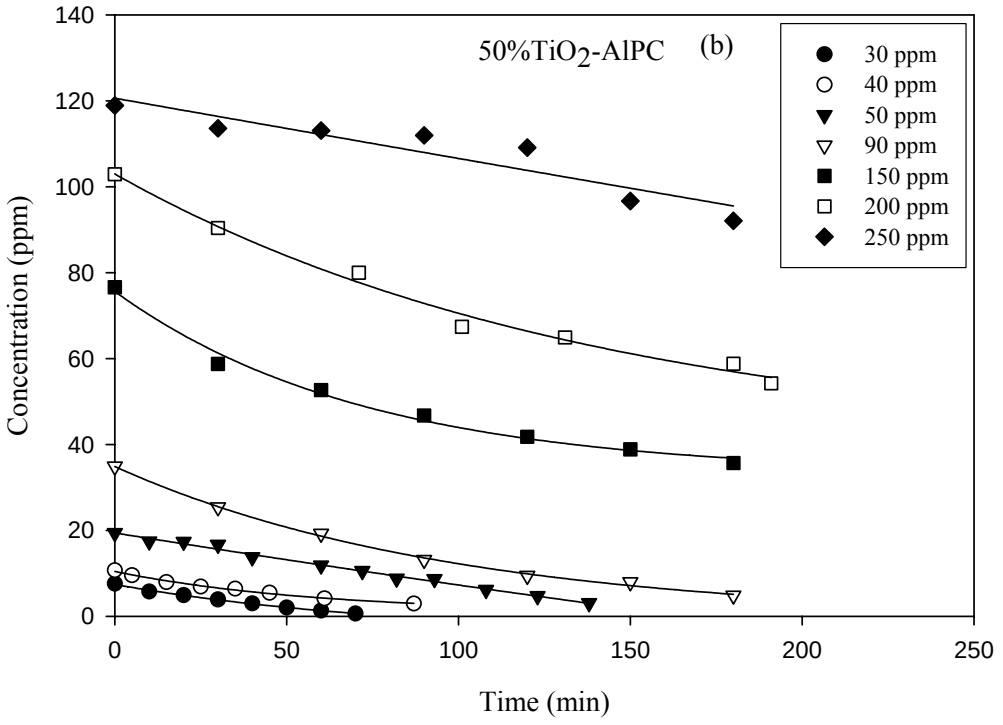

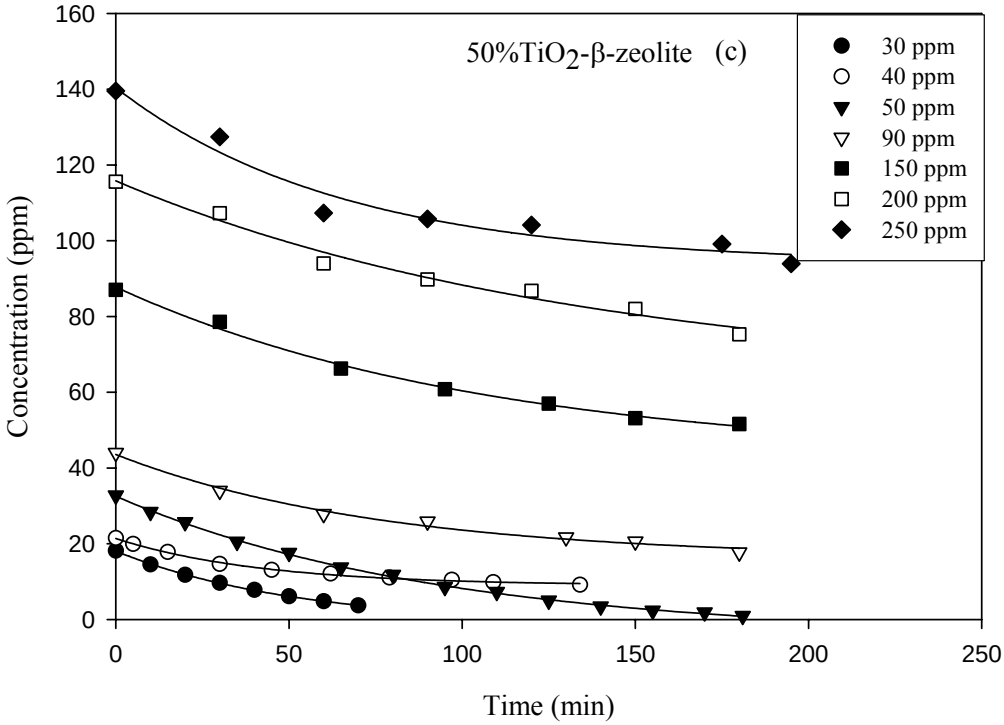

Figure 4.13. Photodegradation of orange II at different initial concentration by 50 (wt %) TiO_2-suppprted on MCM-41 (a), Al-pillared montmorillonite (AlPC) (b) and β-zeolite (c) (catalyst amount = 0.5 g/l, natural pH, calcination temperature = 300 ºC).

At a high dye concentration a significant amount of UV is absorbed by dye molecule rather than TiO_2 particle subsequently reducing the efficiency of the photocatalytic reaction as the concentration of OH• and $O_2^{\bullet-}$ decreased. The influence of initial concentration on photodegradation rate of orange II on the supported TiO_2 catalysts is expressed in terms of Langmuir-Hinshelwood (L-H) model in the following form:

$$r_0 = \frac{kK_eC_0}{1 + K_eC_0} \tag{4.7}$$

Where r_0 is the initial reaction rate (mg/l min), k the reaction rate constant (mg/l min) and K the Langmuir adsorption constant (l/mg). In all experiments mg/l was represented as ppm. L- H equation is applied to evaluate L-H rate constant k and adsorption constant K, but it is only valid for initial rate. During photocatalytic process intermediates are formed and their adsorption (KC) terms must be included in L-H equation. Thus, in this case it is assumed that at initial time interval the intermediate concentration in reaction solution can be considered to be negligible.

A representative plotting of L-H equation using 50 (wt %) TiO_2-MCM-41 among all three supported catalysts is shown in Figure 4.14. A linear expression of equation 4.7 was represented in this figure by plotting the reciprocal initial rate against the reciprocal initial concentration by TiO_2 supported on MCM-41. In this experiment the initial rate was calculated from the first 5 minutes.

The value of k and K was calculated by nonlinear regression using equation 4.7.

$$r_0 = \frac{1.8256 \times 0.007188C_0}{1 + 0.007188C_0} \tag{4.8}$$

The effect of initial concentration on the photodegradation of orange II can be seen by calculating the pseudo-first order kinetic constant and the typical values are presented in Table 4.5.

Table 4.5 Photodegradation rate constant of orange II at different initial concentration on 50 (wt %) TiO_2 supported on MCM-41, Al-pillared montmorillonite (AlPC) and β-zeolite.

TiO_2-MCM-41		TiO_2-AlPC		TiO_2-β-zeolite	
C_0 (ppm)	k_1 (min^{-1})	C_0 (ppm)	k_1 (min^{-1})	C_0 (ppm)	k_1 (min^{-1})
20	0.0171	30	0.0330	30	0.0223
30	0.0236	40	0.0145	40	0.0063
40	0.0083	50	0.0132	50	0.0179
50	0.0179	90	0.0107	90	0.0047
60	0.0043	150	0.0040	150	0.0030
90	0.0056	200	0.0032	200	0.0023
150	0.0051	250	0.0013	250	0.0018
200	0.0031				
250	0.0028				

At low initial concentration, the reaction rate followed pseudo-first order reaction with respect to orange II. In order to evaluate the effect of different process parameters, pseudo-first order rate constant was determined from the kinetic experiments and compared at different conditions.

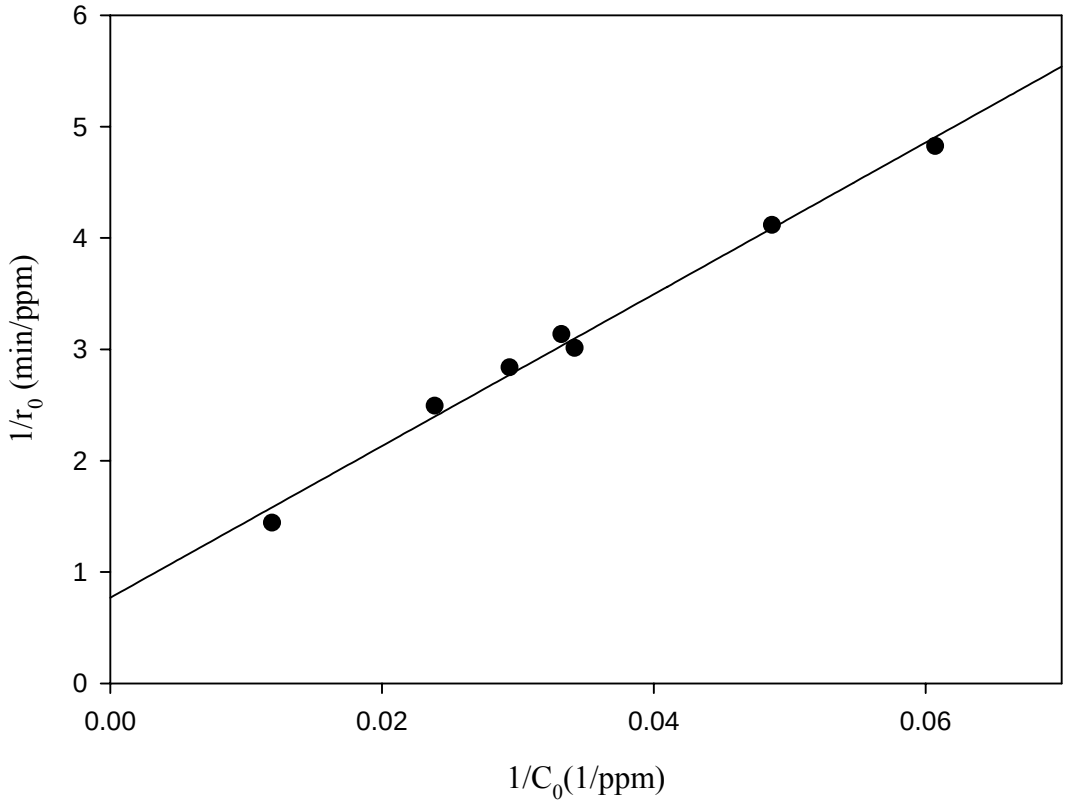

Figure 4.14. Representation of L-H equation by 50 (wt %) TiO_2 supported on MCM-41 (catalyst amount = 0.5 g/l, concentration of orange II = 20-150 ppm, natural pH, calcination temperature = 300 ºC.

4.2.2.2 Effect of TiO_2 (wt %) loading on the Adsorbents

With increasing TiO_2 (wt %) loading, first order rate constant increased until 50 (wt %) loading for all three supported catalysts (Figure 4.15). Subsequently, the rate constant decreased with increased loading of TiO_2 on MCM-41, Al-pillared montmorillonite and β-zeolite. About 50 (wt %) TiO_2 loading performed the best indicating the presence of optimal amount of TiO_2. Earlier, adsorption study of orange II showed increased adsorption with increased TiO_2 (wt %) loading with maximum adsorption occurring at 50-

60 (wt %) loading of TiO_2. Consequently, this has led to the improved photodegradation rate. However, beyond certain loading of TiO_2 (in this case 50 wt %), photodegradation rate decreased due to decrease in adsorption and also due to the increase in size of titania crystallite formed on the support. At lower loading of TiO_2, the overall reaction rate is dictated by the surface reaction, while at higher loading, the extent of adsorption limits the overall reaction.

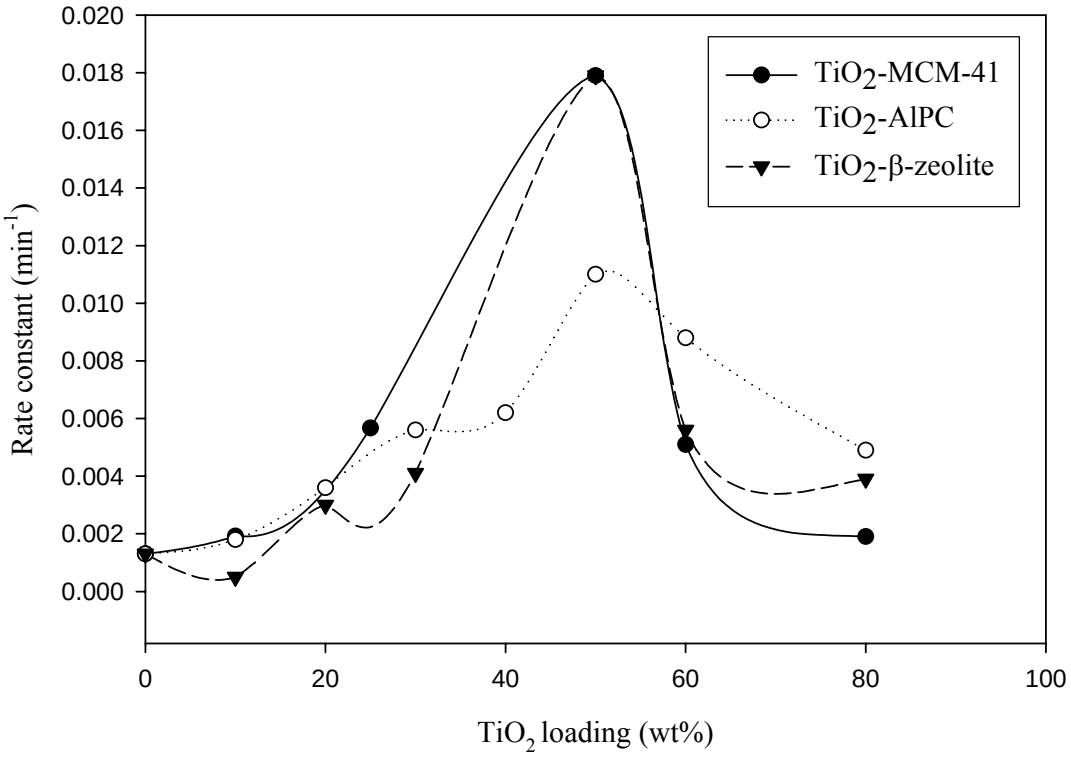

Figure 4.15. Photodegradation rate constant of orange II vs. different TiO_2 (wt %) loading on MCM-41, Al-pillared montmorillonite and β-zeolite (catalyst amount = 0.5 g/l, initial concentration of orange II = 50 ppm, natural pH, catalyst calcination temperature = 300 °C).

The quantization of size may also affect the electronic modification in the TiO_2 particle that provides larger driving force for electron- hole charge transfer within the catalyst (Xu et al., 1999). In addition, the structural homogenization of TiO_2 and adsorption might be lost with increasing loading of TiO_2 on the adsorbent.

4.2.2.3 Comparison between the Supported and Unsupported Catalysts

Kinetic experiments were conducted using both supported and unsupported catalysts. The unsupported catalysts include TiO_2 produced by the sol-gel method and commercial catalyst Degussa-P25. It has been shown earlier that 50 (wt %) TiO_2 loading showed the best photocatalytic efficiency among all the supported catalysts in degrading orange II. The dark adsorption experiments involving supported (50 wt %) and unsupported TiO_2 indicate that effective surface area and adsorption capacity of the supported TiO_2 were much higher than that of bare TiO_2, and Degussa-P25, which favor rapid removal of orange II from the solution (Figure 4.16). Consequently, photocatalytic degradation of orange II (Figure 4.17) by TiO_2 supported on adsorbent was considerably higher than that of bare TiO_2 and the Degussa-P25. All experiments were performed under natural pH condition (pH of supported catalyst approximately varied from 3.92-4.34, pH of Degussa-P25 and sol-gel $TiO_2 \approx 5.16, 8.25$ respectively) using 50 ppm of orange II, and 0.5 g/l of catalyst. A blank experiment without any catalyst was also performed to observe degradation rate of orange II under UV-illumination of 365 nm. As expected, there was no significant removal of orange II when only UV-illumination was applied to the reaction solution. The apparent 1^{st} order rate constants for all the catalysts are presented in Table 4.6.

These results reflect the efficacy of the supported TiO_2 using adsorbent as support. It can be seen that the performance of all three supported catalysts is comparable, while both MCM-41 and β-zeolite show slightly higher rate than TiO_2-montmorillonite. Too strong adsorption in this case for montmorillonite would hinder the mobility of the adsorbed substrate to the photoactive TiO_2 sites as was found in the case of TiO_2-loaded on activated carbon (Yoneyama and Torimoto, 2000).

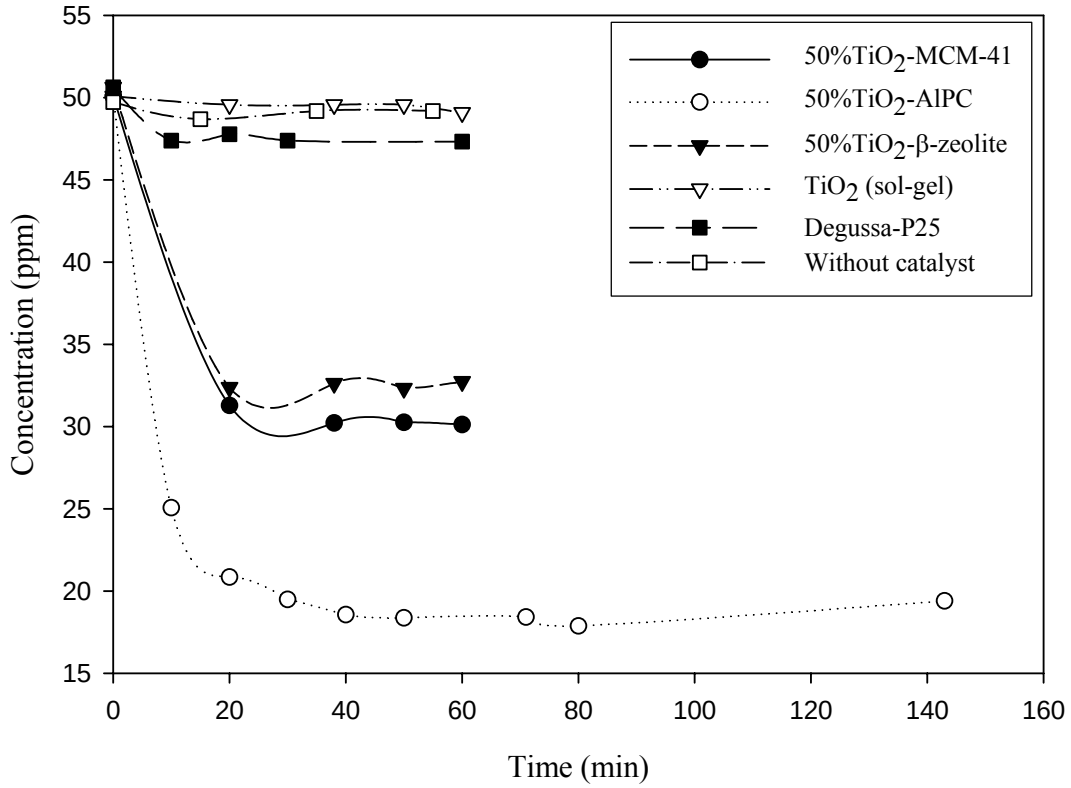

Figure 4.16. Dark adsorption of orange II by 50 (wt %) TiO_2-loaded catalysts, Degussa-P25 and TiO_2 prepared by sol-gel and without any catalyst. (catalyst amount = 0.5 g/l, initial concentration of orange II = 50 ppm, natural pH, calcination temperature = 300 ºC).

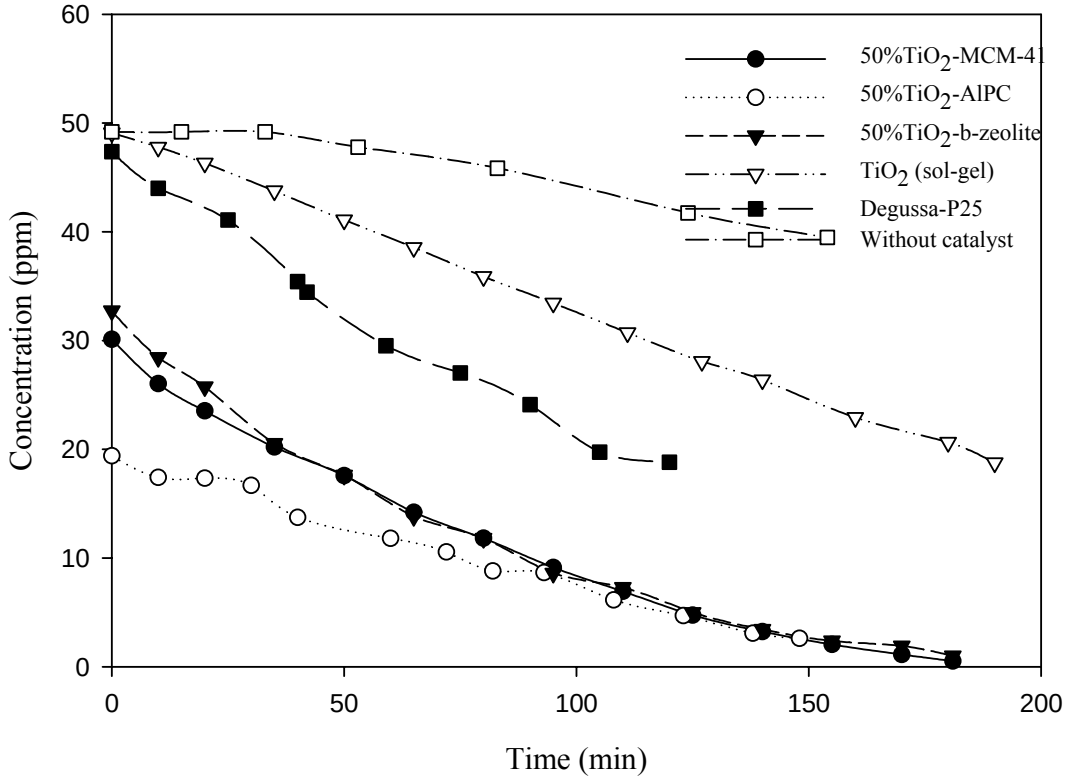

Figure 4.17. Photodegradation of orange II by 50 (wt %) TiO_2-loaded catalysts, TiO_2 prepared by sol-gel and Degussa-P25 and without any catalyst (catalyst amount = 0.5 g/l, initial concentration of orange II = 50 ppm, natural pH, calcination temperature = 300 ºC).

Table 4.6 Apparent first order reaction rate constants for orange II degradation by different catalysts

Catalyst	Rate constant k (min^{-1})	R^2
50% TiO_2-MCM-41	0.0179	0.8927
50% TiO_2-AlPC [a]	0.0132	0.8681
50% TiO_2-β-zeolite	0.0179	0.9333
Degussa-P25	0.0079	0.9736
TiO_2 sol-gel	0.0050	0.9565
Blank	0.0015	0.8028

[a] AlPC reprsents Al-pillared montmorillonite

4.2.2.4 Effect of Amount of Supported Catalyst

These experiments were conducted at higher initial concentration of orange II in order to obtain sufficient data point in a kinetic plot for high concentration of catalyst used in the solution. 50 (wt %) TiO_2-MCM-41 was used as a catalyst in this experiment and initial concentration was 150 ppm. Initially, the rate increased with the increasing concentration of catalyst due to the increasing number of photons and dye molecules available on the catalyst surface. However, for catalyst concentration greater than 2.0 g/l, the rate of degradation decreased slightly possibly due to the agglomeration of the catalysts and decrease in light intensity due to adsorption of the photon by the catalyst as shown in Figure 4.18.

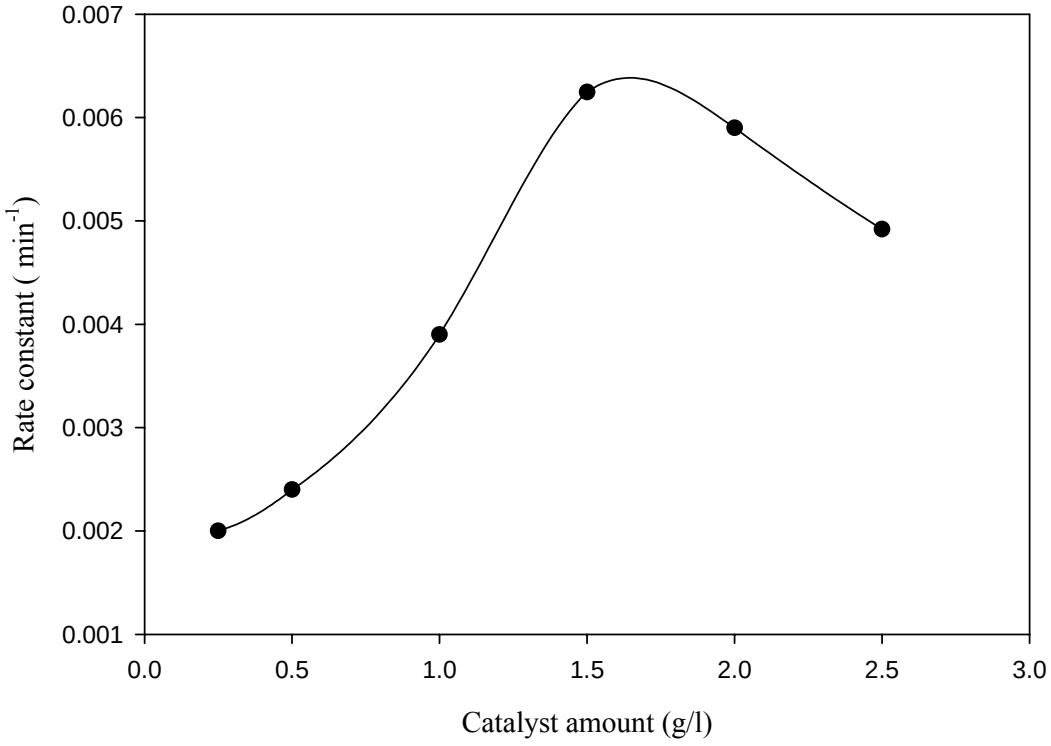

Figure 4.18. Photodegradation rate constant of orange II with different amount of 50 (wt %) TiO_2-MCM-41 (initial concentration of orange II = 150 ppm, natural pH, calcination temperature = 300 ºC).

4.2.2.5 Effect of pH

The effect of solution pH is a complicated one because of its multiple roles. Both ionization state of the catalyst surface and the ionic state of orange II change with the solution pH. The change of pH influenced the adsorption of dye on the catalyst surface as well as photocatalytic degradation. Bahnemann et al. (1994) have reviewed the acid-base properties of metal oxide surfaces which have considerable implication on photocatalytic activity. The point of zero charge of the TiO_2 (Degussa-P25) is at pH 6.8. Thus, the TiO_2 surface is positively charged in acidic media (pH < 6.8) whereas negatively charged (pH >

6.8) in alkaline conditions. In this work, both the supported catalysts and orange II show slightly acidic nature. The natural pH values of MCM-41, Al-pillared montmorilonite and β-zeolite, supported TiO_2 and orange II (50 ppm) in ultrapure water are reported in Table 4.7. It is expected that at low pH, the catalyst surface will be positively charged according to the following equation (see equation (4.2)),

$$Ti - OH + H^+ \leftrightarrow TiOH_2^+$$

The adsorption of anionic orange II on positively charged catalyst surface will be facilitated by low solution pH (pH < 6). But in alkaline solution Coulombic repulsion would take place between the negatively charged photocatalyst surface and negatively charged dye molecule. In addition adsorption would be affected by an increase in the density of TiO^- groups on the semiconductor surface. The adsorption of orange II is very less at pH > 6.8. Moreover, hydroxide radical formed by reaction between hydroxide ions and positive holes might be prevented due to the electrostatic repulsion between hydroxide anions and negatively charged catalyst surface at high pH. (Konstantinou and Albanis, 2004). Thus, the photocatalytic activity of orange II (sulphonated dye) was decreased with increasing pH and exhibited a maximum at pH = 4 (Figure 4.19). The pH was maintained during dark adsorption as well as photooxidation studies. It was observed from the pseudo 1^{st} order reaction rate constant, natural pH condition was better than maintaining the initial pH throughout the reaction. These experiments indicate complex solution behavior at different pH. The solution pH will affect not only the adsorption of parent compound, but also intermediates on the charged catalyst surface. This will also depend on the nature of the substrate to be degraded. Interestingly, when pH was kept constant during the entire photooxidation experiment, performance of TiO_2 supported on MCM-41 and β-zeolite

declined sharply while performance of TiO_2-Al-pillared montmorillonite declined moderately. In these experiments, montmorillonite supported catalyst was better than the catalysts supported on MCM-41 and β-zeolite.

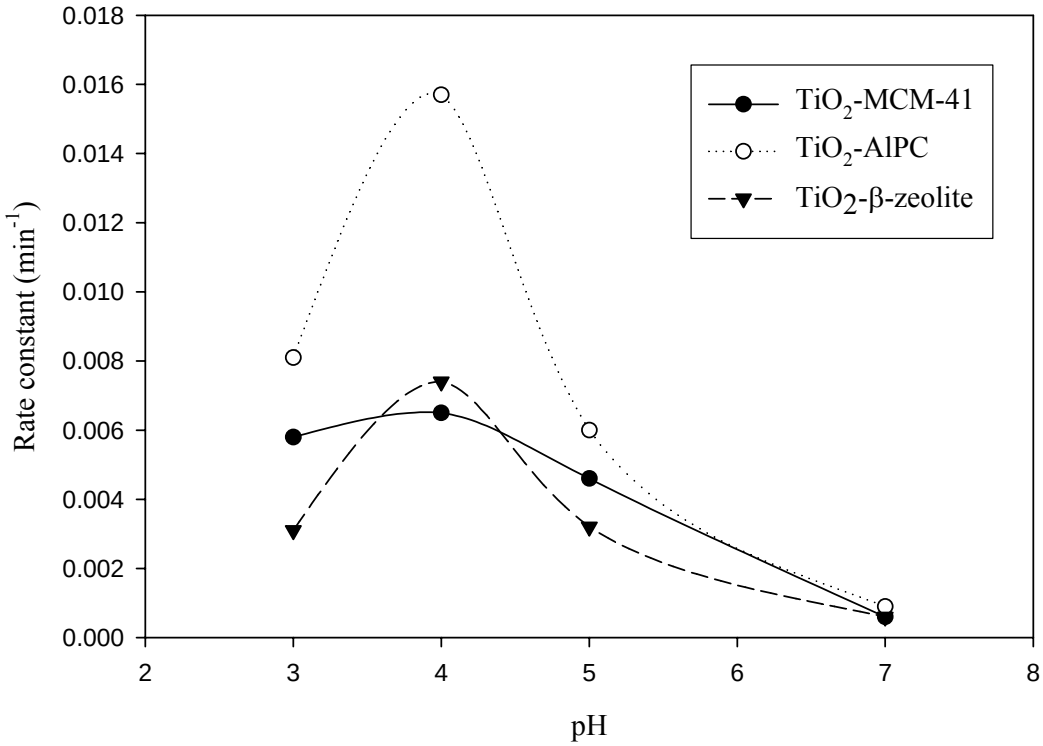

Figure 4.19. Photodegrdation rate of orange II vs. pH by 50 (wt %) loading of MCM-41, Al-pillared montmorillonite and β-zeolite (catalyst amount = 0.5 g/l, initial concentration of orange II = 50 ppm, calcination temperature = 300 ºC).

Table 4.7 pH of different catalyst in ultrapure water

	pH in ultrapure water
Orange II	6.10
MCM-41	6.89
AlPC [a]	5.62
β-zeolite	6.60
TiO_2 (sol-gel)	9.24
50 % TiO_2-MCM-41	4.92
50 % TiO_2-AlPC [a]	4.61
50 % TiO_2- β-zeolite	4.83

[a] AlPC reprsents Al-pillared montmorillonite

4.2.2.6 Effect of Calcination Temperature

Calcination is an important step during catalyst preparation which will affect photocatalytic activity of nanosized TiO_2 resulting from the improvement of the crystallinity. At a certain calcination temperature catalyst is transformed from amorphous to crystalline phase. TiO_2 catalysts supported on three adsorbents MCM-41, Al-pillared montmorillonite and β-zeolite were calcined at 300, 450, 600 and 750 ºC. The photocatalytic activity of the supported catalysts at different calcination temperature is shown in Figure 4.20. The effect of calcination temperature on photocatalytic activity was similar for all three catalysts. The effect is more pronounced for MCM-41 and β-zeolite compared to montmorillonite. Even then, 78.6 % drop in photodegradation rate was

observed for Al-pillared montmorillonite by increasing the calcination temperature from 300 to 750 ºC. The pH was maintained at 3 for all these experiments with different calcination temperatures.

Earlier, characterization of the catalysts using XRD (Table 4.2) and SEM indicated that larger crystallites of anatase were formed at higher calcination temperature on the surface of the supports. It might block the pores of adsorbent supports causing the decrease in surface area (Table 4.1) and subsequently lowering the photocatalytic efficiency of supported catalysts. Similar results were reported by Zhang et al., (2000); Maira et al., (2000) and Deng et al., (2002) for nanoaparticle TiO_2 with calcination temperature. The smaller TiO_2 with larger surface area showed better adsorption which improved the photocatalytic activity. If particle size is very small, the surface structure of atom ensembles can deviate from that of bulk crystal. This could also create significant difference in number and types of catalytic sites present in nanocrystallite and that of large crystals. Fine particles or nano crystals of supported TiO_2 provide rougher surface which would allow multiple reflection thus considerably increasing the number of adsorbed photons to penetrate to the aggregate of particles.

The crystallite structure of anatase plays key role in the photodegardation of organics. Earlier, XRD analysis had shown that the degree of crystallinity of the anatase deposited on all three supports for 50 (wt %) loading of TiO_2 was comparable. In addition, XPS analysis also indicated that the chemical environments (oxidation state) of deposited TiO_2 on various supports were also very similar. The TiO_2 formed on supported catalyst indicated much finer particles than bare TiO_2 prepared by sol-gel method. Finer particles show greater photocatalytic efficiency also by providing greater driving force for charge transfer existed in quantum sized TiO_2 semiconductor particles (Xu et al., 1999).

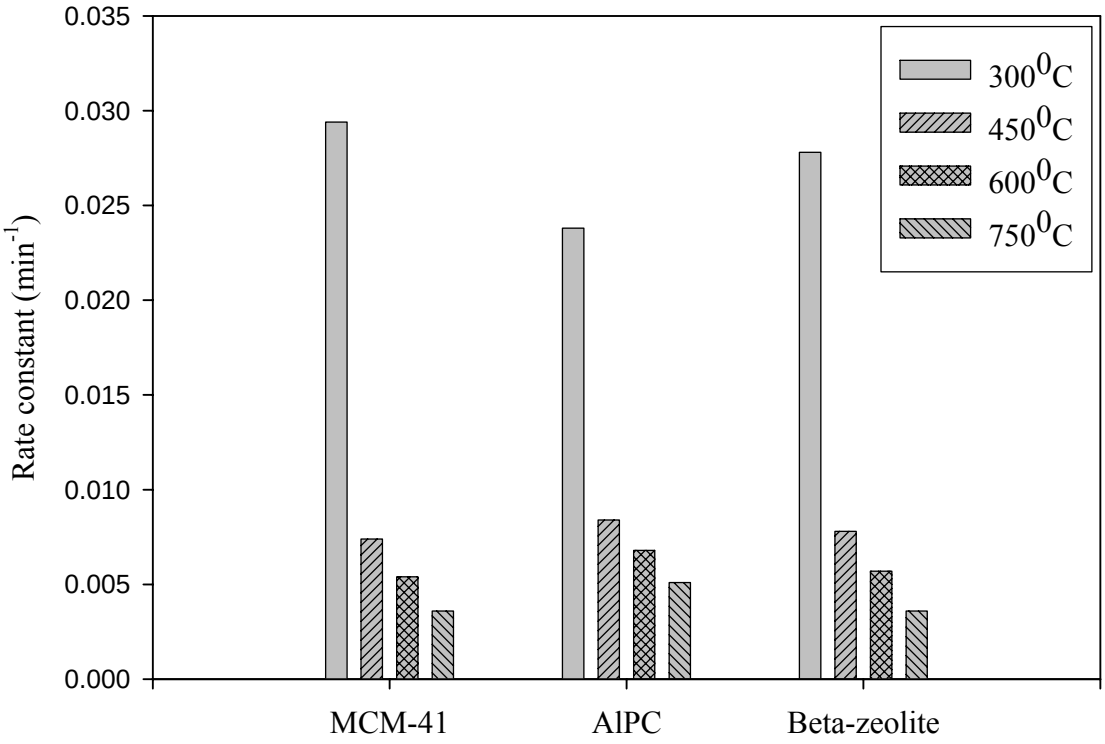

Figure 4.20. Photodegradation rate of orange II by 50 (wt %) TiO_2 supported MCM-41, Al-pillared montmorillonite and β-zeolite at different calcination temperatures (catalyst amount = 1 g/l, initial concentration of orange II = 50 ppm, pH = 3).

4.2.2.7 Total Organic Carbon and Intermediate Analysis

Although, the supported catalysts were very efficient in the degradation of orange II, complete mineralization was much slower as indicated by the TOC analysis of the solution. TOC results of orange II degradation by 50 (wt %) TiO_2 supported on adsorbents, TiO_2 prepared by sol-gel and Degussa-P25 are shown in Figure 4.21. Typically, it took about 3 hours for complete decoloration of the solution, and the concentration of orange II to reach

below detection limit from an initial concentration of 50 ppm, while only 10-20 % of the TOC would reduce by that time. But in case of Degussa-P25, approximately 56 to 60 % TOC reduction was observed. TOC analysis by supported TiO_2 at different initial concentration was also reported in Figure A.1.5 (appendix). There was no significant change in TOC observed in these results. Since orange II is adsorbed on the supported catalyst surface by electrostatic attraction, it is expected that photodegradation takes place at the surface of the catalyst. A rapid exchange of the photoactive species to the reactive surface is essential for complete mineralization. However, the intermediates formed by the photodegradation of orange II are probably strongly adsorbed on the supports inhibiting complete mineralization. The rupture at the N=N bond will lead to the formation of benzene and naphthalene rings followed by a myriad of intermediates such as phenol, oxalate, malonate etc. (Augugliaro et al., 2002; Neamtu et al., 2002) whose anions would also be strongly adsorbed on the surface based on pH. Formation of dibutyl phthalate was confirmed by continuous scanning of the reaction medium during photooxidation of orange II using UV-spectrophotometer when an additional absorbance peak at 260-300 nm occurred and height of this peak increased with time, while the peak absorbance of orange II at 485 nm decreased with time. It was observed from TOC analysis that supported catalyst showed better results for parent compound degradation rather than degradation of intermediates. The initial natural pH (3.92-4.34) of the solution decreased during the photodegradation experiment and the final pH varied from 3.8-4.2 depending on the supported catalysts used in the experiment. At this pH, the adsorption of intermediate anions is quite strong. Thus, the kind of adsorbent, and subsequently TiO_2-adsorbent which would yield the highest activity depends on the target organic compound. The TOC data showed significant variability which is probably due to the interference of

room air as the reactor system was open to the atmosphere. However, there might be other reasons also, which we did not look after due to time constraints and limited scope of the project. At present some experiments are being conducted with greater control environment with a closed head-space, however, those results are not within the scope of this thesis.

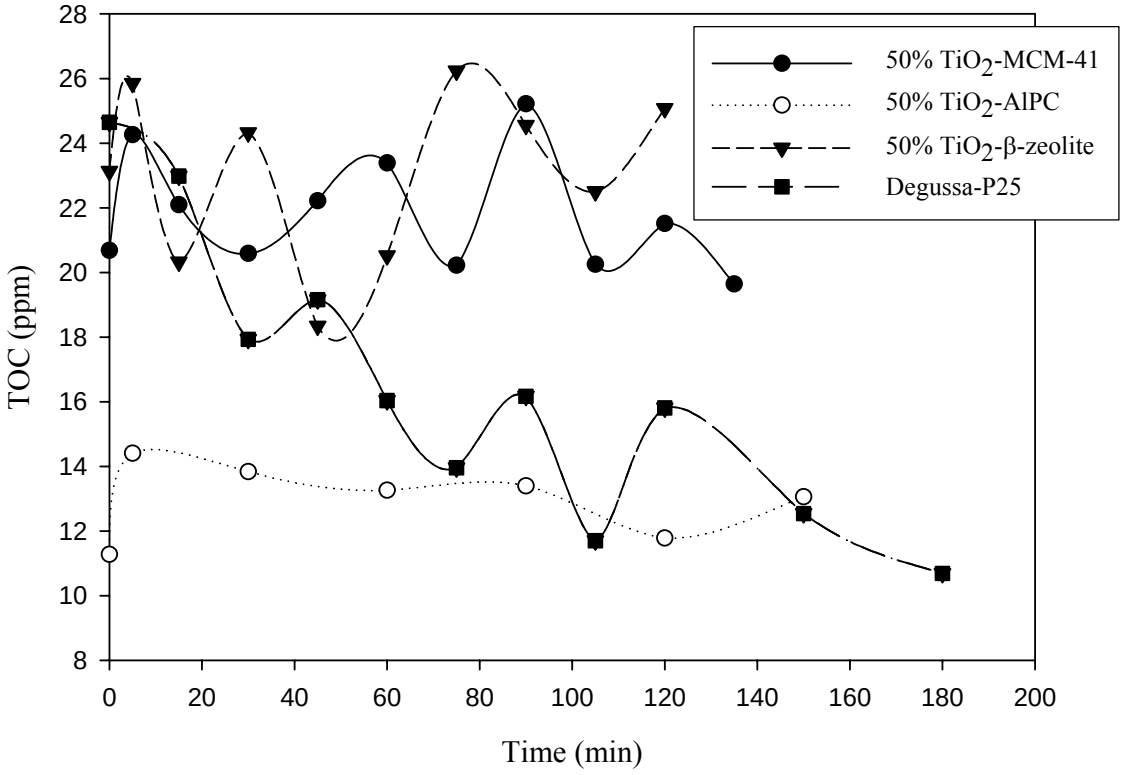

Figure 4.21 TOC concentration with time during photodegradation of orange II by 50 (wt %) TiO_2-loaded catalysts and Degussa-P25 (catalyst amount = 0.5 g/l, initial concentration of orange II = 50 ppm, natural pH, calcination temperature = 300 ºC).

CHAPTER 5
CONCLUSIONS AND RECOMMENDATIONS

5.1 Conclusions

Photocatalytic degradation of organic pollutants using TiO_2 supported on the adsorbents is a promising and potential technique for the treatment of waste streams. The simplicity in photocatalysis process is a major advantage of these methods.

In this thesis photocatalytic efficiency of supported TiO_2 catalyst on three types of adsorbents was compared with that of bare TiO_2 produced by sol-gel method and commercially available Degussa-P25 catalyst using orange II as model compumd. In addition, comparative study of the influence of three different adsorbents on photocatalytic performance of three supported TiO_2 was conducted. Effects of different process parameters such as initial concentration of organics, catalyst amount, pH on the degradation kinetics were evaluated. The effects of TiO_2 (wt %) loading and catalyst calcination temperature on the photodegradation kinetics were also evaluated.

The main conclusions drawn from the present work are as presented below:

- All the supported catalysts showed very good adsorption characteristics compared to bare TiO_2 and Degussa-P25. Photocatalytic efficiency of the supported TiO_2 catalysts over bare TiO_2 produced by sol-gel method and Degussa P25 was greatly improved due to high surface area of the adsorbents used.
- Interestingly, pure supports with very high surface areas showed very poor adsorption of orange II. Surface ionization brought about by the addition of TiO_2

was beneficial for the electrostatic attraction between positively charged surface and the anionic orange II ion.

- Despite lower surface area of TiO_2-montmorillonite catalysts compared to that of TiO_2 supported on MCM-41 and β-zeolite, orange II exhibited stronger adsorption characteristics for TiO_2-montmorillonite. The TiO_2-montmorillonite showed preferential adsorption of orange II due to layered crystalline structure of montmorillonite and the shape selectivity.
- Crystallinity and particle size of TiO_2 are important features, which affect the degradation behavior of the supported catalysts. Fine anatase crystallite size formed on the supports compare to unsupported catalyst is beneficial for photocatalytic degradation as it prevents the recombination of photo excited electron and holes.
- Among the different loadings (10-80 wt %) of TiO_2 on the three supports, catalysts with about 50 (wt %) TiO_2 loading performed the best indicating the presence of an optimal amount of TiO_2. With the increased loading of TiO_2 (beyond 50-60 %) the surface area of the catalysts decreases, thus eventually leading to lower adsorption. Photodegradation rate decreased also due to the increase in size of titania crystallite formed on the support, due to increased loading.
- The photodegradation rate depends on the initial concentration of orange II. It followed Langmuir-Hinshelwood model and showed pseudo-first order reaction kinetics at low initial concentration of orange II.
- Photodegradation rate of the orange II increased with increasing catalyst concentration in the solution upto an optimum concentration beyond which rate declined.

- The performance of three supported catalysts was quite comparable under natural pH condition. Both 50 (wt %) TiO_2 supported on MCM-41 and β-zeolite showed slightly higher photodegradation rate than 50 (wt %) TiO_2 montmorillonite. Too strong adsorption of orange II by montmorillonite hinders the mobility of orange II toward photoactive sites of the catalyst lowering degradation efficiency under natural pH.
- The pH plays a significant and critical role for improving photocatalytic efficiency. The photodegrdation rate showed an optimum at pH= 4. However, 50 (wt %) TiO_2-Al-pillared montmorillonite exhibited higher decomposition rate compared to 50 (wt %) TiO_2 supported on MCM-41 and β-zeolite for experiments where pH was controlled to certain initial value. At strong acidic condition (between pH = 3-4) adsorption was much stronger for the catalysts than those experiments conducted at natural pH.
- Catalysts calcined at 300 ºC exhibit fine crystallites of anatase (approximately 2.4-5.6 nm) and showing better photodegradtion efficiency than other calcinations temperature for all three supported catalysts.
- TOC analysis suggested that complete mineralization was not achieved for the supported catalysts. Intermediates were not degraded as quickly as orange II, most probably due to strong adsorption.

All TiO_2 catalysts using three different supports exhibited similar photodegardation efficiency and there was no apparent advantage or disadvantage of using one support over another. The combination of both TiO_2 and adsorbent (supported TiO_2) showed better photodegradation efficiency than bare TiO_2. However, the performance of the supported catalysts will depend significantly on the nature of the substrate used. The decomposition

of hydrophobic compounds by TiO_2 supported on the adsorbent supports showed better activity than commercial TiO_2. However, for degradation of hydrophilic pollutants supported TiO_2 may not be as active as bare TiO_2. This work suggests that complex manifestation of different factors such as specific surface area, crystal size, crystal phase can influence the photocatalytic activity. Thus, this study opens a new direction for further research to improve supported catalyst.

5.2 Recommendations

This research investigation suggests that supported catalyst showed quite promising results for the degradation of organic dye in water. High surface area of the adsorbent played a significant role improving adsorption as well as overall photocatalytic degradation. However, complete mineralization of the pollutants may be difficult to obtain at reasonable rate using the supported catalysts. This is true mostly for hydrophilic compounds. Therefore, much work is still need to be conducted to make the process viable and efficient for commercial utilization. Some recommendations are proposed in following section:

- The band-gap energy of the TiO_2 of the supported catalyst should be evaluated which can generate sufficient electron-hole pairs that enhance the activity of the photocatalyst for a long time. This can also improve the complete mineralization as well as advanced oxidation at a certain level.
- Catalyst preparation procedure is a basic step to improve the photodegradation efficiency. Here, sol-gel method was used for catalyst preparation. The catalyst preparation procedure was required to generate fine crystallites of TiO_2 with higher

activity. Preparation procedures should also improve proper dispersion of TiO_2 crystallites on the adsorbent supports and provide uniform loading, so that all parts of the catalyst can participate in photodegradation. In this study, siliceous MCM-41 was used. Incorporation of metal ions like Al, in MCM-41 structure can enhance the photocatalytic activity of supported TiO_2. Incorporation of some metal ions such as Fe, Cr, Ir in catalysts can improve the photocatalytic efficiency of supported TiO_2 by generating more electron and hole pairs.

- In this study hydrophilic, polar compound (orange II) was used to evaluate the photodegradation efficiency of the supported catalysts. Photodegradation rate could be enhanced more for non-polar compounds by supported TiO_2 than bare TiO_2 in aqueous media because water molecule which competes with organics which are more polar than polar organics for adsorption and decreases the degradation rate.
- Complete mineralization of the organic pollutant should be pursued using different external oxidants.

REFERENCES

Aguado J., R. V. Grieken, M. J. López-Muñoz, J. Marugán. Removal of Cyanides in Wastewater by Supported TiO_2-based Photocatalysts, Catal. Today, 75, pp. 95-102. 2002.

Anderson M. A., M. J. Gieselman, Q. Xu. Titania and Aluminia Ceramics Membranes, J. Membr. Sci. 39, pp. 243-248. 1988.

Anderson C. and A. J. Bard. An Improved Photocatalyst of TiO_2/SiO_2 Prepared by a Sol-Gel Synthesis, J. Phys. Chem., 99, pp. 9882-9885. 1995.

Anderson C. and A. J. Bard. Improved Photocatalytic Activity and Characterization of Mixed TiO_2/SiO_2 and TiO_2/Al_2O_3 Materials, J. Phys. Chem. B, 101, pp. 2611-2616. 1997.

Anpo M., H. Nakaya, S. Kodama and Y. Kubokawa. Photocatalysis over Binary Metal Oxides; Enhancement of the Photocatalytic Activity of TiO_2 in Titanium-Silicone Oxides, J. Phys. Chem., 90, pp. 1633-1636. 1986.

Anpo M., T. Shima, S. Kodama and Y. Kubokawa. Photocatalytic Hydrogenation of CH_3CCH with H_2O on Small Particle TiO_2: Size Quantization Effects and Reaction Intermediates, J. Phys. Chem. 91, pp. 4305-4310. 1987.

Augugliaro V., C. Baiocchi, A. B. Prevot, E. García-López, V. Loddo, S. Malato, G. Marcí, L. Palmisano, M. Pazzi, E. Pramauro. Azo-dyes Photocatalytic Degradation in Aqueous Suspension of TiO_2 under Solar Irradiation. Chemosphere 49, pp. 1223-1230. 2002.

Bahnemann D. W., J. Cunningham, M. A. Fox, E. Pelizzetti, P. Pichat, N. Serpone, in: R.G. Zepp, G.R. Heltz, D.G. Crosby (eds). Aquatic Surface Photochemistry. pp. 261-268. Lewis Publishers, Boca Raton. 1994.

Beaune O., A. Finiels, P. Geneste, P. Graffin, A. Guida, J. L. Olive and A. Saeedan In M. Guisnet et al. (Ed.). Selective Photocatalytic Oxidation of Hydrocarbon Compounds over Zeolites. Hetero. Catal. and Fine Chem. III, 401, 1993.

Beck J. S., C. Vartuli, W. J. Roth, M. E. Leonowicz, C. T. Kresge, K. D. Schmitt, C. T-W. Chu, D. H. Olson, E. W. Sheppard, S. B. McCullen, J. B. Higgins, J. L. Schlenker. A New Family of Mesoporous Molecular Sieves Prepared with Liquid Crystal Templates, J. Am. Chem. Soc., 114, pp. 10834-10843. 1992.

Belhekar A. A., S. V. Awate and R. Anand. Photocatalytic Activity of Titania Modified Mesoporous Silica for Pollution Control, Catal. Communications, 3, pp. 453-458. 2002.

Blasco T., M. A. Camblor, J. L. G. Fierro, J. Pérez-Pariente. X-Ray Photoelectron Spectroscopy of Ti-Beta Zeolite. Micro. Mater. 3, pp. 259-263. 1994.

Borade R. B. and A. Clearfield. Preparation of Aluminum-rich Beta zeolite, Micro. Mater., 5, pp. 289-297. 1996

Brueva T. R., I. V. Mishin, and G. I. Kapustin. Distribution of Acid-site Strengths in Hydrogen Zeolites and Relationship between Acidity and Catalytic Activity. Thermochemical Acta, 379**,** pp. 15-23. 2001.

Brunauer S., L. Deming, W. Deming, E. Teller. J. Am. Chem.. Soc., 62, pp. 1723. 1940.

Campanati M., G. Fornasari and A. Vaccari. Fundamentals in the Preparation of Heterogeneous Catalysts, Catal. Today, 77, pp. 299-314. 2003.

Carati A., G. Ferraris, M. Guidotti, G. Moretti, R. Psaro and C. Rizzo. Preparation and Characterization of Mesoporous Silica-Alumina and Silica-Titania with a Narrow Pore Size Distribition, Catal. Today, 77, pp. 315-323. 2003.

Chen H., A. Matsumoto, N. Nishimiya and K. Tsutsumi. Preparation and Characterization of TiO_2 Incorporated Y-Zeolite. Coll. Surf. A: Physcochem. Eng. Aspeacts. 157, pp. 295-305. 1999.

Chen Y. and H. Lin. Characteristic of Ti-MCM-41 and its Catalytic Properties in Oxidation of Benzene, J. Por. Mater. 9, pp. 175-184. 2002.

Coutanceau C., J. M. Da Silva, M.F. Alvarez, F. R. Ribeiro and M. Guisnet. Dealumination of Zeolites. Part VII. Influence of the Acid Treatment of a HBEA Zeolite on the Framework Composition and on the Porosity, J. Chem. Phys., 94, pp. 765-781. 1997.

Deng X., Y. Yue and Z. Gao. Gas-phase Photo-oxidation of Organic Compounds over Nanosized TiO_2 Photocatalysts by Various Preparations, Appl. Catal. B: Environ. 39, pp. 135-147. 2002.

Ding Z., H. Y. Zhu, G. Q. Lu and P. F. Greenfield. Photocatalytic Properties of Titania Pillared Clays by Different Drying Methods, J. Coll. and Int. Sci., 209, pp. 193-199. 1999.

Ding Z., J. T. Kloprogge, R. L. Frost, G. Q. Lu and H. Y. Zhu. Porous Clays and Pillared Clays-Based Catalysts. Part 2: A Review of the Catalytic and Molecular Sieve Applications. J. Por. Mater., 8, pp. 273-293. 2001.

Fennandez, G. Lassaletta, V. M. Jimenez, A. Justo. Preparation and Characterization of TiO_2 Photocatalysts Supported on Various Rigid Supports (Glass, Quartz and

Stainless Steel). Comparative Studies of Photocatalytic Activity in Water Purification, Appl. Catal. B: Environ., 7, pp. 49-63. 1995.

Ferino I., D. Meloni, R. Monaci, E. Rombi and V. Solinas. Conversion of Sec-butylbenzene over H-beta Zeolites. J. Mol.. Catal. A: Chem., 192, pp.171-187. 2003.

Guillard C., H. Lachheb, A. Houas, M. Ksibi, E. Elaloui, J. Herrmann. Influence of Chemical Structure of Dyes, of pH and Inorganic Salts on Their Photocatalytic Degradation by TiO_2 Comparison of the Efficiency of Powder and Supported TiO_2, J. Photochem. Photobio. A: Chem., 158, pp. 27-36. 2003.

Han, Y. and S. Yamanaka. Preparation and Adsorption Properties of Mesoporous Pillared Clays with Silica Sol, J. Por. Mater., 5, pp. 111-119. 1998.

Hermann J., J. Matos, J. Disdier, C. Guillard, J. Laine, S. Malato and J. Blanco. Solar Photocatalytic Degradation of 4-chlorophenol using the Synergistic Effect between Titania and Activated Carbon in Aqueous Suspension, Catal. Today, 54, pp. 255-265. 1999.

Hisanaga T. and K. Tanaka. Photocatalytic Degradation of Benzene on Zeolite-incorporated TiO_2 film. J. Hazar. Mater. B, 93, pp. 331-337. 2002.

Hoffmann M. R., S. T. Martin, W. Choi, D. W. Bahnemann. Environmental applications of semiconductor photocatalysis. Chem. Rev., 95, pp. 69-96. 1995.

Hsien Y., C. Chang, Y. Chen and S. Cheng. Photodegradation of Aromatic Pollutants in Water over TiO_2 Supported on Molecular Sieves, Appl. Catal. B: Environ., 31, pp. 241-249. 2001.

Kawi S., S. C. Shen and P. L. Chew. Generation of Brønsted Acid Sites in Si-MCM-41 by Grafting of Phosphorus Specis, J. Mater. Chem., 12, pp. 1582-1586. 2002.

Kim Y. and M. Yoon. TiO_2/Y-Zeolie Encapsulating Intramolecular Charge Transfer Molecules: A New Photocatalyst for Photoreduction of Methyl Orange in Aqueous Medium, J. Mol. Catal. A: Chem., 168, pp. 257-263. 2001.

Konstantinou I. and T. A. Albanis. TiO_2-assisted Photocatalytic degradation of Azo Dyes in Aqueous Solution: Kinetic and Mechanistic Investigations, A Review, Appl. Catal. B: 2004. In press.

Kresge C. T., M. E. Leonowicz, W. J. Roth, J. C. Vartuli, J. S. Beck. Ordered Mesoporous Molecular Sieves Synthesized by a Liquid Crystal Template Mechanism, Nature, 359, pp. 710-712. 1992.

Lepore G. P., L. Persaud and C. H. Langford. Supporting Titanium Dioxide Photocatalysts on Silica Gel and Hydrophobically Modified Silica Gel, J. Photochem. Photobio. A: Chem., 98, pp. 103-111. 1996.

Liqiang J., S. Xiaojun, C. Weimin, X. Zili and D. Yaoguo. The Preparation and Characterization of Nanoparticle TiO_2/Ti Films and Their Photocatalytic Activity, J. Phys. Chem. Solids, 64, pp. 615-623. 2003.

Lopez Nieto J. M. Microporous and Mesoporous Materials with Isolated Vanadium Species as Selective Catalysts in the Gas Phase Oxidation Reactions, Topics in Catal., 15, pp. 189-194. 2001.

Maira A. J., K. L. Yeung, C. Y. Lee, P. L. Yue and C. K. Chan. Size Effect in Gas-Phase Photo-Oxidation of Trichloroethylene Using Nanometer-Sized TiO_2 catalysts, J. Catal., 192, pp. 185-196. 2000.

Malinowska B., J. Walendziewski, D. Robert, J. V. Weber and M. Stolarski. The Study of Photocatalytic Activities of Titania and Titania-Silica Aerogels, Appl. Catal. B: Environ., 46, pp. 441-451. 2003.

Malla P., S. Yamanaka and S. Komarneni. Unusual Water Vapor Adsorption Behavior of Montmorillonite Pillared with Ceramic Oxides, Solid state ionics, 32/33, pp. 354-362. 1989.

Matthews R. W. Purification of Water with Near-UV Illuminated Suspensions of Titanium Dioxide. Wat. Res., 24, pp. 653-660. 1990.

Matos J., J. Laine, J-M Herrmann. Synergy Effect in the Photocatalytic Degradation of Phenol on A Suspended Mixture of Titania and Activated Carbon, Appl. Catal. B: Environ., 18, pp. 281-291. 1998.

Mehrotra K., G. S. Yablonsky, A. K. Ray. Kinetic Studies of Photocatalytic Degradation in a TiO_2 Slurry System: Distinguishing Working Regimes and Determining Rate Dependences, Ind. Eng. Chem. Res., 42, pp. 2273-2281. 2003.

Minero C., F. Catozzo, E. Pelizzetti. Role of Adsorption in Photocatalyzed Reactions of Organic Molecules in Aqueous TiO_2 Suspensions, Langmuir, 8, pp. 481-486. 1992.

Neamtu M., I. Siminiceanu, A. Yediler, A. Kettrup. Kinetics of Decolorization and Mineralization of Reactive Azo Dyes in Aqueous Solution by the UV/H_2O_2 Oxidation, Dyes and Pigments, 53, pp. 93-99. 2002.

Occelli M. L. New Routes to the Preparation of Pillared Montmorillonite Catalysts, J. Mol. Catal., 35, pp. 377-389. 1986.

Ohtani B., Y. Ogawa and S. I. Nishimoto. Photocatalytic Activity of Amorphous-Anatase Mixture of Titanium (IV) Oxide Particle Suspended in Aqueous Solutions. J. Phys. Chem. B, 101, pp. 3746-3752. 1997.

Ollis D.F. and H. Al-Ekabi (Eds). Photocatalytic Purification and Treatment of Water and Air. Amsterdam: Elsevier. 1993.

Ooka C., S. Akita, Y. Ohashi, T. Horiuchi, K. Suzuki, S. Komai, H. Yoshida and T. Hattori. Crystallization of Hydrothermally Treated TiO_2 Pillars in Pillared Montmorillonite for Improvement of Photocatalytic Activity, J. Mater. Chem., 9, pp. 2943-2952. 1999.

Ooka C., H. Yoshida, M. Horio, K. Suzuki and T. Hattori. Adsorptive and Photocatalytic Performance of TiO_2 Pillared Montmorillonite in Degradation of Endocrine Disruptors having Different Hydrophobicity, Appl. Catal. B: Environ. 41, pp. 313-321. 2003.

Qiang W., H. Xijun, P. L. Yue, S. Z. Xiu and Q. L. Gao. Copper/MCM-41 as Catalyst for the Wet Oxidation of Phenol, Appl. Catal. B: Environ. 32, pp.151-156. 2001.

Reddy B. M., B. Chowdhuri, E. P. Reddy, A. Fernández. An XPS Study of Dispersion and Chemical State of MoO_3 on Al_2O_3-TiO_2 Binary Oxide Support. Appl. Catal. A: General 213, pp. 279-288. 2001.

Reddy E. P., L. Davydov., P. Smirniotis. TiO_2-loaded Zeolites and Mesoporous Materials in the Sonophotocatalytic Decomposition of Aqueous Organic Pollutants: The Role of the Support, Appl. Catal. B: Environ. 42, pp. 1-11. 2003.

Salerno P. and S. Mendioroz. Preparation of Al-pillared Montmorillonite from Concentrated Dispersions, Appl. Clay Sci., 22, pp.115-123. 2002.

Sampath S., H. Uchida and H. Yoneyama. Photocatalytic Degradation of Gaseous Pyridine over Zeolite-Supported Titanium Dioxide, J. Catal., 149, pp. 189-194. 1994.

Sauer T., G. Cesconeto Neto, H. J. Jose, R. F. P. M. Moreira. Kinetics of Photcatalytic Degradation of Reactive Dyes in a TiO_2 Slurry Reactor. J. Photochem. Photobio. A: Chem. 149, pp. 147-154. 2002.

Schiavello M., Photocatalysis and Environment. Trends and Applications. Nato Asi Series. Kluwer Academic Publishers, Dordrecht. 1988.

Schmidt R., D. Akporiaye, M. Stocker, O. H. Ellestad. Synthesis of Mesoporous MCM-41 Materials with High Levels of Tetrahedral Aluminium. J. Chem. Soc. Chem. Commun., pp. 1493-1494. 1995.

Serpone N. and Pelizzetti E. (Eds.), Photocatalysis, Fundamentals and Applications, New York: Wiley. 1989.

Shifu C. Photocatalytic Degradation of Organic Pesticide Containing Phosphorous by TiO_2 Supported on Fiber Glass. Environ. Sci., 17, pp. 33-35. 1996.

Shimizu K., T. Kaneko, T. Fujishima, T. Kodama, H. Yoshida and Y. Kitayama. Selective Oxidation of Liquid Hydrocarbons Over Photoirradiated TiO_2 Pillared Clays, Appl. Catal. A: General, 225, pp. 185-191. 2002

Sing K. S. W., D. H. Everett, Haul R. A. W., L. Moscou, R. A. Pierotti, J. Rouquerol and T. Siemieniewska, Reporting Physisorption Data for Gas/Solid Systems with Special Reference to the Determination of Surface Area and Porosity. Pure and Appl. Chem., 57, no. 4, pp. 603-619. 1985.

Stelzer J., M. Paulus, M. Hunger, J. Wietkamp. Hydrophobic Properties of Al-Silica Zeolite Beta. Mesopor. and Micropor. Mater., 22, pp. 1-8. 1998.

Sunada, F. and A. Heller. Effects of Water, Salt Water and Silicone Over Coating of the TiO_2 Photocatalyst on the Rates and Products of Photocatalytic Oxidation of Liquid 3-Octanol and 3-Octanone Environ. Sci. Technol., 32, pp. 282-286. 1998.

Takeda N., T. Torimoto, S. Sampath, S. Kuwabata and H. Yoneyama. Effect of Inert Supports for Titanium Dioxide Loading in Enhancement of Photodecomposition Rate of Gaseous Propionaldehyde, J. Phys. Chem., 99, pp. 9986-9991. 1995.

Takeda N., M. Ohtani, T. Torimoto, S. Kuwabata and H. Yoneyama. Evaluation of Diffusibility of Assorbed Propionaldehyde on Titanium dioxide-Loaded Adsorbent Photocatalyst Films from its Photodecomposition Rate. J. Phys. Chem. B, 101, pp. 2644-2649. 1997.

Takeda N., N. Iwata, T. Torimoto and H. Yoneyama. Influence of Carbon Black as an Adsorbent Used in TiO_2 Photocatalyst Films on Photodegradation Behaviors of Propyzamide. J. Catal., 177, pp. 240-246. 1998.

Tanguay J. F., S. L. Suib and R. W. Coughlin. Dichloromethane Photodegradation using Titanium Catalysts, J. Catal., 117, pp. 335-347. 1989.

Torimoto T., S. Ito, S. Kuwabata and H. Yoneyama. Effects of Adsorbents Used as Supports for Titanium Dioxide Leading on Photocatalytic Degradation of Propyzamide, Environ. Sci. Technol., 30, pp. 1275-1281. 1996.

Torimoto T., Y. Okawa, N. Takeda and H. Yoneyama. Effect of Activated Carbon Content in TiO_2-loaded Activated Carbon on Photodegradation Behaviors of Dichloromethane, J. Photochem. Photobio. A: Chem., 103, pp. 153-157. 1997.

Vartuli J. C., K. D. Schmitt, C. T. Kresge, W. J. Roth, M. E. Leonowicz, S. B. McCullen, S. D. Hellring, J. S. Beck, J. L. Schlenker, D. H. Olson, E. W. Sheppard. Effects of Surfactants/Silica Molar Ratios on the Formation of Mesoporous Molecular Sieves: Inorganic Mimicry of Surfactant Liquid Crystal Phases and Mechanistic Implications. Chem. Mater., 6, pp. 2317-2326. 1994.

Xu Y. and C. H. Langford. Enhanced Photoactivity of a Titanium (IV) Oxide Supported on ZSM5 and Zeolite A at Low Coverage, J. Phys. Chem., 99, pp. 11501-11507. 1995.

Xu Y. and C. H. Langford. Photoactivity of Titanium dioxide Supported on MCM-41, Zeolite X, and Zeolite Y, J. Phys. Chem. B, 101, pp 3115-3121. 1997.

Xu Y., W. Zheng and W. Liu, Enhanced Photocatalytic Activity of Supported TiO_2 Dispersing Effect of SiO_2, J. Photochem. Photobio. A: Chem., 122, pp. 57-60. 1999.

Xu N., Z. Shi, Y. Shi, Y. Fan, J. Dong, J. Shi and M. Z-C. Hu. Effects of Particle Size of TiO_2 on Photocatalytic Degradation of Methylene Blue in Aqueous Suspensions, Ind. Eng. Chem. Res., 38, pp. 373-379. 1999.

Yamanaka S., P. B. Malla and S. Komarneni. Water Adsorption Properties of Alumina Pillared Clay, J. Coll. Int. Sci., 134, no. 1, pp. 51-57. 1990.

Yasuyuki H. and A. Ayame. Investigation of Oxidation States of Titanium in Titanium Silicalite-1 by X-ray Photoelectron Spectroscopy. Catal. Today, 71, pp. 177-187. 2001.

Yoneyama H. and T. Torimoto. Titanium Dioxide/Adsorbent Hybrid Photocatalysts for Photodestruction of Organic Substances of Dilute Concentrations, Catal. Today, 58, pp. 133-140. 2000.

Yoo K. and G. Smirniotis. The Influence of Si/Al Ratios of Synthesized Beta Zeolites for Alkylation of Isobutene with 2-butene., Appl. Catal. A: General, 227, pp. 171-179. 2002.

Zhang Q., L. Gao and G. Jingkun, Effects of Calcination Temperature on the Photocatalytic Properties of Nanosized TiO_2 Powders Preapared by $TiCl_4$ Hydrolysis, Appl. Catal. B: Environ., 26, pp. 207-215. 2000.

Zhao X. S., G. Q. (Max) Lu and G. J. Millar. Advances in Mesoporous Molecular Sieve MCM-41, Ind. Eng. Chem. Res., 35, pp. 2075-2090. 1996.

Zhu C., L. Wang, L. Kong, X. Yang, L. Wang, S. Zheng, F. Chen, F. MaiZhi and H. Zong. Photocatalytic Degradation of Azo Dyes by Supported TiO_2 + UV in Aqueous Solution, Chemosphere, 41, pp. 303-309. 2000.

APPENDIX

A.1 Supplementary Figures and Tables of Experiments

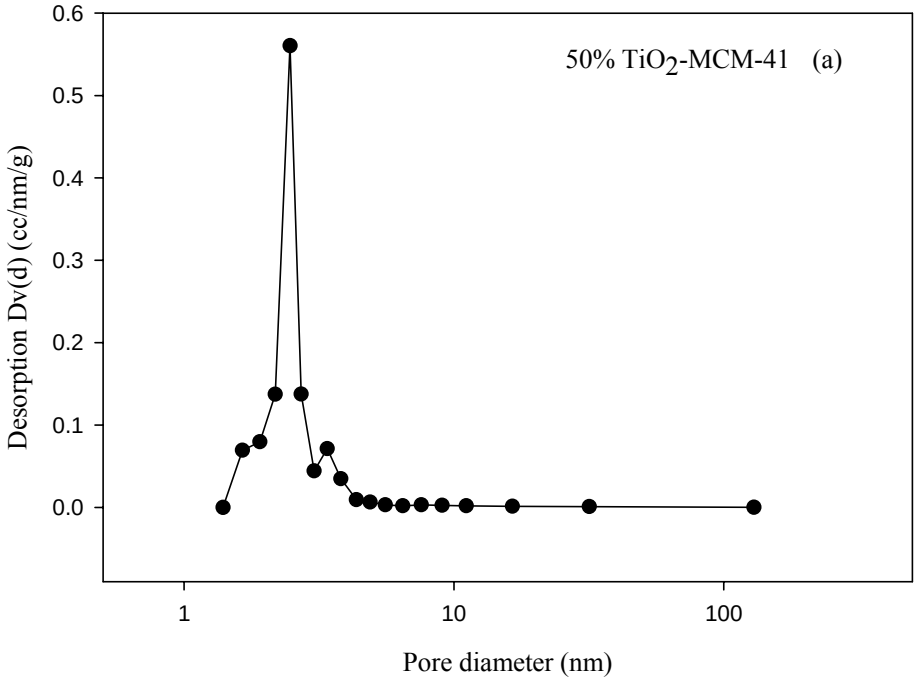

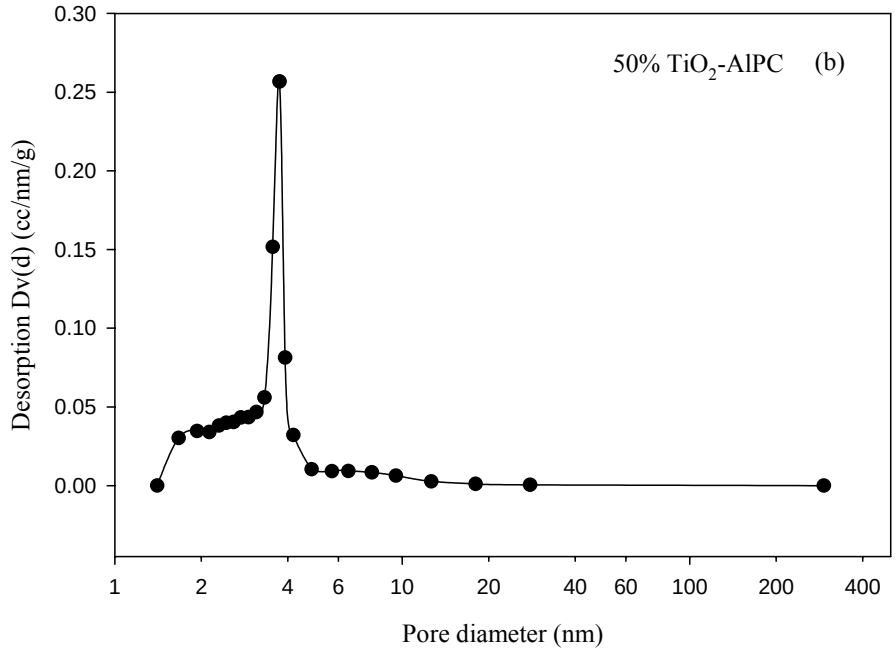

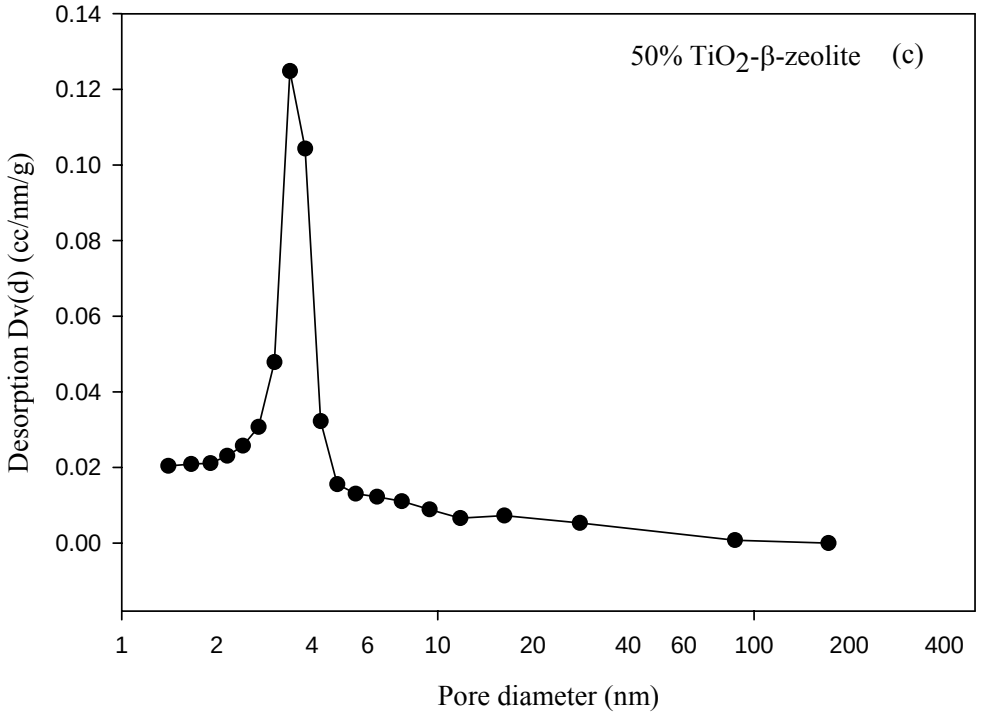

Figure A.1.1. BJH pore size distribution of 50 (wt %) TiO_2 loaded on MCM-41 (a), Al-pillared montmorillonite (AlPC) (b) and β-zeolite (c) (calcined at 300 º C).

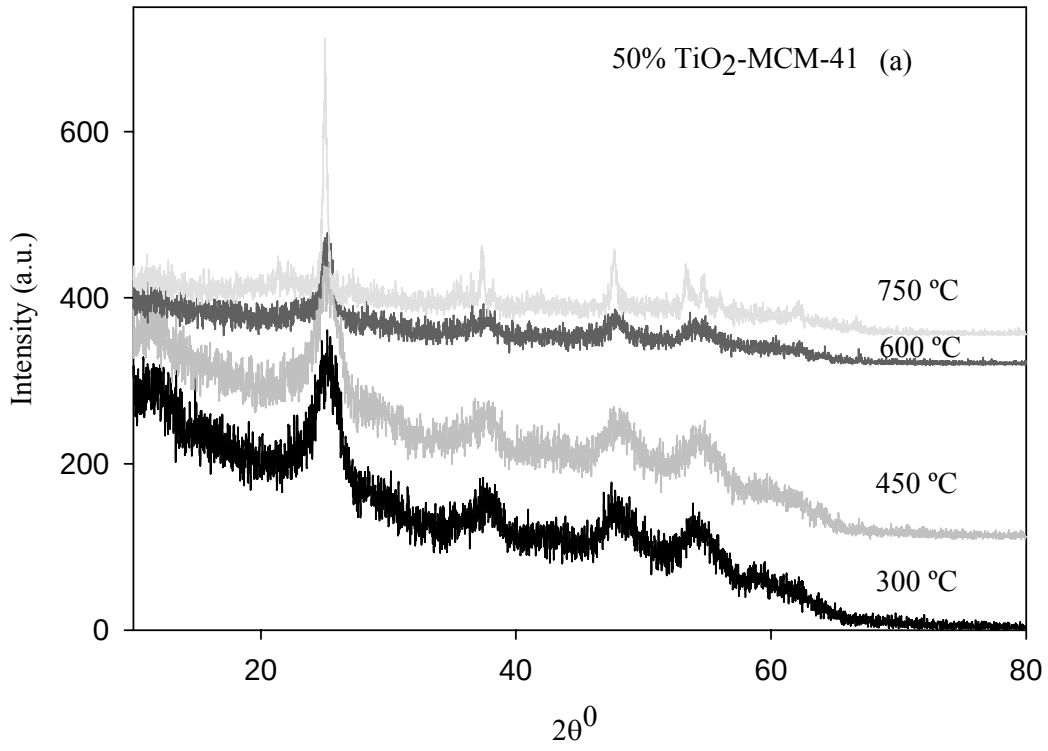
50% TiO2-MCM-41 (a)
Intensity (a.u.)
750 ºC
600 ºC
450 ºC
300 ºC
0
200
400
600
20
40
60
80
2θ0

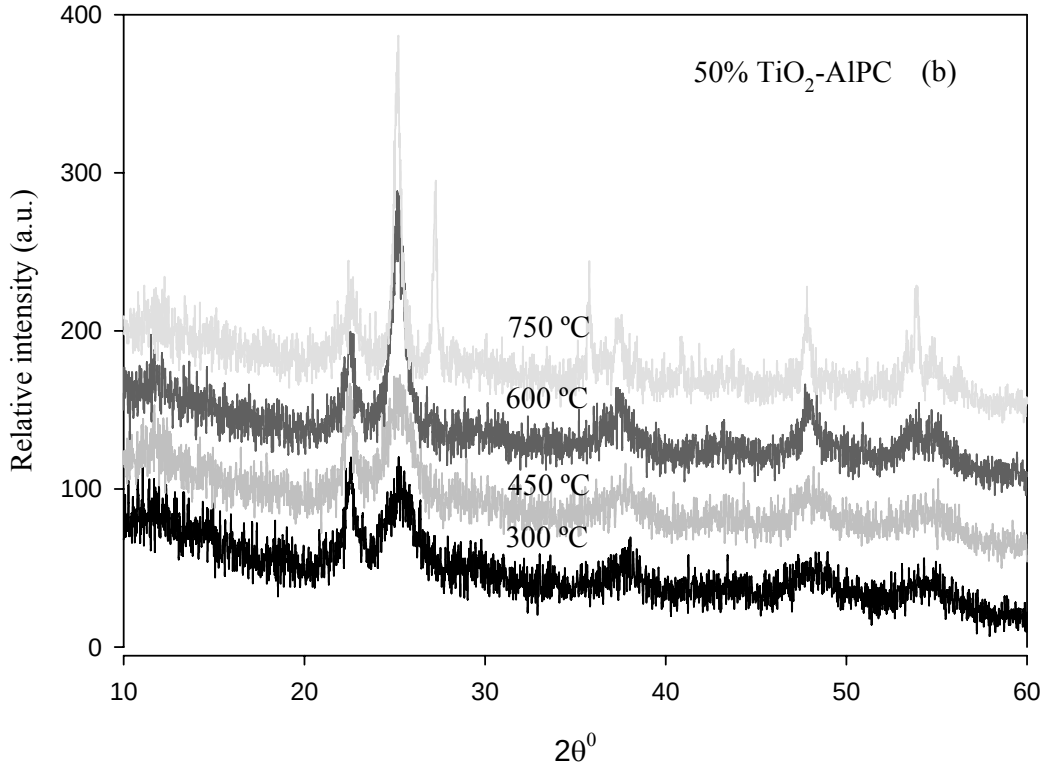
50% TiO2-AlPC (b)
Relative intensity (a.u.)
750 ºC
600 ºC
450 ºC
300 ºC
0
100
200
300
400
10
20
30
40
50
60
2θ0

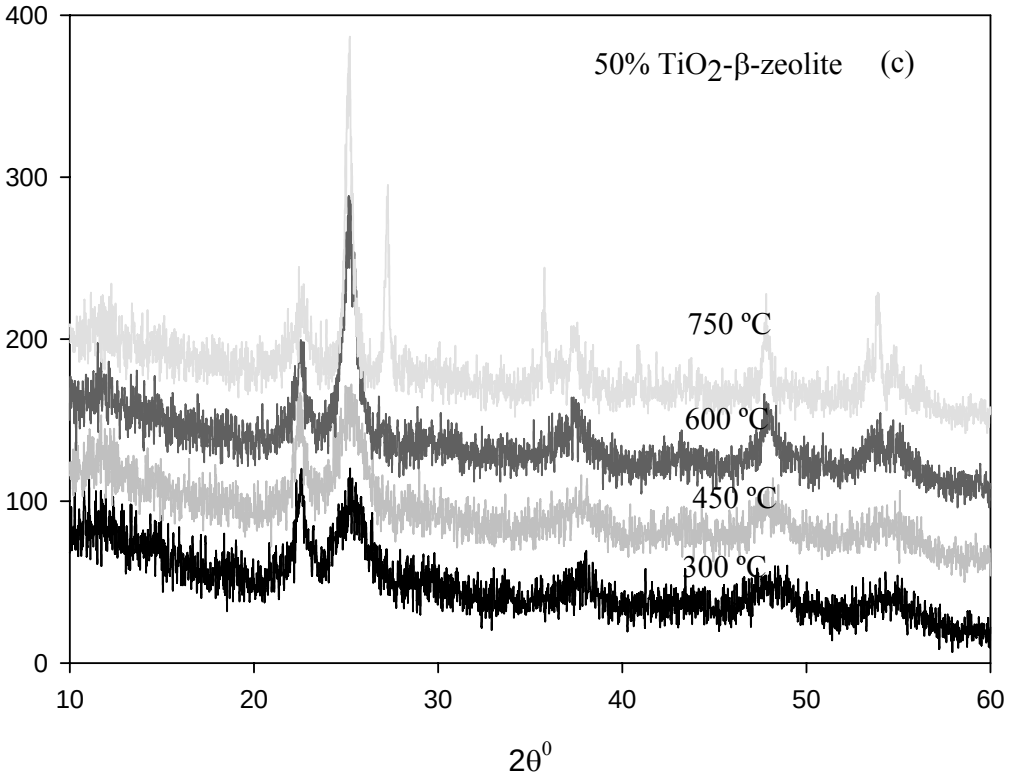

Figure A.1.2. XRD diffraction pattern of 50(wt %) TiO_2 loaded on MCM-41 (a), Al-Pillared montmorillonite (AlPC) (b) and β-zeolite (c) at different calcination temperatures.

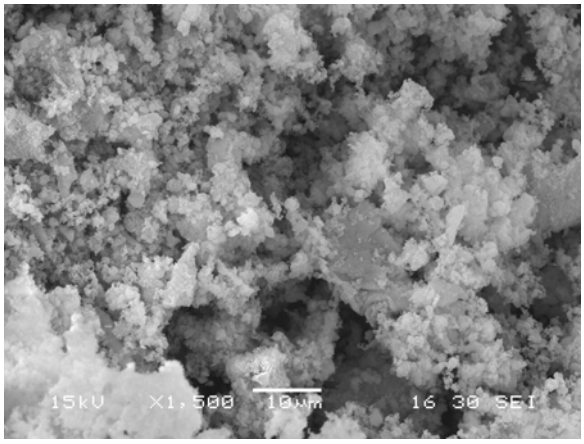

(a) 10% TiO_2-MCM-41

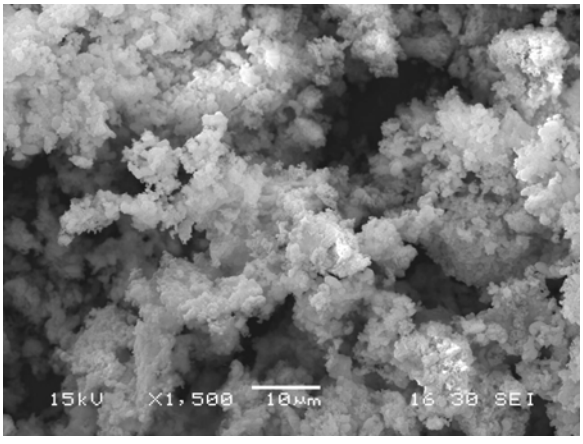

(b) 25% TiO_2-MCM-41

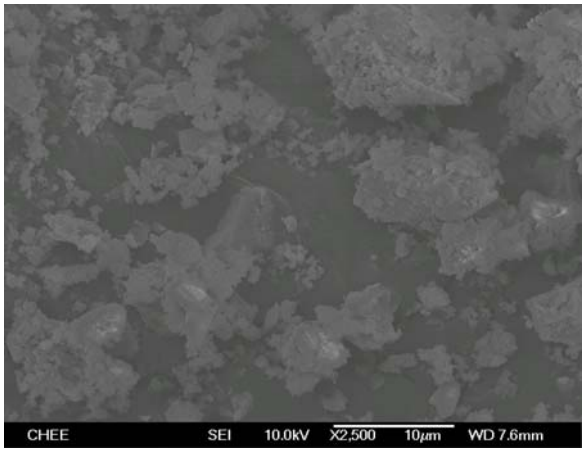

(c) 80% TiO_2 MCM-41

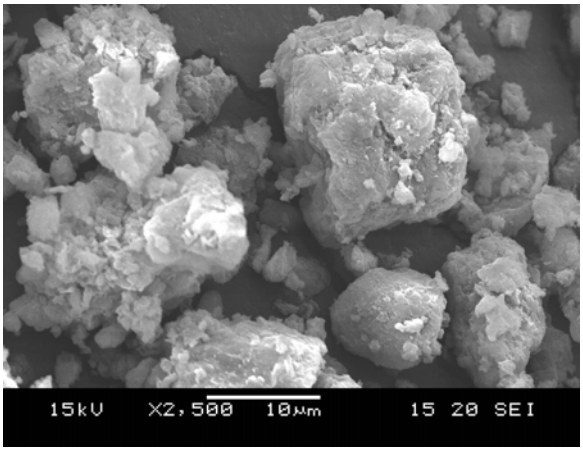

(d) 10% TiO_2-Al-pillared montmorillonite

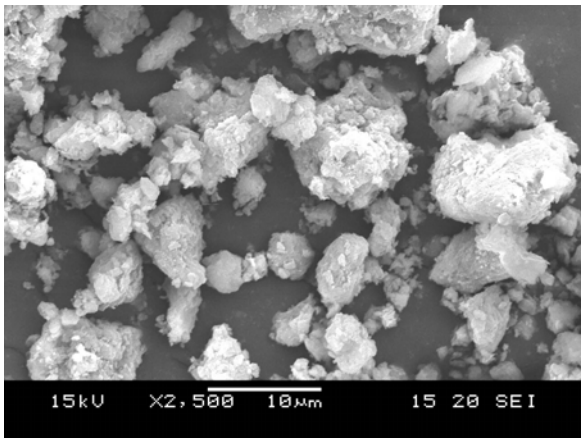

(e) 20% TiO_2-Al-pillared montmorillonite

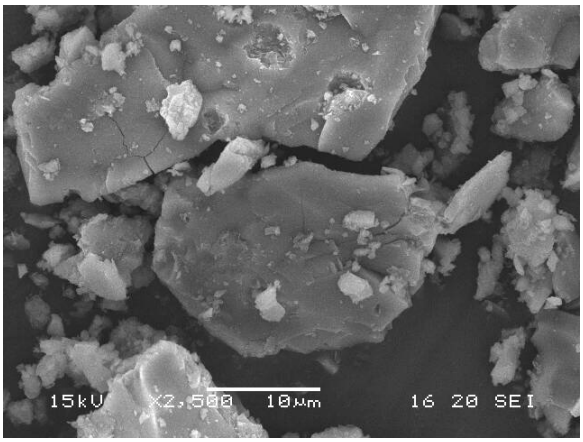

(f) 80% TiO_2-Al-pillared montmorillonite

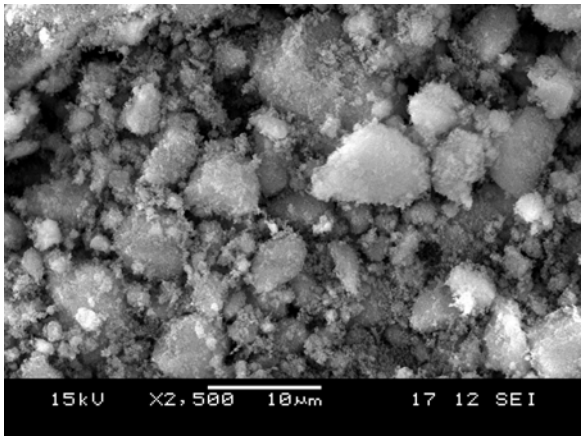

(g) 10% TiO_2-β zeolite

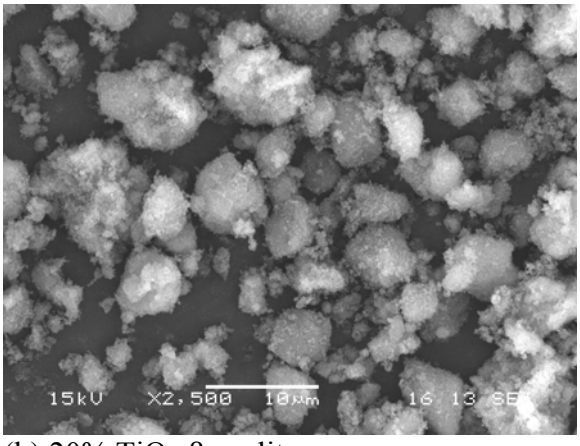

(h) 20% TiO_2-β zeolite

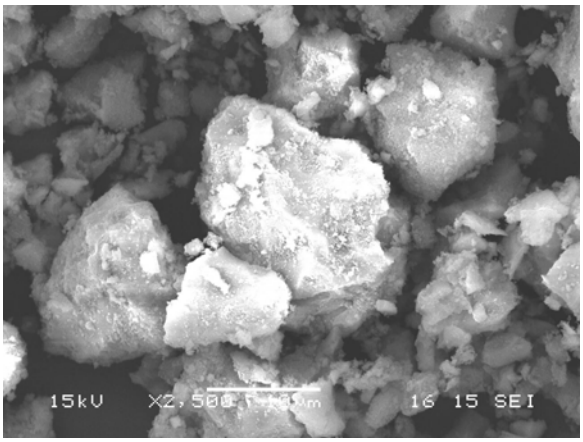

(i) 80% TiO_2-β zeolite

Figure A.1.3. SEM of 10% TiO_2-MCM-41 (a), 25% TiO_2-MCM-41 (b), 80% TiO_2-MCM-41 (c), 10% TiO_2-Al-pillared montmorillonite (d), 20% TiO_2-Al-pillared montmorillonite (e), 80% TiO_2-Al-pillared montmorillonite (f), 10% TiO_2-β-zeolite (g), 20% TiO_2-β-zeolite (h), 80% TiO_2-β-zeolite (i) (Calcined at 300 ºC).

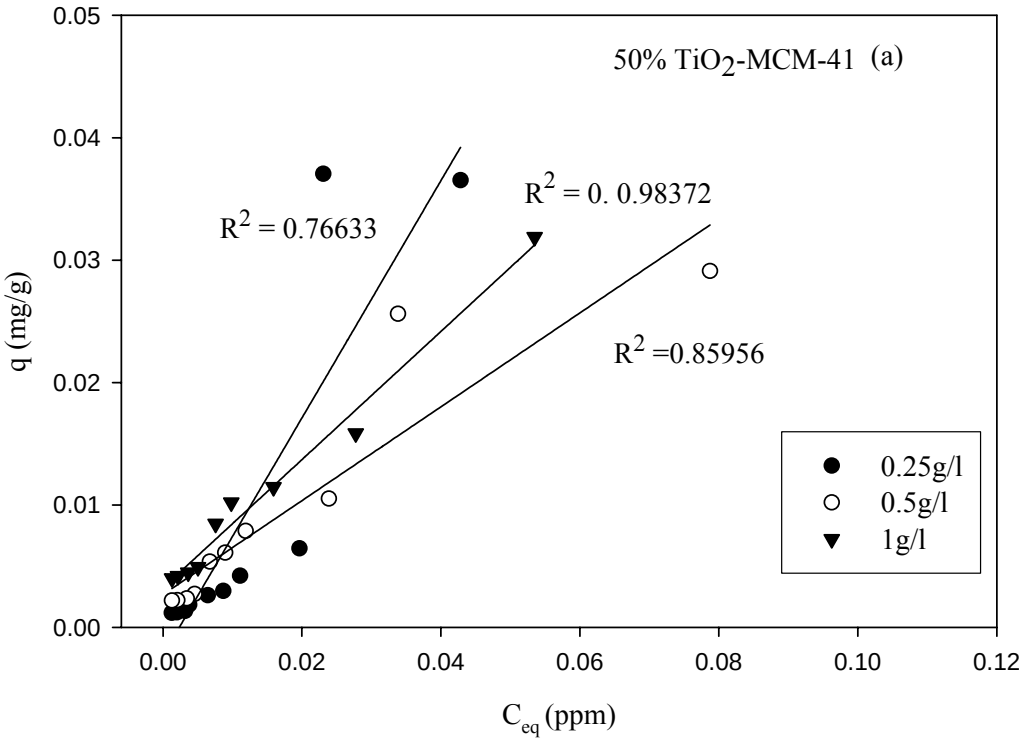

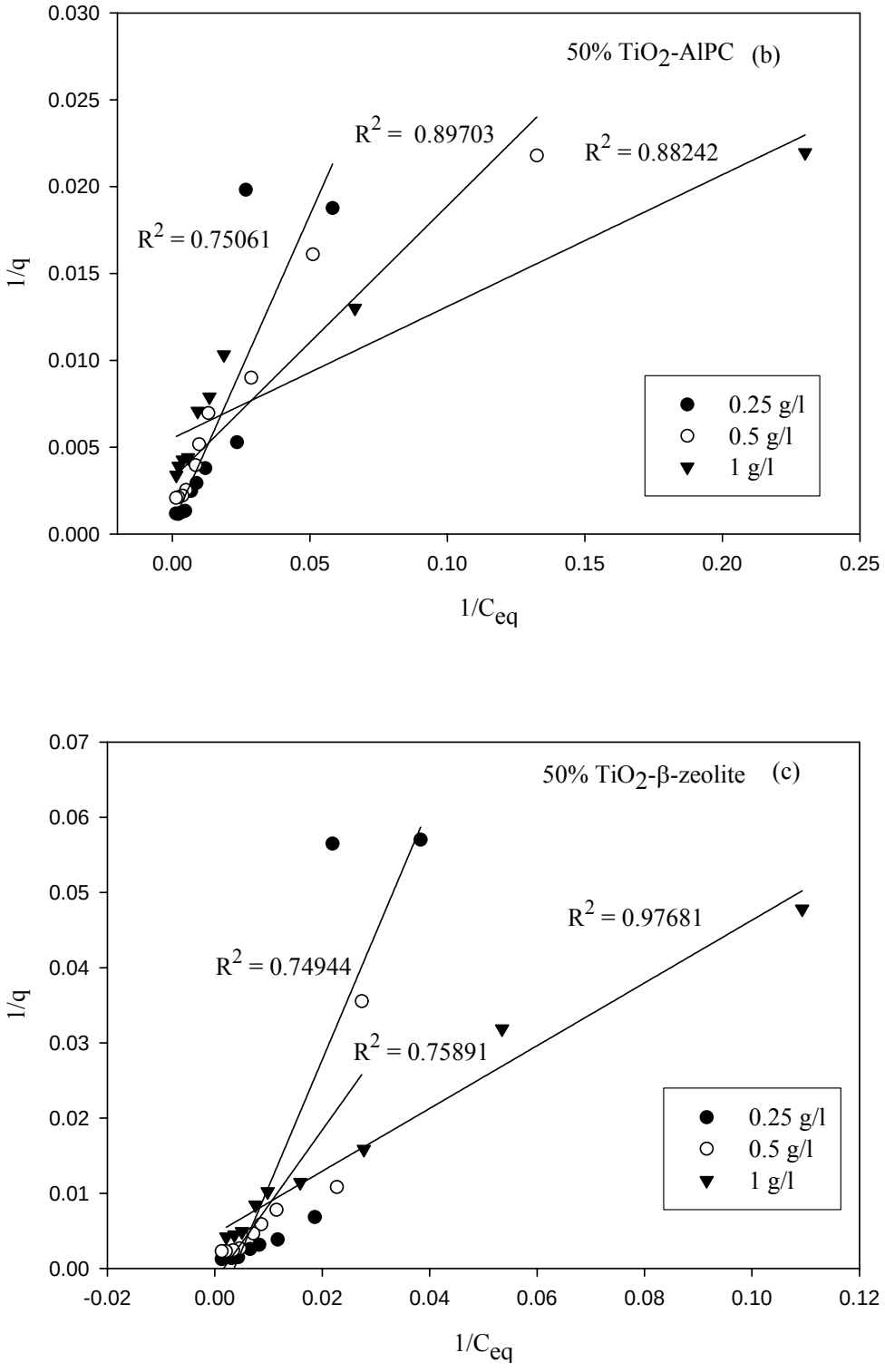

Figure A.1 4. Langmuir adsorption isotherm of 50 (wt %) TiO_2 supported on MCM-41 (a), Al-pillared montmorillonite (b) and β-zeolite (c).

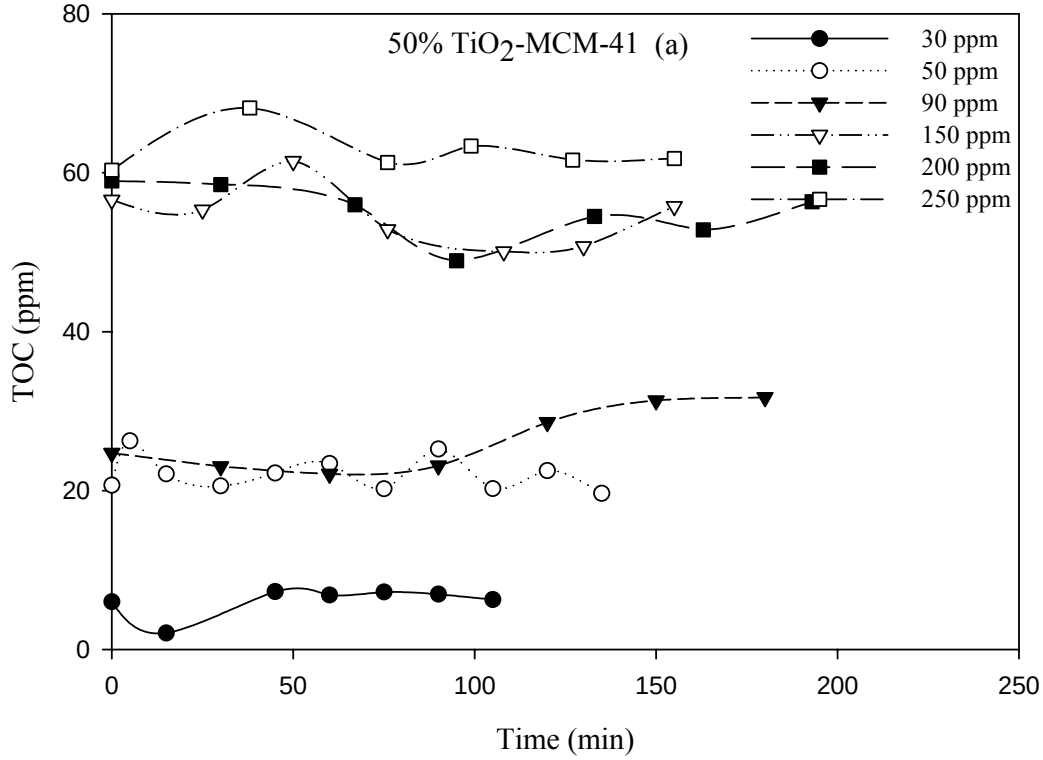
50% TiO2-MCM-41 (a)
30 ppm
50 ppm
90 ppm
150 ppm
200 ppm
250 ppm
TOC (ppm)
Time (min)
0
20
40
60
80
0
50
100
150
200
250

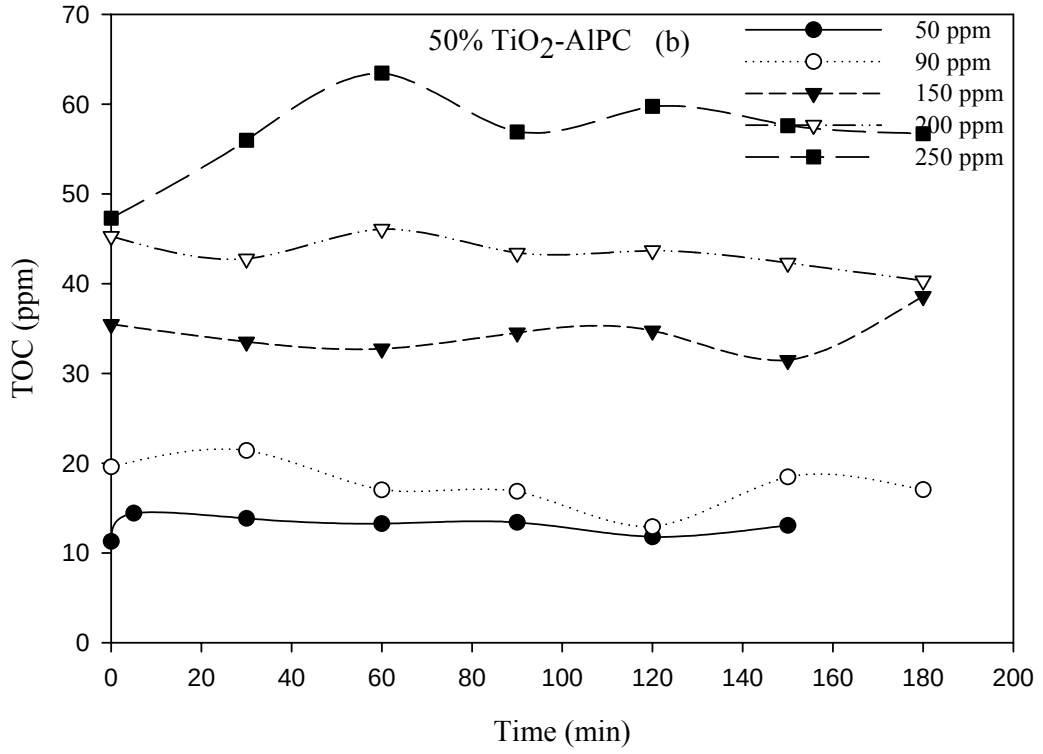
50% TiO2-AlPC (b)
50 ppm
90 ppm
150 ppm
200 ppm
250 ppm
TOC (ppm)
Time (min)
0
10
20
30
40
50
60
70
0
20
40
60
80
100
120
140
160
180
200

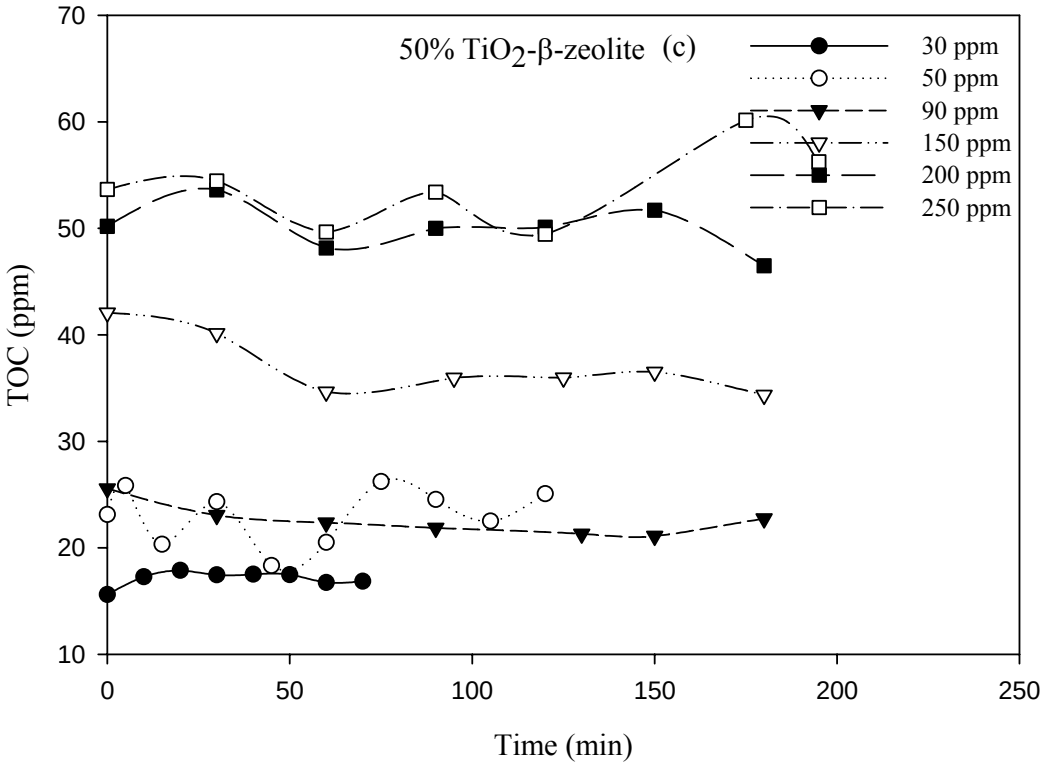

Figure A.1.5 TOC concentration with time during photodegradation of orange II by 50 (wt %) TiO_2-loaded MCM-41 (a), Al-pillared montmorillonite (b) and β-zeolite (c) at different initial concentrations (catalyst = 0.5 g/l, natural pH, calcination temperature = 300 ºC).

Table A.1.1 Pore diameter (calculated from BJH adsorption) at different TiO_2 (wt %) loading

TiO_2-MCM-41		TiO_2-ALPC		TiO_2-β-zeolite	
TiO_2 loading (wt %)	**Pore diameter (nm)**	**TiO_2 loading (wt %)**	**Pore diameter (nm)**	**TiO_2 loading (wt %)**	**Pore diameter (nm)**
0	2.520	0	0.740	0	0.740
10	2.409	10	0.740	10	0.745
25	2.482	20	1.410	20	2.729
30	2.560	50	3.399	50	4.277
50	2.430	60	3.036	60	4.844
60	2.760	80	2.724	80	1.700
80	1.416				

A.2 Experimental Data

Table A.2.1 (Data for Figure 4.2)

TiO_2-MCM-41		TiO_2-ALPC		TiO_2-β-zeolite	
TiO_2 loading (wt %)	**BET surface area (m^2/g)**	**TiO_2 loading (wt %)**	**BET surface area (m^2/g)**	**TiO_2 loading (wt %)**	**BET surface area (m^2/g)**
0	1022	0	397.10	0	612.20
10	760.13	10	295.35	10	579.88
25	606.26	20	296.44	20	486.62
30	589.59	50	242.77	50	356.50
50	527.23	60	219.60	60	305.55
60	334.42	80	209.60	80	265.43
80	248.25				

Table A.2.2 (Data for Figure 4.3)

TiO_2-MCM-41		TiO_2-ALPC		TiO_2-β-zeolite	
TiO_2 loading (wt %)	**Pore volume (cc/g)**	**TiO_2 loading (wt %)**	**Pore volume (cc/g)**	**TiO_2 loading (wt %)**	**Pore volume (cc/g)**
0	0.5870	0	0.6300	0	0.7850
10	0.5509	10	0.4700	10	0.7550
25	0.5740	20	0.2800	20	0.5900
30	0.4565	50	0.2637	50	0.4520
50	0.4285	60	0.2040	60	0.3470
60	0.2425	80	0.1918	80	0.2210
80	0.1632				

Table A.2.3 (Data for Figure 4.8)

50% TiO_2-MCM-41		50% TiO_2-AlPC		50% TiO_2-β-zeolite	
Eq. conc (ppm)	**Amnt. adsorbed/surface area (ppm/m^2/g)**	**Eq. conc (ppm)**	**Amnt. adsorbed/surface area (ppm/m^2/g)**	**Eq. conc (ppm)**	**Amnt. adsorbed/surface area (ppm/m^2/g)**
12.6990	0.0326	7.5470	0.0945	18.1630	0.0343
29.5570	0.0370	19.5690	0.1279	36.5520	0.0395
41.8660	0.0901	34.8445	0.2290	44.0220	0.1295
83.9920	0.1204	76.5800	0.2957	87.0550	0.1799
111.5150	0.1553	102.9050	0.3986	115.5900	0.2382
148.2050	0.1767	118.9100	0.5198	139.5250	0.3020
219.8800	0.3466	200.6400	0.8133	214.8600	0.5267
290.7500	0.4007	274.3700	0.9324	292.8300	0.5800
479.8050	0.4257	467.5000	0.9751	485.3500	0.6140
773.2600	0.4338	761.3200	0.9912	783.0800	0.6139

Table A.2.3 (Data for Figure 4.8) (Contd.)

TiO_2 (sol-gel)		Degussa P25	
Eq. conc. (ppm)	**Amnt. adsorbed/surface area (ppm/m^2/g)**	**Eq. conc. (ppm)**	**Amnt. adsorbed/surface area (ppm/m^2/g)**
31.0000	6.2500e-3	18.0170	0.0793
40.0000	3.6750e-3	38.3700	0.0898
49.0820	0.0125	48.6260	0.0374
80.2280	4.2500e-3	90.6260	0.0140
148.7040	0.0407	151.9600	0.0551
302.0040	0.0490	300.1360	0.0714
397.7760	0.0278	397.7760	0.0890
496.2120	0.0290	502.4890	0.0345
599.0000	0.0125	599.0000	0.0400
672.0000	0.0248	800.0000	0.0000
732.8200	0.0258	1032.6000	0.0000

Table A.2.4 (Data for Figure 4.9)

TiO_2-MCM-41		TiO_2-ALPC		TiO_2-β-zeolite	
Ti^+ conc. (mM)	H^+ conc. (mM)	Ti^+ conc. (mM)	H^+ conc. (mM)	Ti^+ conc. (mM)	H^+ conc. (mM)
1.0000e-3	1.1220e-6	1.0000e-3	6.4565e-6	1.0000e-3	6.4565e-7
0.0260	7.5858e-7	0.0210	1.6596e-5	0.0210	2.3442e-6
0.0420	2.5704e-5	0.0420	6.1660e-5	0.0310	1.3490e-5
0.0521	6.6069e-5	0.0521	1.2023e-4	0.0420	1.8197e-5
0.0625	9.3325e-5	0.0625	1.0000e-4	0.0521	4.5709e-5
0.0830	1.2023e-4	0.0830	1.9055e-4	0.0625	8.5114e-6
				0.0830	8.5114e-5

Table A.2.5 (Data for Figure 4.10a)

10%		25%		50%		60%		80%	
Time (min)	Conc (ppm)	Time (min)	Conc (ppm)	Time (min)	Conc (ppm)	Time (min)	Conc (ppm)	Time (min)	Conc (ppm)
0	50.626	0	50.076	0	50.078	0	49.722	0	50.931
20	49.561	21	45.860	15	31.278	26	31.232	20	36.641
65	50.038	30	44.600	30	30.212	53	30.725	40	36.717
150	50.076	65	44.510	35	30.255	63	30.437	50	36.959
		150	44.248	53	30.112			60	36.959
				85	30.119				

Table A.2.6 (Data for Figure 4.10b)

10%		20%		30%		40%		50%	
Time (min)	**Conc (ppm)**	**Time (min)**	**Conc (ppm)**	**Time (min)**	**Conc (ppm)**	**Time (min)**	**Conc (ppm)**	**Time (min)**	**Conc (ppm)**
0	50.626	0	50.078	0	50.931	0	50.910	0	50.078
20	47.890	20	43.000	20	45.332	36	26.726	10	25.062
40	48.230	40	42.981	49	45.199	56	27.081	20	20.845
80	48.190	80	43.058	79	45.521	66	26.524	30	19.486
						80	26.981	40	18.560
								60	18.370
								71	18.413
								80	17.876
								143	19.389

Table A.2.6 (Data for Figure 4.10b) (Contd.)

60%		80%	
Time (min)	**Conc (ppm)**	**Time (min)**	**Conc (ppm)**
0	50.9100	0	50.9100
26	19.2910	36	23.7260
50	19.5810	56	24.0810
66	19.4980	66	23.5240
80	19.4560	80	23.5240

Table A.2.7 (Data for Figure 4.10c)

10%		20%		30%		50%		60%	
Time (min)	**Conc (ppm)**	**Time (min)**	**Conc (ppm)**	**Time (min)**	**Conc (ppm)**	**Time (min)**	**Conc (ppm)**	**Time (min)**	**Conc (ppm)**
0	50.626	0	50.572	0	49.687	0	50.626	0	50.931
20	50.078	20	50.626	25	44.313	20	32.379	27	44.894
40	50.078	40	50.372	60	44.598	38	32.615	37	45.199
80	50.078	80	50.578	69	44.598	50	32.318	49	45.199
						60	32.734	79	45.521

Table A.2.7 (Data for Figure 4.10c) (Contd.)

80%	
Time (min)	**Conc (ppm)**
0	50.910
20	38.731
40	37.402
50	37.067

Table A.2.8 (Data for Figure 4.11a)

Catalyst amount					
0.25g/l		**0.5g/l**		**1g/l**	
log(C)	**log(q)**	**log(C)**	**log(q)**	**log(C)**	**log(q)**
1.706846	2.190164	1.621861	1.977733	1.211574	1.528878
1.954942	2.374858	1.924238	2.103811	1.440695	1.799916
2.061697	2.525071	2.047333	2.214261	1.770815	1.961554
2.191577	2.581540	2.170863	2.270376	1.934347	2.062093
2.424441	2.733101	2.342186	2.562864	2.093737	2.101335
2.498131	2.870076	2.463520	2.625806	2.431637	2.360271
2.697944	2.914682	2.681065	2.652101		
2.899109	2.921749	2.888326	2.660277		

Table A.2.9 (Data for Figure 4.11b)

Catalyst amount					
0.25g/l		**0.5g/l**		**1g/l**	
log(C)	**log(q)**	**log(C)**	**log(q)**	**log(C)**	**log(q)**
1.629450	2.276701	1.291569	1.793189	1.727175	1.986064
1.920462	2.421538	1.542134	2.046070	1.870550	2.103085
2.058274	2.532296	1.884115	2.157076	2.037466	2.150327
2.168085	2.607283	2.012436	2.286748	2.242939	2.356695
2.329967	2.874157	2.075218	2.402021	2.426397	2.370254
2.474770	2.904190	2.302418	2.596465		
2.686082	2.942207	2.438337	2.655849		
2.897110	2.929255	2.669782	2.675283		
		2.881567	2.682380		

Table A.2.10 (Data for Figure 4.11c)

Catalyst amount					
0.25g/l		**0.5g/l**		**1g/l**	
log(C)	**log(q)**	**log(C)**	**log(q)**	**log(C)**	**log(q)**
1.729853	2.165660	1.643670	1.965305	0.961198	1.320514
1.931178	2.414773	1.939794	2.108010	1.556669	1.799916
2.083054	2.502236	2.062920	2.230066	1.798063	1.941422
2.182429	2.585528	2.144652	2.333145	2.007449	1.990960
2.365188	2.825296	2.332156	2.574656	2.297564	2.308244
2.506045	2.860530	2.466616	2.616518	2.439112	2.349355
2.720763	2.853698	2.686055	2.641236	2.668274	2.377215
2.902318	2.910347	2.893806	2.641216	2.875952	2.397836

Table A.2.11 (Data for Figure 4.12)

MCM-41		AlPC		β-zeolite	
Time (min)	**Conc. (ppm)**	**Time (min)**	**Conc. (ppm)**	**Time (min)**	**Conc. (ppm)**
0	49.5610	0	48.6260	0	48.6260
10	49.5610	10	48.6260	10	48.6260
20	49.5610	20	48.6260	30	48.6260
30	48.6260	30	47.7770	45	48.1900
45	48.1900	45	47.3820	60	47.0050
60	47.3820	60	45.9710	75	47.0050
75	46.3030	75	45.0590	90	46.3030
90	45.0590	95	44.5100	111	45.9710
111	44.2480	111	43.7510	127	45.3520
127	43.2840	127	42.8370		

Table A.2.12 (Data for Figure 4.13a)

20 ppm		30 ppm		40 ppm		50 ppm		60 ppm	
Time (min)	**Conc (ppm)**	**Time (min)**	**Conc (ppm)**	**Time (min)**	**Conc (ppm)**	**Time (min)**	**Conc (ppm)**	**Time (min)**	**Conc (ppm)**
0	16.477	0	20.542	0	29.278	0	30.119	0	34.042
5	14.441	5	19.328	5	27.613	5	28.5251	5	32.28
10	12.614	10	16.334	10	25.276	10	26.028	21	28.586
16	10.662	25	12.699	27	22.326	20	23.522	36	25.419
23	9.629	45	8.373	38	19.553	35	20.197	52	23.168
30	7.804	60	4.973	50	17.221	50	17.587	74	22.444
40	6.024	75	3.551	65	15.587	65	14.207	94	21.106
62	5.038	90	2.555	85	13.633	80	11.812	114	19.755
82	3.577	105	1.826	106	12.523	95	9.130	134	17.267
118	2.102	120	1.257			110	6.936	160	15.958
						125	4.745	190	14.352
						140	3.235		
						155	2.045		
						170	1.126		
						181	0.5231		

Table A.2.12 (Data for Figure 4.13a) (contd.)

90 ppm		30 ppm	
Time (min)	**Conc (ppm)**	**Time (min)**	**Conc (ppm)**
0	41.886	0	83.992
5	39.841	25	73.688
30	32.948	50	65.192
60	26.762	76	52.448
90	23.782	108	44.864
120	19.989	130	41.584
150	17.472	155	39.880
180	15.011		

Table A.2.13 (Data for Figure 4.13b)

30 ppm		40 ppm		50 ppm		90 ppm		150 ppm	
Time (min)	**Conc (ppm)**	**Time (min)**	**Conc (ppm)**	**Time (min)**	**Conc (ppm)**	**Time (min)**	**Conc (ppm)**	**Time (min)**	**Conc (ppm)**
0	7.574	0	10.68	0	19.389	0	34.845	0	76.580
10	5.752	5	9.529	10	17.402	30	25.396	30	58.724
20	4.917	15	7.939	20	17.348	60	19.210	60	52.648
30	3.901	25	6.919	30	16.679	90	13.137	90	46.740
40	2.975	35	6.401	40	13.747	120	9.412	120	41.784
50	2.036	45	5.480	60	11.803	150	7.955	150	38.857
60	1.295	61	4.151	72	10.550	180	4.806	180	35.678
70	0.636	87	2.933	82	8.795				
				93	8.674				
				108	6.137				
				123	4.709				
				138	3.070				

Table A.2.13 (Data for Figure 4.13b) (contd.)

200 ppm		250 ppm	
Time (min)	**Conc (ppm)**	**Time (min)**	**Conc (ppm)**
0	102.905	0	118.910
30	90.375	30	113.580
71	79.990	60	113.050
101	67.400	90	111.945
131	64.905	120	109.100
180	58.775	150	96.650
191	54.225	180	92.065

Table A.2.14 (Data for Figure 4.13c)

30 ppm		40 ppm		50 ppm		90 ppm		150 ppm	
Time (min)	**Conc (ppm)**	**Time (min)**	**Conc (ppm)**	**Time (min)**	**Conc (ppm)**	**Time (min)**	**Conc (ppm)**	**Time (min)**	**Conc (ppm)**
0	18.163	0	21.489	0	32.734	0	44.022	0	87.055
10	14.564	5	19.956	10	28.428	30	33.987	30	78.600
20	11.827	15	17.870	20	25.737	60	27.865	65	66.270
30	9.678	30	14.656	35	20.526	90	25.915	95	60.820
40	7.825	45	13.090	50	17.616	130	21.682	125	57.015
50	6.147	62	12.125	65	13.803	150	20.587	150	53.190
60	4.813	79	11.107	80	11.803	180	17.731	180	51.640
70	3.740	97	10.512	95	8.594				
		109	9.8672	110	7.292				
		134	9.1521	125	4.984				
				140	3.429				
				155	2.367				
				170	1.907				
				181	0.979				

Table A.2.14 (Data for Figure 4.13c) (contd.)

200 ppm		250 ppm	
Time (min)	**Conc (ppm)**	**Time (min)**	**Conc (ppm)**
0	115.59	0	139.525
30	107.25	30	127.410
60	93.995	60	107.315
90	89.820	90	105.780
120	86.785	120	104.145
150	82.055	175	99.135
180	75.335	195	93.940

Table A.2.15 (Data for Figure 4.14)

$1/c_0$	$1/r_0$
0.0607	4.8263
0.0487	4.1169
0.0342	3.0120
0.0332	3.1370
0.0294	2.8377
0.0239	2.4938
0.0119	1.4422

Table A.2.16 (Data for Figure 4.15)

TiO_2-MCM-41		TiO_2-ALPC		TiO_2-β-zeolite	
TiO_2 (wt %)	Rate const (min^{-1})	TiO_2 (wt %)	Rate const (min^{-1})	TiO_2 (wt %)	Rate const (min^{-1})
0	0.0013	0	0.0013	0	0.0013
10	0.0019	10	0.0018	10	0.0005
25	0.0056	20	0.0036	20	0.0030
50	0.0179	30	0.0056	30	0.0041
60	0.0051	40	0.0062	50	0.0179
80	0.0019	50	0.0110	60	0.0056
		60	0.0088	80	0.0039
		80	0.0049		

Table A.2.17 (Data for Figure 4.16)

50 % TiO_2-MCM-41		50 % TiO_2-ALPC		50 % TiO_2-β-zeolite	
Time (min)	**Conc. (ppm)**	**Time (min)**	**Conc. (ppm)**	**Time (min)**	**Conc. (ppm)**
0	50.078	0	50.078	0	50.626
20	31.278	10	25.062	20	32.379
38	30.212	20	20.845	38	32.615
50	30.255	30	19.486	50	32.318
60	30.119	40	18.560	60	32.734
		50	18.370		
		71	18.413		
		80	17.876		
		143	19.389		

Table A.2.17 (Data for Figure 4.16) (contd.)

TiO_2 (sol-gel)		Degussa P25		Without catalyst	
Time (min)	**Conc. (ppm)**	**Time (min)**	**Conc. (ppm)**	**Time (min)**	**Conc. (ppm)**
0	50.078	0	50.626	0	49.722
20	49.561	10	47.382	15	48.687
38	49.561	20	47.777	35	49.189
50	49.561	30	47.382	55	49.189
60	49.082	60	47.330		

Table A.2.18 (Data for Figure 4.17)

50 % TiO_2-MCM-41		50 % TiO_2-ALPC		50 % TiO_2-β-zeolite	
Time (min)	**Conc. (ppm)**	**Time (min)**	**Conc. (ppm)**	**Time (min)**	**Conc. (ppm)**
0	30.119	0	19.389	0	32.734
10	26.028	10	17.402	10	28.428
20	23.522	20	17.348	20	25.737
35	20.197	30	16.679	35	20.526
50	17.587	40	13.747	50	17.616
65	14.207	60	11.803	65	13.803
80	11.812	72	10.550	80	11.803
95	9.130	82	8.796	95	8.594
110	6.936	93	8.674	110	7.292
125	4.745	108	6.137	125	4.984
140	3.235	123	4.709	140	3.429
155	2.045	138	3.070	155	2.367
170	1.126	148	2.607	170	1.907
181	0.523			181	0.979

Table A.2.18 (Data for Figure 4.17) (contd.)

TiO_2 (sol-gel)		Degussa P25		Without catalyst	
Time (min)	**Conc. (ppm)**	**Time (min)**	**Conc. (ppm)**	**Time (min)**	**Conc. (ppm)**
0	49.082	0	47.382	0	49.189
10	47.777	10	43.993	15	49.189
20	46.303	25	41.081	33	49.189
35	43.751	40	35.427	53	47.779
50	41.081	42	34.443	83	45.857
65	38.552	59	29.535	124	41.742
80	35.870	75	27.021	154	39.484
95	33.438	90	24.112		
111	30.719	105	19.738		
127	28.076	120	18.813		
140	26.381				
160	22.915				
180	20.635				
190	18.744				

Table A.2.19 (Data for Figure 4.18)

Catalyst amount (g/l)	Rate const. (min^{-1})
0.25	0.0020
0.5	0.0024
1.0	0.0039
1.5	0.0062
2.0	0.0059
2.5	0.0049

Table A.2.20 (Data for Figure 4.19)

50 % TiO_2-MCM-41		50 % TiO_2-ALPC		50 % TiO_2-β-zeolite	
pH	Rate const (min^{-1})	pH	Rate const (min^{-1})	pH	Rate const (min^{-1})
3	0.0058	3	0.0081	3	0.0031
4	0.0065	4	0.0157	4	0.0074
5	0.0046	5	0.0060	5	0.0032
7	0.0006	7	0.0009	7	0.0006

Table A.2.21 (Data for Figure 4.20)

	300 ºC	**450 ºC**	**600 ºC**	**750 ºC**
50% TiO_2-MCM-41	0.0256	0.0074	0.0054	0.0036
50% TiO_2-AlPC	0.0238	0.0084	0.0068	0.0051
50% TiO_2-β-zeolite	0.0278	0.0078	0.0057	0.0036

Table A.2.22 (Data for Figure 4.21)

50 % TiO_2-MCM-41		**50 % TiO_2-ALPC**		**50 % TiO_2-β-zeolite**	
Time (min)	**Conc. (ppm)**	**Time (min)**	**Conc. (ppm)**	**Time (min)**	**Conc. (ppm)**
0	20.685	0	11.28	0	23.129
5	24.26	5	14.403	5	25.851
15	22.092	30	13.84	15	20.321
30	20.587	60	13.26	30	24.321
45	22.215	90	13.4	45	18.34
60	23.388	120	11.78	60	20.518
75	20.221	150	13.06	75	26.230
90	25.215			90	24.552
105	20.247			105	22.500
120	21.514			120	25.070
135	19.641				

Table A.2.22 (Data for Figure 4.21) (contd.)

Degussa P25	
Time (min)	**Conc. (ppm)**
0	24.64
15	22.98
30	17.93
45	19.16
60	16.04
75	13.96
90	16.17
105	11.7
120	15.81
150	12.54
180	10.69